MOLECULAR DYNAMICS SIMULATION STUDY OF CYANOBIPHENYL-BASED LIQUID CRYSTALS

by

Xiaoyu Wei

A dissertation submitted to the faculty of
The University of Utah
in partial fulfillment of the requirements for the degree of

Doctor of Philosophy

Department of Materials Science and Engineering

The University of Utah

August 2016

The University of Utah Graduate School

STATEMENT OF DISSERTATION APPROVAL

The dissertation of **Xiaoyu Wei**

has been approved by the following supervisory committee members:

Dmitry Bedrov	, Chair	**6/14/2016** Date Approved
Matthew Glaser	, Member	**4/9/2016** Date Approved
Feng Liu	, Member	**6/14/2016** Date Approved
Ling Zang	, Member	**6/15/2016** Date Approved
Jules John Magda	, Member	**6/14/2016** Date Approved

and by **Feng Liu** , Chair/Dean of

the Department/College/School of **Materials Science and Engineering**

and by David B. Kieda, Dean of The Graduate School.

ABSTRACT

Atomistic molecular dynamic (MD) simulations of cyanobiphenyl liquid crystal both in the bulk and at interfaces have been conducted using the highly transferable, quantum chemistry-based force field from our group. The influence of induced polarization effects force field details on the predicted thermodynamic, dynamic, and structural properties of 4-cyano-4'-pentylbiphenyl (5CB) bulk systems have been systematically investigated in the 292-368 K temperature range. Variations in the magnitude of molecular dipole moment and the details of dihedral potential for biphenyl unit were investigated using both polarizable (POL) and nonpolarizable (NP) versions of the aforementioned force field. The predicted densities for the nematic and isotropic phases of bulk 5CB were found to be in excellent agreement with available experimental data. However the simulation predicted nematic-isotropic transition temperature (T_{NI}) show an overestimation when the partial atomic charges were taken directly from high-level quantum chemistry calculations. Subsequent rescaling of partial charges significantly improved the prediction of T_{NI} and other thermodynamic and dynamic properties. We also studied the interface anchoring effect and energetics of 5CB in contact with free surface, pure water, and aqueous solution of surfactant C_{10}TAB in both nematic and isotropic phases via atomistic molecular dynamic simulation. The resulting anchoring behaviors of 5CB at different interfaces are in good agreement with experiment. For the free surface system, we demonstrated that a

small change of the biphenyl torsional parameter of 5CB can lead to stronger positional ordering both at the interface and in the bulk. Overall the results show our force field is fully capable of capturing the crucial planar to homeotropic anchoring reorientation of 5CB in a complex four component environment. Initial data and comparison on structure, conformations, and dynamics of cyanobiphenyl-$(CH_2)_7$-cyanobiphenyl (CB7CB) in twist-bend nematic, regular nematic, and isotropic phases were provided. The simulation predicted order parameter, average bend angle β and the nanoscale angular modulation of β are in good agreements with experiments.

Dedicated to my mother and father

TABLE OF CONTENTS

ACKNOWLEDGEMENTS

The author would like to gratefully acknowledge the tremendous support from Dr. Dmitry Bedrov and Dr. Justin Hooper for their guidance, discussions, and encouragement throughout my years of learning as a graduate student. Special thanks are given to Dr. Wenmei Ming and all my colleagues for the helpful discussions and their unique insights.

The author expresses his gratitude for the financial support from Soft Materials Research Center under National Science Foundation Materials Research Science and Engineering Centers Grants DMR-0820579 and DMR-1420736. The computational resources provided by the University of Utah Center for High Performance Computing are deeply appreciated.

CHAPTER 1

INTRODUCTION TO LIQUID CRYSTALS

1.1 General Overview

Liquid crystals (LCs) are a truly fascinating category of materials with a wide array of applications that made them of a great interest both to scientific and engineering communities ever since their discovery in 1888 by Friedrich Reinitzer. As a matter of fact, the reader might very well be looking at this text on a LC display right now, and this application alone has created a multibillion-dollar industry. Let us briefly review what the liquid crystal are. As the name suggest, it is a state of matter that possess properties of both liquid (fluidity and viscosity, deforms upon stress) and solid crystalline materials (long range ordering, optical, electric, and magnetic anisotropy). There are mainly two kinds of LCs, thermotropic and lyotropic. A thermotropic LC material displays a series of phase transitions with increasing temperature before it becomes an isotropic liquid. These phases are called "mesophases" from the Greek *meso* which means "in between." In lyotropic LC materials the phase transition is mainly concentration dependent in a multicomponent solution. One of the most common mesophases is a nematic phase, which is illustrated in Figure 1.1a and characterized by a long-range orientational order and the lack of positional order of constituent LC molecules. The average preferred orientational direction is called the director **n** and is the primary reason for the anisotropy of macroscopic optical,

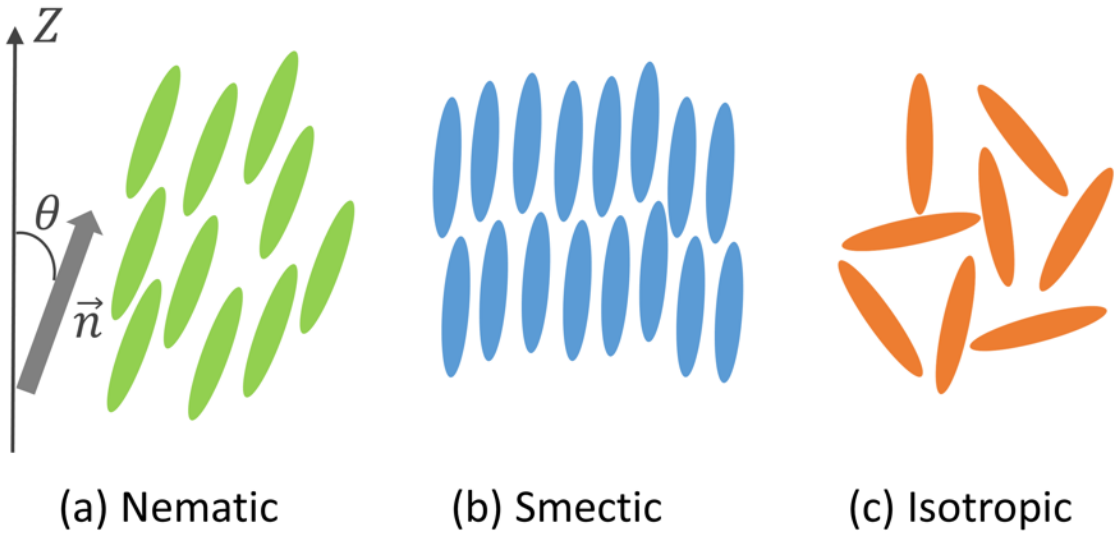

Figure 1.1. Schematic representation of nematic (a), smectic (b) and isotropic (c) phases.

electrical, magnetic, and mechanical properties of LC materials in this phase. The other commonly studied mesophases include smectic (Figure 1.1b) and columnar phases, a more detailed descriptions of which can be found in the excellent review by de Gennes and Prost.[1] The materials that exhibit LC mesophases usually have the following common traits for molecules comprising them: asymmetric shape, have both rigid and flexible moieties, have a relatively large dipole moment. Extensive efforts of numerous researchers have significantly advanced our understanding of the phase behavior of LC materials. However, a fundamental understanding of correlations between the macroscopic properties of LC materials and the molecular level structure still represents a great challenge in soft matter physics and materials science.

1.2 Theories for Nematic-Isotropic Transition

In order to discuss the theories describing the nematic-isotropic (NI) transition quantitatively we need to define two key characteristics, namely, the nematic order parameter and director. Since most nematogens have rigid cores and are rod-shaped, we consider a vector $\mathbf{u}^i$ to denote the backbone of the molecule *i* and will use it to describe its orientation. The rotational symmetry of the nematogen makes $\mathbf{u^i}$ and $-\mathbf{u^i}$ indistinguishable, and its cylindrical symmetry means the angle distribution is independent of the azimuthal angle φ. Those symmetries forbid the use of the $<cos\theta>$ to characterize the degree of alignment, and therefore, we resort to the 2nd rank tensor instead. It is defined as

$$Q_{\alpha\beta} = \frac{1}{N}\sum_{i=1}^{N}\left(\frac{3}{2}\mu_\alpha^i\mu_\beta^i - \frac{1}{2}\delta_{\alpha\beta}\right) \tag{1.1}$$

where μ_α^i $(\alpha, \beta = x, y, z)$ are the Cartesian components of the molecular axis unit vector of molecule *i* and $\delta_{\alpha\beta}$ is the Kronecker symbol, and $Q_{\alpha\beta}$ is a spatially invariant dimensionless tensor. In the case of uniaxial nematic, the largest eigenvalue is the order parameter $S_{\alpha\beta}$ we use and the corresponding eigenvector is the director **n**, which represents the average molecular orientation of the nematic phase. $S_{\alpha\beta}$ = 1 for a perfectly aligned system and $S_{\alpha\beta}$ = 0 in the isotropic system.

1.2.1 Landau-de Gennes Phenomenological Model

According to Landau,[2] the free energy of a system can be interpreted as a power series of the order parameter tensor Q. de Gennes[1] has extended this idea to describe the NI phase transition phenomenon in LC materials. This symmetry based theory is famous for its simplicity and the ability to capture important aspects of the NI phase transition, and it

ensures the smooth transition of orientation at the boundary of adjacent small local nematic droplets with size of coherence length ξ that persisted in isotropic phase. The thermodynamic potential $G(p,T,Q)$ near the transition point can be constructed as

$$G(p,T,Q) = G_0(p,T,Q) + \frac{1}{2}AQ^2 + \frac{1}{3}BQ^3 + \frac{1}{4}CQ^4 + OQ^5 \tag{1.2}$$

where G_0 is the free energy potential of the isotropic phase, A, B, C…are functions of p and T. $A = a(T - T_{NI}^*)$ and a is a constant greater than zero and T_{NI}^* is the lower limit for the metastable isotropic phase when supercooled, while B, C are considered temperature independent in the vicinity of $A = 0$ (T near T_{NI}). Clearly, if $T > T_{NI}^*$, then $A > 0$ and the free energy curve minima is at $S_2 = 0$, while if $T < T_{NI}^*$, $A < 0$ and a minima of G can be find at $S_2 > 0$, and at T = T_{NI}, the nematic and isotropic phases can coexist. The second and third order invariant are $Q^2 = \frac{1}{2}(3q^2 + \eta^2)$ and $Q^3 = \frac{3}{4}q(3q^2 - \eta^2)$, respectively. In the case of uniaxial nematic phase $\eta = 0$, and therefore $Q^2 = \frac{3}{2}q^2$ and $Q^2 = \frac{9}{4}q^3$, taken into (1.2) the free energy density now becomes

$$G = G_0 + \frac{3}{4}a(T - T_{NI}^*)q^2 + \frac{1}{4}Bq^3 + \frac{9}{16}Cq^4 + Oq^5 \tag{1.3}$$

and at the free energy minimum, $\frac{dG}{dq^2} = 0 = \frac{3}{2}a(T - T_{NI}^*)q + \frac{3}{4}Bq^2 + \frac{9}{4}Cq^3 + Oq^4$ and the solution

$$\begin{cases} q = 0 \\ q = \frac{B}{6C}\sqrt{1 \pm \frac{24a(T-T_{NI}^*)C}{B^2}} \end{cases} \tag{1.4}$$

corresponds to isotropic and nematic phases, respectively.

1.2.2 Maier-Saupe Theory

Maier and Saupe[3–5] proposed a model based on the molecular field approximation of long-range interactions from the orientation-dependent London-van der Waals forces. Assuming that molecules have a spherical symmetry, the free energy can thus be written as

$$F(p,T) = F_0(p,T) + \left(-\frac{1}{2}u(p,T)S^2\right) + k_BT\int f(\theta)\ln[4\pi f(\theta)]d\Omega \qquad (1.5)$$

where $F_0(p,T)$ is the free energy of isotropic phase, and the second term is the free energy associated with London-van der Waals interactions, u is a positive interaction parameter independent of temperature. The last term describes the entropy change due to angular distribution $f(\theta)$ of LC molecules, $d\Omega$ denotes a small solid angle around $f(\theta)$. To minimize F for all variations regarding $f(\theta)$ with $\int \delta f(\theta)d\Omega = 1$ as constraint, the equation of $F(p,T)$ becomes

$$\delta F(p,T) = \lambda\int \delta f(\theta,\phi)d\Omega$$

and

$$\delta F(p,T) = \int \delta f\{(u(p,T)S * \delta S) + f(\theta)\, k_BT\ln[4\pi f(\theta)] + 1\}d\Omega$$

$$\delta S = \int \frac{1}{2}(3cos^2\theta - 1)\,\delta f(\theta,\phi)d\Omega$$

$$\ln[4\pi f(\theta)] + 1 = \lambda + \frac{1}{2k_BT}u(p,T)S(3cos^2\theta - 1) \qquad (1.6)$$

The angular distribution becomes

$$f(\theta) = \frac{1}{4\pi Z}\exp[\frac{3cos^2\theta}{2k_BT}u(p,T)S] \qquad (1.7)$$

where partition function $Z = \int \exp(\frac{3cos^2\theta}{2k_BT}u(p,T)S)d\Omega$ and λ is an unknown Lagrange

multiplier. To make the theory self-consistent, $S = \frac{1}{2} < 3cos^2\theta - 1 >= \int \frac{1}{2}(3cos^2\theta - 1)\, f(\theta) d\Omega$ and after parametric transformation,

$$S = \frac{3}{4}\left[\frac{\exp(x^2)}{x\int_0^x \exp(y^2)dy} - \frac{1}{x^2}\right] - \frac{1}{2} \tag{1.8}$$

$$\frac{k_B T}{u(p,T)} = \frac{3}{2}\frac{S}{x^2} \tag{1.9}$$

at T_{NI}, $\frac{k_B T_{NI}}{u(p,T_{NI})} = 4.55$, and $S_{NI} = 0.44$. Maier-Saupe theory model predicts the order parameter very well compare to experiments if the London-van der Waals interactions u are carefully selected to match the observed transition temperature.

1.2.3 Onsagar Hard Rod Model

In Onsagar's hard rod model[6] of LC phase transition, the many-body configurational energy is approximated by a pair-wise volume exclusion repulsion interactions that is orientation-dependent, and the NI phase transition is considered as a balance between positional and orientation entropy. For the systems of elongated rods with length $L >>$ diameter D, the concentration of rods c, the rod volume fraction of $\Phi = c\frac{1}{4\pi}LD^2$ and the angle between two rods is γ one can write the Helmholtz free energy rods as

$$F = F_0 + k_B T\left(\int f(a)\ln[4\pi f(a)]d\Omega + \frac{1}{2}c\iint f(a)\, f'(a)\beta_1(aa')d\Omega d\Omega'\right) \tag{1.10}$$

where the second term corresponds to orientational entropy and the third term is the positional entropy due to excluded volume interactions ($\beta_1(aa') = 2L^2 D sin(\gamma)$ is the excluded volume). The minimum free energy can be obtained by solving the equation via variational derivative of (1.9) subject to the same normalization condition of $\int \delta f(\theta) d\Omega = 1$,

$$\ln[4\pi f(a)] = \lambda - 1 - c \int f'(a)\beta_1(aa')d\Omega \quad (1.11)$$

using trial function, *f(a) = (const) cosh(αcos(θ))*, where α and θ is a variation parameter and angle between vector *a* and the *Z* axis, respectively. At the nematic-isotropic transition point, the critical volume fraction $\Phi_c = D/L$, and as a result, the NI transition is easier to achieve for more elongated rods, and the critical order parameter is around 0.84, which is rather large compared to the value of 0.44 predicted by the Maier-Saupe theory. The reason for such overestimation is that in actuality, the relatively weak repulsion-dispersion, electrostatic, and induced polarization interactions cannot be treated as small perturbations to the excluded volume interactions. All these interactions play an important role in defining the variety of mesophases. Nevertheless, the Onsagar model has provided the first ever qualitative understanding of the fundamental physics behind the NI transition.

1.3 4-Cyano-4'-pentylbiphenyl (5CB) and Its Homologues

In this thesis, the primary object of investigation is the 4-Cyano-4'-pentylbiphenyl (5CB) LC compound. The 5CB molecule has $C_{18}H_{19}N$ chemical formula, and together with its nCB homologues, they represent the well-known chemically stable thermotropic LCs family. nCBs were first synthesized by Gray and coworkers[7] in 1972, when they were searching for room temperature LCs to be used in display devices. nCBs are among the most-studied and characterized LC materials both by experiments and simulations. Figure 1.2a shows that the 5CB molecule is comprised of a cyano group connected to a biphenyl unit, which in turn, is attached to a flexible pentyl tail (the number of carbons on the tail defines *n* in the nCB, e.g., 8CB in Figure 1.2b). The cyano group is responsible for the large molecular dipole moment of about 4.6 Debye, the biphenyl unit provides conjugated

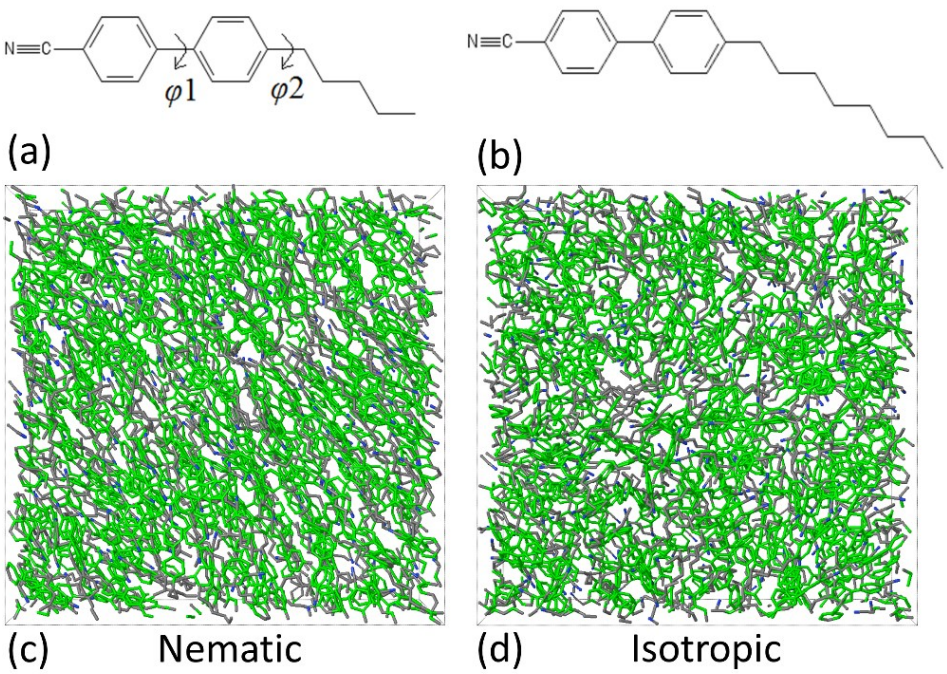

Figure 1.2. Chemical structure and simulation snapshots of 5CB. Panels (a) and (b) are the skeletal formula of 4-Cyano-4'-pentylbiphenyl and its 8CB homologue. Panels (c) and (d) are snapshots of 5CB system in the nematic and isotropic phases, respectively.

bonds with delocalized electrons, and together with the alkyl tail they dictate the phase behavior of nCB. The intermolecular van der Waals forces also contributed to the formation of nematic phase as the biphenyl group has strong interaction with the local surrounding molecules and tends to align parallel to them. The experimentally observed nematic-isotropic phase transition temperature is 306.7-308 K.[8,9] Figure 1.2c and 1.2d show snapshots from our molecular simulations that illustrate the bulk structure of 5CB LC in the isotropic and nematic phases. Structurally, the dimension of this rod like molecule is about 20 Å long and 5 Å wide, the equilibrium dihedral angles of inter-ring φ_1 and ring-tail φ_2, indicated in Figure 1.2a, are around 32°and 90°,[10] respectively.

For the nCB family, there is an interesting phenomenon referred as an "odd-even" effect, due to the intricate and complex interplay of inter and intramolecular interactions, the nCBs with odd number of carbon atoms on the tail group exhibit significant alternation of thermodynamic properties compare to the even number cyanobiphenyls[11,12] (see Figure 1.3). More specifically, in terms of free energy consideration, this phenomenon arises from the complex interplay between energetic terms (intermolecular repulsion/dispersion and electrostatic interactions) and the entropy terms[1,13] (positional, orientational, and conformational probability distributions). The delicate balance between these terms means that even small changes in free energy can affect the mesophase stability as well as the dielectric permittivity[14] and viscosity.[15,16] This effect further demonstrates the extreme sensitivity of macroscopic properties of LC materials to small perturbations in the chemical details of molecules (e.g., the appearance of nematic and smectic phase when n > 5 and 8, respectively.[17–19])

Despite being one of the most studied mesogens the understandings of the molecular scale phenomena of 5CB LCs and its homologues is still incomplete. For example, the influence of the induced polarization effect on the phase behavior, conformational, flexoelectric, and dynamic properties are often hard to measure via traditional experiment method, this is especially true in the case of measurements of the fourth rank orientational order parameter P_4.[20,21]

1.4 Anchoring Effect of Liquid Crystals

It is known that the presence of interfaces (air, solid, or liquid) will induce ordering of LC that is different than in the bulk nematic phase, such phenomenon is called "surface-

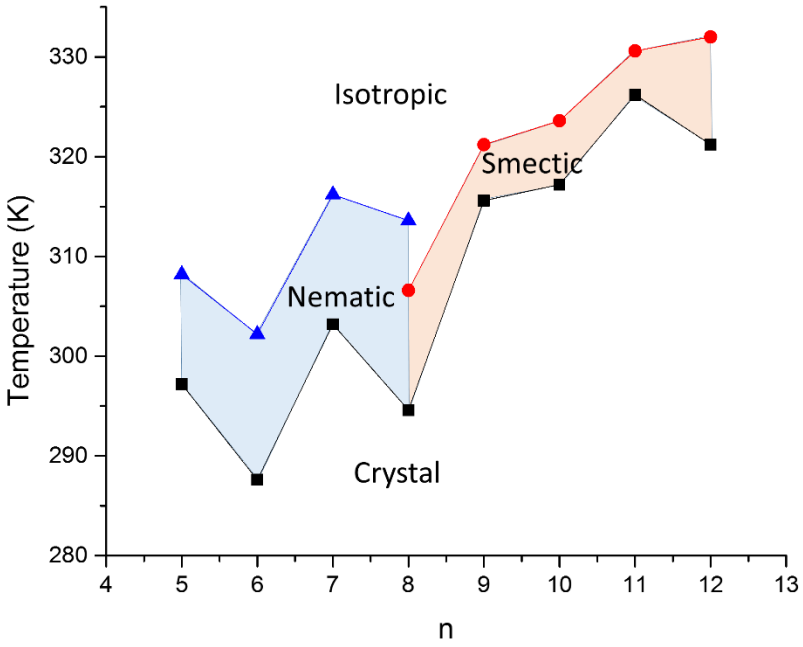

Figure 1.3. Experimentally observed odd-even effect[22] in both phase transition temperatures and phase sequence of the nCB family.

anchoring." Figure 1.4a and 1.4b schematically illustrates the planar and homeotropic anchoring alignment of LC in contact with pure water and air, respectively. This effect was first brought to attention by the commercial application of LCDs where the alignment of the LC materials at the interface between display cell wall and the LC was dictating the performance of the device.[23] The influence of surface anchoring on the orientation of nematic LC phase can be explained by a two-step process: first, at distances smaller than few molecular lengths, i.e., for the first layer of LC molecules in direct contact with the interface, the surface exerts a perturbation of translational symmetry and the LC molecules have a tendency to adapt some positional ordering with the mean anchoring orientation of **a** and the thickness of this ordered layer corresponding to the coherence length ξ.

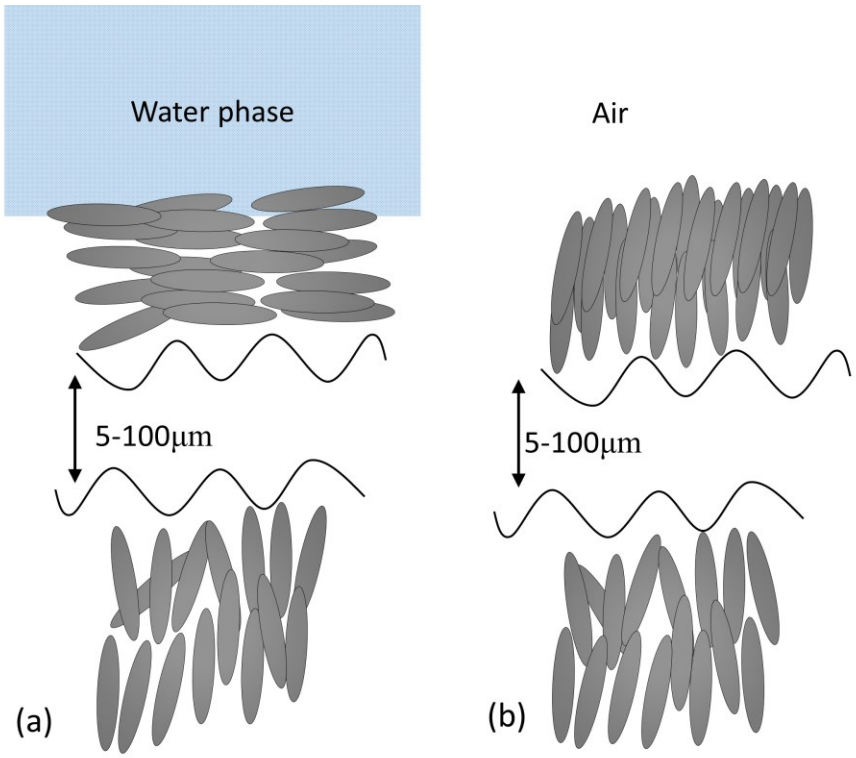

Figure 1.4. Schematic illustration of LC anchoring alignment at water (a) and air (b) interfaces.

Eventually, at distances greater than ξ, the average orientation of bulk LC molecules will be moved away from the original bulk phase "easy axis" and get anchored by the surface orientation of **a** due to the elastic forces which tend to orient all the molecules parallel to each other.[24,25]

The interfacial free energy γ_s can be defined as

$$\gamma_s = \gamma_0 + \frac{1}{2}W_\theta sin^2(\theta_a - \theta_0) + \frac{1}{2}W_\varphi sin^2(\varphi_a - \varphi_0) \qquad (1.12)$$

where γ_0 is the orientation-independent surface free energy, W_a and W_φ is the polar anchoring potential and θ_a and θ_0 are the zenith orientation of anchoring direction of a and the easy axis of the bulk, respectively, and similarly, φ_a and $\varphi_0$are the azimuthal angles. The zenith anchoring coefficient W_θ is on the order of 10^{-2}-10^{-3} mJ/m^2, and the azimuthal

anchoring potential W_φ is orders of magnitude smaller.[26] As a consequence, the subtle changes in the surface energetics on the similar scale can lead to a change of anchoring direction of LC material.

While the properties of solid-LC interface have been well-studied due to strong commercial interest for LCD applications, these days more and more attention is given to the aqueous-LC interfaces due to rich anchoring behavior exhibited by LCs at those interfaces and controlled by interactions with surfactants, polymers, and biomolecules such as DNA, lipids, and proteins adsorbed at the interface. One of the most important properties of the aqueous interface is the high mobility provided for the adsorbents,[27] it permits fast reorganization and formation of new domains in the surfactants self-assembly monolayer (SAM). Together with the ability to manipulate composition and concentration of surfactants at the surface enables new opportunities such as novel sensors for detection of various bio- and chemical events and label-free DNA hybridization detection.[28]

1.5 A Novel Twist-Bend Nematic Phase

Very recently, a new type of nematic phase has been discovered by Chen et al.,[29] identifying the fifth type of the nematic ordering observed in LC materials since the discovery of the uniaxial nematic phase in the 19th century,[29] Such novel mesophase was first predicted theoretically by Meyer,[30] suggesting that this new phase is due to the spontaneous formation of the flexoelectric polarization of the bending gradient. Latter Dozov[31] has attributed this phase to the negative elastic bend constant of the banana-shaped mesogens and suggesting that if the imposed elastic bend is stronger than splay and twist then a twist-bend nematic phase (N_{TB}) can form. Figure 1.5a shows the structure of N_{TB}

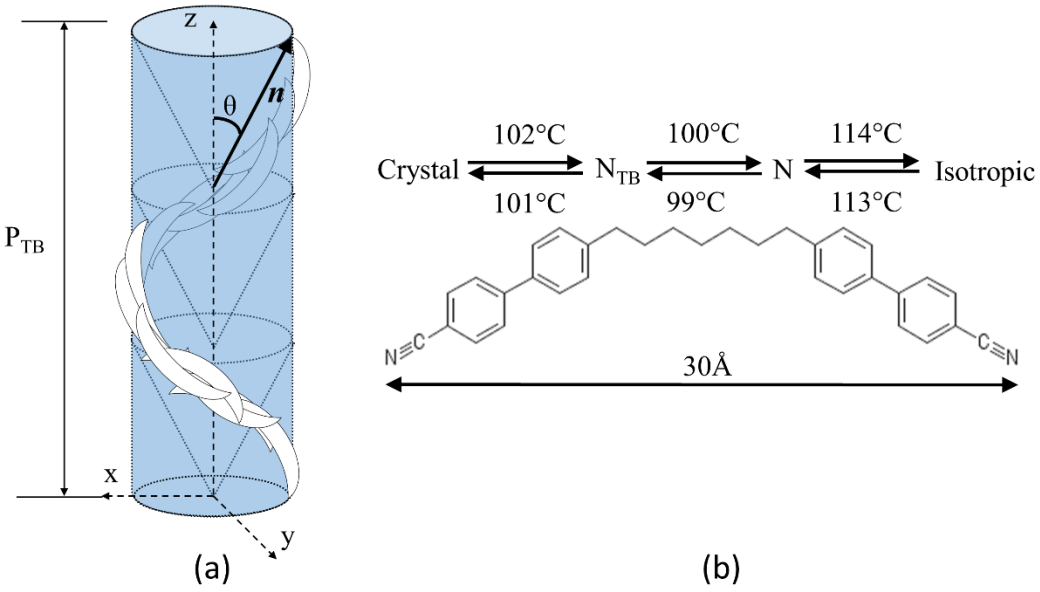

Figure 1.5. Schematic illustration of the N_{TB} phase structure (a), the director **n** is spontaneously distorted forming a helicoid of constant polar angle θ and a pitch P_{TB} of about 8 nm. (b) Skeletal formula and phase diagrams of CB7CB.

phase, the precession of the director **n** field of N_{TB} phase forms oblique helicoid, with a constant conical angle $0 < \theta < \pi/2$ with Z axis, and an extremely short helicoid pitch of P_{TB} on the order of ~10 nm, $n(z) = (sin\theta cos\varphi, sin\theta cos\varphi, cos\varphi), \varphi = q \cdot Z$ is the azimuthal angle, $q = \pm 2\pi/P_{TB}$ is the wave vector of the director distortion. The Frank-Oseen elastic free energy of N_{TB} for one-dimensional oscillation of the director can be expressed as

$$F_{TB} = \frac{1}{2}(K_2 sin^4\theta \times q^2 + K_3 sin^2\theta \times q^2 + C sin^2\theta \times q^4) \qquad (1.13)$$

here K_2 and K_3 is the twist and bend elastic constant, respectively, C is the fourth order elastic coefficient. After the minimization of (1.13), the spontaneous tilt angle $sin^2\theta = -K_3/3K_2$, and the wave vector $q^2 = -K_3/3C$. These two values can be used as order

parameters to describe the N- N_{TB} phase transition, and the sign of the wave vector q is used to distinguish the chirality of the helicoid.[31,32]

The specific LC molecule that exhibits the N_{TB} phase is an achiral odd dimer 1''7''-bis(4-cyanobiphenyl-4'-yl)heptane (CB7CB), along with its n-odd CBnCB homologues, assumes a banana shaped all-trans conformations, as shown in Figure 1.5a. It shows a N-N_{TB} transition temperature of 100°C and T_{NI} of 113°C upon cooling, with about 1°C hysteresis upon cooling, the melting temperature Crystal-->N_{TB} is about 102°C[29,33] when heating. The N-N_{TB} is a first order phase transition, but the phase identification and characterization is proven to be a challenging task due to similarity of textures shown by optical polarizing microscopy (OPM) for the N_{TB} and chiral smectic C^* (SmC^*) phases. Some early investigations[34,35] have mislabeled the n-odd CBnCB to be of smectic in nature. However, as has been later discovered, the N_{TB} phase differs from the SmC^* phase in the following ways. First, there is no positional order, and therefore no periodic density variation. Second, this new chiral phase is formed by achiral molecules, whereas most SmC^* phases are formed by chiral molecules. Thirdly, the wave vector q in the N_{TB} phase is temperature dependent and can be used as an order parameter for N_{TB}, whereas q in SmC^* is invariant to temperature and determined by the length of the smectic molecule. And lastly, the doubly degenerate helicoid superstructure is formed due to the negative nematic bend elasticity, rather than dipole-dipole interactions of smectic mesogens.

1.6 Molecular Dynamics Simulation Technique

Thanks to the rapid growth of CPU throughput (and emergence of GPU architectures), atomistic molecular dynamics (MD) simulations have become a very powerful tool to

investigate the microscopic origin of macroscopically observed properties and phenomena in a variety of materials. These days, MD simulations are an integrated part of materials science and engineering field. In the past few decades, a tremendous amount of work has been done to investigate various aspects of LC materials using MD simulations employing models ranging from fully-atomistic to coarse-grained.[13,36–45] These simulations greatly improved our understanding of both the statistical models and experimentally observed phenomena of the mesophases. One of the key advantages of MD simulations that made this technique particularly interesting for materials scientists is the ability to manipulate with specific interactions, which is impossible to do in the real world, so one can study the effects of various contributions (e.g., partial atomic charges, molecular polarizability, molecular flexibility, etc.) separately. The ability of MD simulations to use such "what if" scenarios at the molecular scale has become a key component in the design and optimization of novel materials.[20] Another useful aspect of MD simulations is that they facilitate bridging between theory and experiment. For example, a theoretical model can be tested/validated against well-defined virtual experiment of molecular simulation, while interpretation of real experimental measurements can be facilitated using the insight obtained from correlations observed in MD simulations.[46]

1.6.1 Simulation Methodology

MD simulation is well suited for exploring thermodynamic, structural, dynamic, and interfacial behavior of LC materials. However, in order to accurately predict those properties, it is crucial to have an accurate, reliable and transferable force field as the input parameters describing various inter and intramolecular interactions operative in the system.

For simulations described below, we have employed the many-body polarizable APPLE&P force field[47] that has been developed in our group and successfully applied to variety of soft-condensed matter materials.[48–53]

The total potential energy $U^{tot}(r)$ for each interaction site (r) in the system is defined as

$$U^{tot}(r) = U^{NB}(r) + \sum_{bends} U^{bend}\left(\theta_{ijk}\right) + \sum_{dihedrals} U^{dihedral}\left(\varphi_{ijkl}\right) + \sum_{impropers} U^{improper}\left(\varphi_{ijkl}^{imp}\right) \quad (1.14)$$

where the sums are over all bonds, bends, dihedrals, and improper dihedrals in the system. The potential energy from bonds, bends, dihedrals, and out-of- plane improper dihedrals are defined as

$$U^{bend}\left(\theta_{ijk}\right) = \frac{1}{2} k_{\alpha\beta\gamma}^{bend} (\theta_{ijk} - \theta_{ijk}^{0})^2 \quad (1.15)$$

$$U^{dihedral}\left(\varphi_{ijkl}\right) = \sum_n \frac{1}{2} k_{\alpha\beta\gamma\delta,n}^{dihedral} [1 - cos(n\varphi_{ijkl})] \quad (1.16)$$

$$U^{improper}\left(\varphi_{ijkl}^{imp}\right) = \frac{1}{2} k_{\alpha\beta\gamma\delta}^{imp} (\varphi_{ijkl}^{imp})^2 \quad (1.17)$$

where θ_{ijk} and θ_{ijk}^{0} are the instantaneous and equilibrium bending angles formed by atoms i, j, and k, φ_{ijkl} is the dihedral angle of atoms i, j, k, and l, and φ_{ijkl}^{imp} is the out of plane improper dihedrals angle for an sp2 orbital at site j, $k_{\alpha\beta\gamma}^{bend}$, $k_{\alpha\beta\gamma\delta,n}^{dihedral}$, and $k_{\alpha\beta\gamma\delta}^{imp}$ are the force constants, and α, β, γ, and δ are the atom type correspond to site i, j, k, and l, respectively. The nonbonded interaction potential $U^{NB}(r)$ is comprised of repulsion and dispersion $U^{RD}(r)$, fixed charges coulombic $U^{coul}(r)$, and polarization energy $U^{pol}(r)$ from induced dipole-dipole and induced dipole-induced dipole interactions,

$$U^{NB}(r) = U^{RD}(r) + U^{coul}(r) + U^{pol}(r) = \sum_{i>j}(A_{\alpha\beta} exp\left(-B_{\alpha\beta} r_{ij}\right) - C_{\alpha\beta} r_{ij}^{-6} + D\left(\frac{12}{B_{\alpha\beta} r_{ij}}\right)^{12}) + \sum_{i>j}(\frac{q_i q_j}{4\pi\varepsilon_0 r_{ij}}) - \frac{1}{2}\sum_i \vec{\mu}_i \vec{E}_i^0 \quad (1.18)$$

where $\vec{\mu}_i = \alpha_i \vec{E}_i^{tot}$ is an induced dipole at force center i, α_i is the isotropic atomic

polarizability, $\vec{E}_i^{tot}$ is the total electrostatic field at the atomic site i due to permanent charges q_i and induced dipole $\vec{\mu}_j$, ε_0 is the permittivity of free space, $A_{\alpha\beta}$ and $B_{\alpha\beta}$ serve to specify the repulsive core of the potential, and $C_{\alpha\beta}$is the dispersion parameter for interaction between atoms *i* and *j* with atom types *α* and *β*. The term $D\left(12/B_{\alpha\beta}r_{ij}\right)$,[12] with $D = 5 \times 10^{-5}$ kcal/mol for all pair interactions, is essentially zero at typical nonbonded atomic separations, but becomes the dominant term at r_{ij}<1Å, ensuring that the repulsive interaction at close approaches remains monotonic in nature. Nonbonded interactions are included for atoms separated by three or more covalent bonds.

1.6.2 Force Field Development

Force field development for specific material/compound requires obtaining the above mentioned parameters which is a very challenging task that usually involves three steps. First, the valence interactions (bond lengths, bending angles and constants, dihedral parameters, etc.) are fitted against data obtained from *ab initio* calculations on representative compounds or molecular segments in the gas phase. These parameters are fit to reproduce the gas phase geometries and energies due to bending angle distortions, and conformational energy surface. Second, the parameters describing electrostatic interactions (partial atomic charges, atomic polarizabilities) are fit to describe the electrostatic potential around representative molecule(s) as obtained from high-level *ab initio* calculations. Thirdly, the repulsion-dispersion parameters of van-der-Waals interactions are obtained by fitting them to binding energies obtained from *ab initio* calculations on small molecular clusters as well as by empirical adjustments to reproduce available thermodynamic properties such as heats of vaporization (H^{vap}), densities, phase

behavior, transport properties, etc. As we discuss in the next chapter, the process of obtaining an accurate force field is extremely challenging task requiring multiple iterations and simultaneous optimization of large set of parameters that are often have complex interdependence.

1.7 Thesis Overview

In Chapter 2, we describe the force field development for 5CB mesogen as well as discuss the influence of some key parameters/interactions on the prediction of thermodynamic and dynamic properties of 5CB bulk systems in a wide range of temperatures. The predicted densities for the nematic and isotropic phases of bulk 5CB were found to be in excellent agreement with available experimental data. We will demonstrate that the utilization of partial atomic charge distributions fit directly to the high-level QC calculations results in overestimation of the 5CB dipole moment, therefore leading to over estimation of the T_{NI}. Rescaling the charges to allow the molecular dipole to be closer to experimentally reported values of 5CB dipole in condensed phases significantly improves the prediction of T_{NI} as well as other thermodynamic and dynamic properties of isotropic and nematic phases of 5CB. We also will demonstrate how the flexibility of the central biphenyl dihedral can affect the phase behavior of 5CB.

In Chapter 3, we provide in depth view of the effect of induced polarization interactions on the structural properties of bulk 5CB systems. Calculation of radial distribution function and orientation correlation function indicates two preferred antiparallel configurations in the nematic phase, which are in accordance with X-ray diffraction experiment as well as other simulation works. We show that in the first coordination shell, the induced

polarization will lead to a closer packed 5CB molecules. For the conformational property, we will show the inter-ring and ring-tail dihedral angle distribution using both the original and modified force fields. We also will present the dihedral distribution of 5CB in both nematic and isotropic phase.

In Chapter 4, all-atom MD simulations utilizing non-polarizable force fields were used to comprehensively study the anchoring effect of 5CB molecules at vacuum, water and surfactant laden aqueous interfaces. We will show the anchoring behavior of 5CB at these three vastly different interface environments and demonstrate how small changes of torsional parameter in the biphenyl moiety in 5CB, can affect the interfacial ordering of 5CB in the vacuum interface systems, as well as 5CB aqueous interface systems. Through order parameter calculation we are able to directly grasp the anchoring effect of the LC near the interface with respect to the bulk phase behavior, and the degenerate planar anchoring induced 2D isotropic phase at the 5CB water interface agrees well with the experiment. We show the direction of anchoring for 5CB via relative order parameter calculation, for the homeotropic anchoring created by the vacuum and surfactant interface we see the angle between the local director and Z axis is near parallel close to the surface, whereas the water interface induced planar anchoring of 5CB is perpendicular to the Z axis.

In Chapter 5, we present a first look of the novel N_{TB} phase using full atomistic MD simulation, the thermodynamic, structure, and dynamic properties of the bent-shape mesogen CB7CB will be shown. Specifically, we will show investigation the correlation between temperature and conical angle θ and pitch P_{TB}, and predicted both N-N_{TB} and T_{NI} transition temperatures. We demonstrated the structure correlation of CB7CB by calculating radial distribution function and orientation correlation function. Transport

properties are measured as a function of temperature using mean squared displacement.

1.8 References

[1] P.G. de Gennes and J. Prost, *The Physics of Liquid Crystals*, 2nd ed. (Clarendon Press, 1995), pp. 10-27.

[2] L.D. Landau, Zh. Eks. Teor. Fiz. **7**, 19 (1937).

[3] W. Maier and A. Saupe, Z. Naturforsch. A **13**, 564 (1958).

[4] W. Maier and A. Saupe, Z. Naturforsch. **15A**, 882 (1959).

[5] W. Maier and A. Saupe, Z. Naturforsch. A **15**, 287 (1960).

[6] L. Onsager, Ann. N. Y. Acad. Sci. **51**, 627 (1949).

[7] G.W.G.W. Gray, K.J.J. Harrison, and J.A.A. Nash, Electron. Lett. **9**, 130 (1973).

[8] G.A. Oweimreen and M.A. Morsy, Thermochim. Acta **346**, 37 (2000).

[9] T. Mansaré, R. Decressain, C. Gors, and V.K. Dolganov, Mol. Cryst. Liq. Cryst. **382**, 97 (2002).

[10] S. Sinton and A. Pines, Chem. Phys. Lett. **76**, 263 (1980).

[11] G.W. Gray and A. Mosley, J. Chem. Soc. Perkin Trans. **2** 97 (1976).

[12] G.W. Gray, K.J. Harrison, J.A. Nash, J. Constant, D.S. Hulme, J. Kirton, and E.P. Raynes, in *Liq. Cryst. Ordered Fluids* (1974), pp. 617–643.

[13] M. Glaser, in *Adv. Comput. Simulatons Liq. Cryst.*, edited by P. Pasini and C. Zannoni (Springer Netherlands, 2000), pp. 263–331.

[14] T. Matsushita and S. Koseki, J. Phys. Chem. B **109**, 13493 (2005).

[15] L.T.S. Siedler, A.J. Hyde, R.A. Pethrick, and F.M. Leslie, Mol. Cryst. Liq. Cryst. **90**, 255 (2011).

[16] P. Zeng-Hui, X. Li, Z. Ran, and H. Jun, Acta Phys. Sin. **58**, 5560 (2009).

[17] D. Demus, J. Goodby, G.W. Gray, H.-W. Spiess, and V. Vill, editors , *Handbook of Liquid Crystals Set* (Wiley-VCH Verlag GmbH, Weinheim, Germany, 1998).

[18] P.J. Collings and M. Hird, *Introduction to Liquid Crystals: Chemistry and Physics* (1997).

[19] S. Chandrasekhar, *Liquid Crystals* (Cambridge University Press, Cambridge, 1992).

[20] S.J. Picken, W.H. de Jeu, S.J. Picken, W.F. van Gunsteren, P.T. van Duijnen, and W.H. de Jeu, Liq. Cryst. **33**, 1359 (2006).

[21] A. Sanchez-Castillo, M.A. Osipov, and F. Giesselmann, Phys. Rev. E - Stat. Nonlinear, Soft Matter Phys. **81**, 1 (2010).

[22] G. Tiberio, L. Muccioli, R. Berardi, and C. Zannoni, ChemPhysChem **10**, 125 (2009).

[23] D. Demus and L. Richter, Textures of Liquid Crystals, 1st ed. (Wiley-VCH Verlag, 1980).

[24] V.K. Gupta and N.L. Abbott, Phys. Rev. E. Stat. Phys. Plasmas. Fluids. Relat. Interdiscip. Topics **54**, 4540 (1996).

[25] B. Jerome, Reports Prog. Phys. **54**, 391 (1991).

[26] O.D. Lavrentovich, Liq. Cryst. **24**, 117 (1998).

[27] N. a. Lockwood, J.K. Gupta, and N.L. Abbott, Surf. Sci. Rep. **63**, 255 (2008).

[28] A.D. Price and D.K. Schwartz, J. Am. Chem. Soc. **130**, 8188 (2008).

[29] D. Chen, J.H. Porada, J.B. Hooper, A. Klittnick, Y. Shen, M.R. Tuchband, E. Korblova, D. Bedrov, D.M. Walba, M.A. Glaser, J.E. Maclennan, and N.A. Clark, Proc. Natl. Acad. Sci. **110**, 15931 (2013).

[30] R.B. Meyer, in *Mol. Fluids*, edited by B. R and W. G (Gordon and Breach, New York, 1976), pp. 271–343.

[31] I. Dozov, Europhys. Lett. **56**, 247 (2001).

[32] C. Meyer, G.R. Luckhurst, and I. Dozov, Phys. Rev. Lett. **111**, 067801 (2013).

[33] C. Meyer, G.R. Luckhurst, and I. Dozov, J. Mater. Chem. C **3**, 318 (2015).

[34] P.A. Henderson, O. Niemeyer, and C.T. Imrie, Liq. Cryst. **28**, 463 (2001).

[35] J.W. Emsley, G.R. Luckhurst, G.N. Shilstone, and I. Sage, Mol. Cryst. Liq. Cryst. **102**, 223 (1984).

[36] J. Zhang, J. Su, and H. Guo, J. Phys. Chem. B **115**, 2214 (2011).

[37] J. Zhang, J. Su, Y. Ma, and H. Guo, J. Phys. Chem. B **116**, 2075 (2012).

[38] Z. Zhang and H. Guo, Soft Matter **8**, 5168 (2012).

[39] I. Cacelli, G. Prampolini, and A. Tani, J. Phys. Chem. B **109**, 3531 (2005).

[40] M. Bizzarri, I. Cacelli, G. Prampolini, and a Tani, J. Phys. Chem. **108**, 10336 (2004).

[41] I. Cacelli, L. De Gaetani, G. Prampolini, and A. Tani, J. Phys. Chem. B **111**, 2130 (2007).

[42] C. Amovilli, I. Cacelli, G. Cinacchi, L. De Gaetani, G. Prampolini, and A. Tani, Theor. Chem. Acc. **117**, 885 (2007).

[43] D. Sandström, A. V. Komolkin, and A. Maliniak, J. Chem. Phys. **106**, 7438 (1997).

[44] Z. Wang, J.A. Lupo, S. Patnaik, and R. Pachter, Comput. Theor. Polym. Sci. **11**, 375 (2001).

[45] A. V. Komolkin, A. Laaksonen, and A. Maliniak, J. Chem. Phys. **101**, 4103 (1994).

[46] M. P. Allen, Comput. Soft Matter **23**, 289 (2004).

[47] O. Borodin, J. Phys. Chem. B **113**, 11463 (2009).

[48] J.B. Hooper, O.N. Starovoytov, O. Borodin, D. Bedrov, and G.D. Smith, J. Chem. Phys. **136**, 194506 (2012).

[49] D. Bedrov and O. Borodin, J. Phys. Chem. B **114**, 12802 (2010).

[50] O. Borodin and D. Bedrov, J. Phys. Chem. C 140723165951001 (2014).

[51] D. Bedrov, O. Borodin, Z. Li, and G.D. Smith, J. Phys. Chem. B **114**, 4984 (2010).

[52] D. Bedrov, O. Borodin, G.D. Smith, T.D. Sewell, D.M. Dattelbaum, and L.L. Stevens, J. Chem. Phys. **131**, 224703 (2009).

[53] J.B. Hooper, G.D. Smith, and D. Bedrov, J. Chem. Phys. **139**, 104503 (2013).

CHAPTER 2

INFLUENCE OF ELECTROSTATIC INTERACTIONS ON THE PROPERTIES OF CYANOBIPHENYL LIQUID CRYSTALS PREDICTED FROM ATOMISTIC MOLECULAR DYNAMICS SIMULATIONS

2.1 Introduction

Ever since the first synthesis by Gray et al.[1] in 1973, a significant amount of research effort has been dedicated to the study of 4-Cyano-4'-pentylbiphenyl (5CB) and its homologues (nCB) that demonstrate classical liquid crystal (LC) behavior. Aside from the most famous application in LC displays, these materials have been considered for a variety of other technologies including nonlinear optical devices, molecular photonic materials, sensors, and many others.[2-7] One of the key characteristics of these materials is the high sensitivity of their macroscopic properties to the thermodynamic conditions and the molecular structure of the mesogens.[8] A small variation in the number of ethylene groups in the alkyl tail can noticeably influence the formation and stability of the nematic and smectic phases, both of which are crucial for the above mentioned applications. For bulk 5CB, the experimentally observed nematic to isotropic (NI) phase transition temperature (T_{NI}) is between 306.7-308 K.[9,10] However, the understanding of molecular parameters that determine the phase transition phenomena in 5CB and other nCB LCs is still incomplete,

particularly with respect to understanding the effects born of the details of electrostatic interactions between the mesogens. Due to the strong polar nature of 5CB, the dipole-dipole contribution to the total intermolecular energies is not only important in determining optical anisotropy under applied electric fields, but also considered one of the key interactions affecting the accuracy of predictions from molecular.[11] Moreover, the synthesis of better performing LC materials requires the knowledge on how the subtle changes at the molecular level affect the macroscopic behavior. For example, as we will demonstrate later on, small changes in the biphenyl dihedral potential or the atomic partial charges can lead to noticeable changes in the properties of 5CB bulk systems. Therefore, it is of great interest to obtain a better understanding of such correlations.

One of the unique advantages of investigating systems via molecular dynamics (MD) simulations is the ability to separate the contributions from various interactions and to determine the influence of the details of interaction potentials on micro and macroscopic properties of materials. Thanks to the constantly increasing performance and efficiency of computers, MD simulations of LC materials have become a great tool to investigate the link between molecular level details and the macroscopic properties, including the phase behavior. Different levels of modeling have been used for these investigations, ranging from a single-site Gay-Berne model,[12–15] many-site coarse-grained models,[16–20] and united-atom models,[21–23] all the way to fully atomistic models,[24–27] as well as hybrid models.[27–33] Clearly, the reliability of any MD simulation strongly depends on the accuracy of the force field employed. Indeed, in the past two decades many attempts have been made towards developing and optimizing force fields for 5CB and related systems. For example, Cacelli et al.[31] investigated the thermodynamic and structural properties of bulk 5CB using a

hybrid model with a force field obtained from *ab initio* fragmentation reconstruction method. Simulations using this force field predicted T_{NI}, order parameter, molecular conformations, and phase transition related enthalpy changes that were in a good agreement with experimental data. However, the predicted density was overestimated by about 6%. In order to further improve the quality of their model, Cacelli et al. proposed to adopt an all-atom model and extend the partial atomic charge distribution to the alkyl tail to have a better description of electrostatic interactions. Komolkin et al.[34] carried out simulations using both all-atom and united-atom models of 5CB at 300 K. Although the observation times in these simulations were limited to 300 ps, they found that for the all-atom model the dihedral angle distribution between two phenyl rings peaked at 25°, which was considered to be in a good agreement with the NMR measured[35] angle of 32°. However, their united-atom model predicted a planar dihedral angle between two rings. Wang et al.[25] found that using semiempirically fitted partial atomic charges in the CHARMM force field in their all-atom simulations could not accurately reproduce T_{NI} as the system remained in the nematic phase even at 400 K. Refitting the partial atomic charges to *ab initio* calculations resulted in a force field that did not provide good predictions of the order parameter when compared to experimental data. The authors suggested that the short run time of 300 ps might not be sufficient to observe the expected phase transition. Tiberio et al.[36] showed that, by carefully tuning the available in the literature parameters of the Lennard-Jones potentials, an accurate T_{NI} can be predicted for bulk 5CB. They also reported that if the standard AMBER[37] force field was directly employed without optimization, a 120 K overestimation of T_{NI} was observed, and thus showed a poor transferability of the generic force field to 5CB. Recently, Zhang et al.[21] conducted MD

simulations of the 5CB systems using the TraPPE-UA[38] force field with carefully-tuned parameters of the Lennard-Jones potentials. The resulting order parameter, density, dipole moment, molecular conformations, and diffusion anisotropy ratio were all found in excellent agreement with experiments. However, owing to the intrinsic faster dynamics from UA models, their diffusion coefficients were two times larger than the experimental data.

In this work, we adapt the Atomistic Polarizable Potential for Liquids, Electrolytes, and Polymers (APPLE&P) force field[39] for simulations of 5CB. APPLE&P has proven capable of reproducing accurate results for density, self-diffusion coefficients, conductivity, and viscosities for numerous materials including ionic liquids,[40] electrolytes,[41–43] and polymers.[44] The force field parameters specific for 5CB (i.e., those that could not be transferred from the APPLE&P database) were parameterized against high-level *ab initio* calculations. Using the fitted potentials, we have studied the influence of many-body polarization interactions and the magnitude of 5CB dipole on the ability of MD simulations to predict bulk properties of 5CB, including T_{NI}, density, and dynamics. To the best of our knowledge, the effect of induced and permanent dipole moments on the phase behavior of 5CB has not been investigated. And yet, one can expect that for such a polar compound like 5CB, the interplay of these electrostatic interactions can be crucial in defining structural, thermodynamic, and dynamic properties of bulk phases.[28] In order to obtain a more comprehensive understanding of the influence of polarizability, for each temperature investigated, we carried out simulations both with polarizable (POL) and nonpolarizable (NP) versions of the force field. The latter was obtained by setting the atomic polarizability parameters to zero for all atoms while the parameters for all other interactions (valence and

nonbonded) were kept the same. In addition, we also investigate the influence of the magnitude of 5CB dipole moment and the flexibility of biphenyl dihedral on the phase behavior as well as structural and dynamic properties of 5CB bulk.

2.2 Methodology

2.2.1 Force Field Development

The parameterization of the 5CB force field was accomplished following the general approach employed previously for a wide variety of systems.[40,45–47] This approach, utilizing the APPLE&P transferrable polarizable force field, has been shown to successfully model both thermodynamic and dynamic properties for a wide variety of systems, including polymers,[44] molecular crystals,[48] and ionic liquids.[40,45,49] While we refer to the APPLE&P force field as transferrable, it is not generic in nature. In general, the repulsion/dispersion (R/D) terms and associated polarizabilities exist for many atom types in their most frequent chemical groupings (e.g., neutral/anionic/cationic nitrogen, aliphatic/aromatic carbon), which may be used as a basis for expansion of the force field to additional molecules/groups. However, even if all atoms for specific chemical functionality are present, additional work is generally necessary in the form of fitting partial atomic charges, bond lengths, bend angles and constants, dihedral constants, and improper dihedral (out-of-plane) constants, in order to obtain a force field which faithfully reproduces the interactions of a desired molecule.

The initial 5CB force field was constructed by using as-transferred R/D and polarizability parameters from the APPLE&P force field. Partial atomic charges were calculated for the mesogenic portion of the molecule by fitting each atom's partial charge

to accurately reproduce *ab initio* calculations of the electrostatic potential on a grid around a single 5CB molecule in a minimum energy configuration, as calculated via the Gaussian09[50] package at the M052X//cc-pvTz level. In this fit we have constrained the same charge for atoms that are chemically indistinguishable within the molecule. Fitting charges in this manner yielded a dipole moment of 6.00 D, compared to the 6.17 D predicted by the *ab initio* calculation. Transferrable polarizabilities were sufficient to reproduce the out of plane (transverse to the aromatic ring) polarizability of the molecule well, but due to the isotropic nature of our polarizability implementation, coupled with the lack of polarization between charges and atoms separated by one or two bonds, it is impossible for our model to simultaneously reproduce the polarizability both transverse to and directed along the long-axis of the biphenyl unit of the nematogen. Taking into account that the stacking of aromatic rings is an important type of interaction in the liquid crystalline phase, we chose to prioritize the reproduction of polarizability values perpendicular to the nematogen and to give less weighting to the fitting of polarizability values along the biphenyl unit. This led to force field values of 34.3 $Å^3$, 25.5 $Å^3$, and 23.9 $Å^3$, compared to 51.8 $Å^3$, 25.5 $Å^3$, and 20.5 $Å^3$ from *ab initio* calculations for molecular polarization directions along, transverse, and perpendicular to the long-axis of the biphenyl unit of 5CB, respectively. The only remaining quantity to be fit for the 5CB molecule was the dihedral potential curve representing the biphenyl torsional rotation across the center of the mesogen. Since passage of the dihedral through the planar state (0°/180° dihedral angle) can be expected to play a role in dynamic properties of individual molecules as well as structural relaxation of the whole system, using *ab initio* calculations we have investigated the energy profile at a variety of different levels of theory, as shown in Figure

2.1b. The general trend tends to indicate that the height of the transition barrier increases as the level of theory increases, e.g., upon transitioning from density functional (M052X) to correlated electron *ab initio* (MP2) method, or increasing the size of the basis set from M052X//cc-pvDz to M052X//cc-pvTz. In general, our force field can be seen to fit well the dihedral energy data at the MP2//cc-pvDz level of theory.

In this study, we have investigated two versions of the developed force fields, POL and NP. For both types of the force fields the valence parameters were the same, the differences were only in the treatment of nonbonded interactions. For the POL force field, the general expression for nonbonded interactions $U^{NB}(r)$ is defined as the following,

$$U^{NB}(r) = \sum_{i>j}\left(A_{\alpha\beta} exp\left(-B_{\alpha\beta} r_{ij}\right) - C_{\alpha\beta} r_{ij}^{-6} + D\left(\frac{12}{B_{\alpha\beta} r_{ij}}\right)^{12}\right) + \sum_{i>j}\left(\frac{q_i q_j}{4\pi\varepsilon_0 r_{ij}}\right) - \frac{1}{2}\sum_i \vec{\mu}_i \vec{E}_i^0 \quad (2.1)$$

where $\vec{\mu}_i = \alpha_i \vec{E}_i^{tot}$ is an induced dipole at force center *i,* α_i is the isotropic atomic polarizability, $\vec{E}_i^{tot}$ is the total electrostatic field at the atomic site *i* due to permanent charges q_i and induced dipole $\vec{\mu}_j$, ε_0 is the permittivity of free space, $\vec{E}_i^0$ is the electric field due to fixed charges only, $A_{\alpha\beta}$ and $B_{\alpha\beta}$ serve to specify the repulsive core of the potential, and $C_{\alpha\beta}$is the dispersion parameter for interaction between atoms *i* and *j* with atom types α and β. The term $D\left(12/B_{\alpha\beta} r_{ij}\right)^{12}$, with $D = 5 \times 10^{-5}$ kcal/mol for all pair interactions, is essentially zero at typical nonbonded atomic separations, but becomes the dominant term at r_{ij}<1Å, ensuring that the repulsive interaction at close approaches remains monotonic in nature. Nonbonded interactions are included for atoms separated by three or more covalent bonds. The Thole screening[51] is imposed upon the induced dipoles to mitigate the onset of

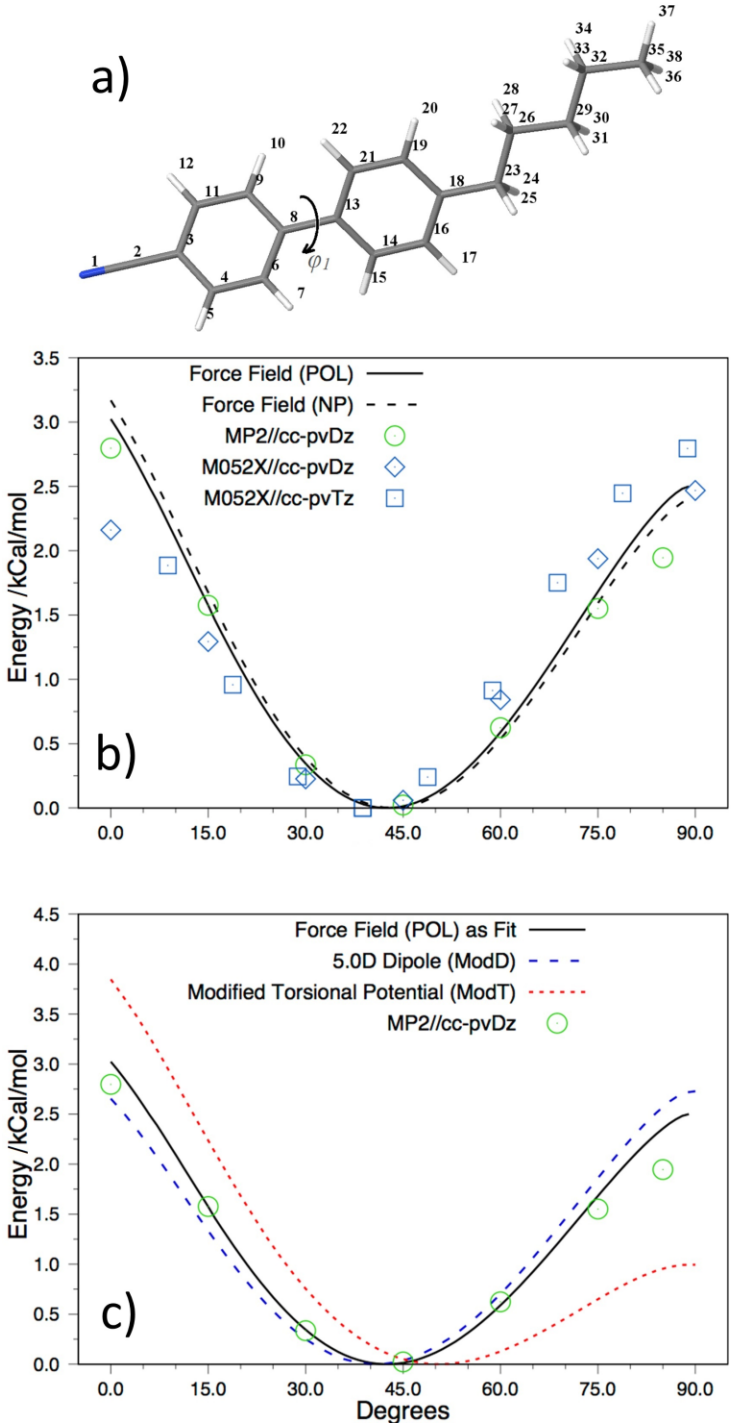

Figure 2.1. All-atom model of 5CB molecule (a). Dihedral angle φ1 is designated to depict the inter-ring conformations. (b) Dihedral potential energy profile of the biphenyl group in 5CB as obtained from different levels of theory and original force field fit. (c) Comparison of the dihedral potential energy profiles obtained from original, *modT* and *modD* force field as well as the *ab initio* calculation.

the “polarization catastrophe” for closely interacting atoms, with a screening constant of $\alpha_T = 0.2$. Additionally, the interaction between an induced dipole and a partial charge separated by three bonds is reduced by 80%.

To obtain a NP version of the force field the partial atomic charges were kept the same as in the POL force field, while atomic polarizabilities were set to zero, thus allowing no induced dipoles to be generated on the atoms, forcing electrostatic interactions comprised only of interactions between fixed partial atomic charges. It is important to note that the purpose of carrying out simulations using NP models is gaining better understanding of the influence of polarization interactions on the thermodynamic and structural properties of 5CB and, therefore, no additional adjustments to NP force field were made. We found that turning the induced polarization off did not affect the quality of the electrostatic potential description obtained from *ab initio* calculations nor the quality of dihedral potential as illustrated in Figure 2.1b.

2.2.2 Simulation Protocol

The MD simulations using developed force fields were carried out in cubic simulation cells with ~53 Å in length and subject to periodic boundary conditions. The systems were comprised of 384 5CB molecules (i.e., 14592 atoms). The system size was carefully chosen considering the balance between the potential influence of the finite size effect and the computational resources. All simulations were conducted using our in-house molecular simulation software, which is able to handle induced polarization interactions. The Ewald summation method[52] was used for electrostatic interactions between partial atomic charges and between partial charges and induced dipoles, while the velocity-Verlet form of the

SHAKE algorithm[53] was employed to constrain bond lengths. Interactions between induced dipoles were gradually reduced to zero using a cubic damping function, with damping occurring over a 1 Å distance, starting at 9 Å. All van der Waals interactions and the real part of the electrostatic interactions in the Ewald summation were cutoff at 10 Å. For the polarizable systems, induced dipole/induced dipole interactions were calculated with an iterative approach. A multiple timestep integration method[54] was employed with three different time scales: a short timestep of 0.5 fs for intramolecular interactions (bonding, bending, dihedral, and out-of-plane deformation motions), a medium timestep of 1.5 fs for torsions and short-range (7.0 Å) nonbonded interactions, and a large timestep of 3 fs for the full-range nonbonded interactions and the reciprocal part of electrostatic interactions. The thermostat and barostat used for temperature and pressure control in the NPT ensemble had frequencies of 0.01 and 0.005 fs^{-1}, respectively.

Two initial configurations of 5CB bulk were prepared. One was set up in the nematic phase which was equilibrated at 292 K and had an initial orientational order parameter around 0.7 (see discussion below). Another system was set up in an isotropic phase and equilibrated at 368 K, with an initial order parameter of about 0.1. Simulations of additional temperatures in the range 292-368 K were conducted starting from these two configurations. Systems started from the first configuration we label as "fromNem" while from the second as "fromIso." For all investigated temperatures, simulations were conducted starting using "fromNem" configuration and equilibrated in the NPT ensemble. For temperature near the NI transition we also conducted simulations using the "fromIso" initial configurations to ensure the stability of the predicted equilibrium phase. At these close-to-transition temperatures, ideally one would expect to obtain the same phase

(nematic or isotropic) independent of the initial configuration from which the simulation was initiated. Production runs varied between 10 ns to 700 ns depending on the temperature. At each temperature the trajectory length was long enough for 5CB molecules to reach the diffusive regime, i.e., to have displacements noticeably larger than molecule dimensions.

2.3 Results and Discussion

2.3.1 Order Parameter and Density

We begin our analysis of 5CB bulk properties predicted from simulations by examining the nematic order parameter which allows us to identify what state (nematic or isotropic) is more stable at a given temperature, and hence, to determine the temperature of the NI phase transition. The ability of simulations to reproduce this transition is one of the key criteria of the quality of employed force field. The nematic order parameter (S_2) is defined as the maximum eigenvalue of the average ordering tensor ($Q_{\alpha\beta}$):

$$Q_{\alpha\beta} = \frac{1}{N}\sum_{i=1}^{N}\left(\frac{3}{2}\mu_\alpha^i\mu_\beta^i - \frac{1}{2}\delta_{\alpha\beta}\right) \quad (2.2)$$

where μ_α^i $(\alpha, \beta = x, y, z)$ are the Cartesian components of the molecular axis unit vector of molecule *i*. For 5CB we took the long axis of the biphenyl core as the axis of the molecule. The value of S_2 is 1.0 in a perfectly aligned system where all molecules are aligned along the system director **n** and is 0.0 in the completely isotropic system. However, due to the finite system size in MD simulations, the value of S_2 cannot reach zero exactly, instead it is usually saturates at a small value. For system sizes simulated here, the isotropic phase has S_2 about 0.1-0.2. The corresponding maximum eigenvector represents the system director **n**. Experimentally the order parameter can be extracted using

diamagnetism, birefringence, polarized Raman scattering, x-ray diffraction, NMR, and EPR[55,56] techniques and a value of around 0.5-0.55 is typically reported for the nematic phase.

2.3.1.1 Order Parameter Evolution

First we examine the evolution of S_2 during simulation. Figure 2.2a shows the evolution of instantaneous values of S_2 for the systems simulated using the as-fit POL force field at different temperatures and starting from nematic initial configuration (fromNem) with an initial order parameter of S_2=0.73. As can be seen from this figure, systems at low temperatures (e.g., <303 K) have very small fluctuations of S_2 that stay in the vicinity of the initial value for the entire trajectory. As the temperature increases, the fluctuations in S_2 also increase, however the magnitude still remains in the nematic range of $S_2 > 0.5$. At higher temperatures (e.g., 340 K and 360 K) S_2 drops to low values (below 0.3) indicating a clear transition to an isotropic phase.

Observation of the phase transitions in brute force MD simulations is a challenging problem, as it requires nucleation of another phase on the time and length scales accessible to simulation. Typically, the brute force MD simulations of first order phase transitions as a function of temperature (e.g., liquid-vapor equilibrium) result in significant hysteresis of predicted phase diagrams as the nucleation processes require significant overheating (or overcooling) of simulated systems to ensure large enough fluctuations capable to overcome a relatively large enthalpy change (λH) between two phases. Luckily, for NI transition in bulk LC the corresponding λH term is relatively small and hence, appropriate fluctuations and new phase nuclei can be obtained on time scales that are accessible to MD simulations.

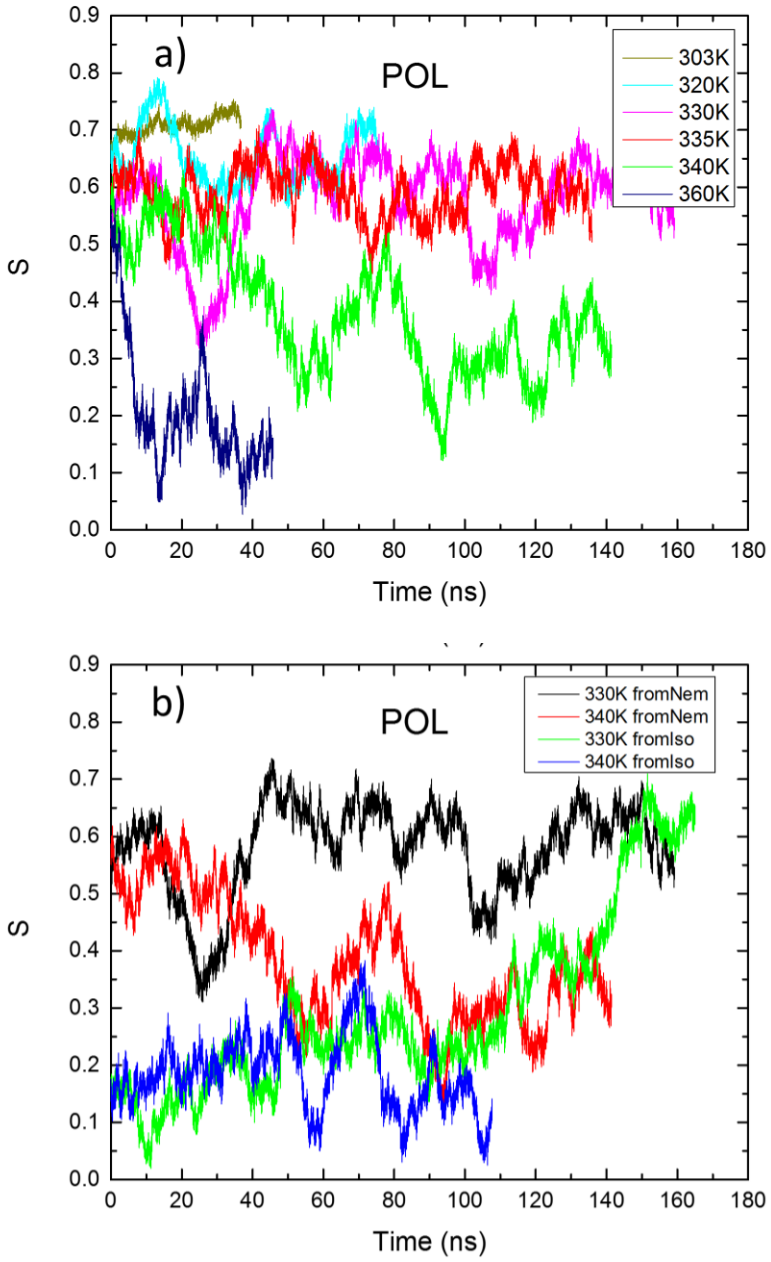

Figure 2.2. Time evolution of the order parameter (S_2) at different temperatures: (a) obtained from MD simulations using POL force field and temperature range 303 K and 360 K starting from nematic phase, (b) obtained from simulations using POL force field at 330 K and 340 K starting from configurations in nematic and isotropic phases, and (c) obtained from simulations using NP force field at 330 K starting from nematic and isotropic phases.

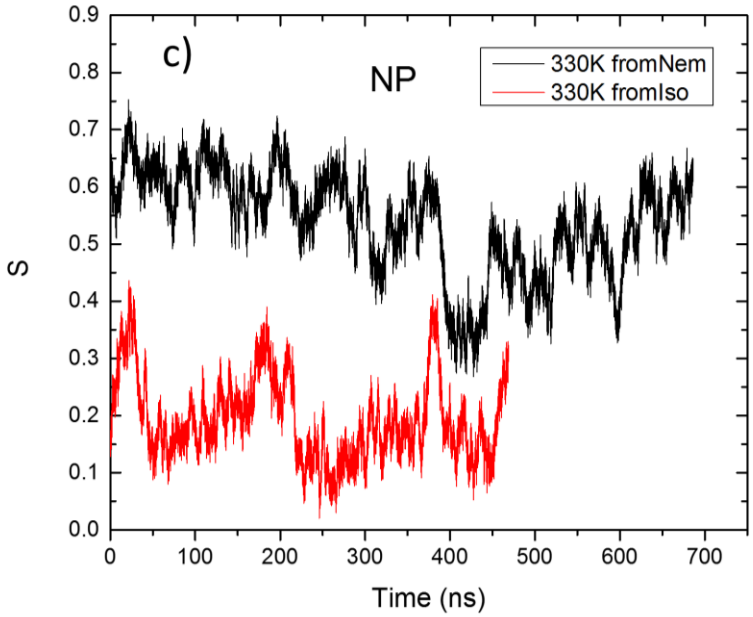

Figure 2.2 Continued.

For example, in Figure 2.2a, we can see that at 360 K the transition from nematic to isotropic phase occurred on a time scale of less than 10 ns. Yet, at 340 K the transition was more gradual and required more than 100 ns to occur. To ensure the stability of the nematic or isotropic phases at temperatures near T_{NI}, we have conducted simulations using both the nematic (fromNem) and isotropic (fromIso) initial configurations. Figure 2.2b shows evolution of S_2 for the POL force field systems starting with each configuration at 330 K and 340 K. While at 330 K both systems eventually converged to a nematic state, at 340 K both simulations predict an isotropic phase. In such a case, we can definitively pin down the transition point in the 330 K < T_{NI} < 340 K range. However, in some systems this approach resulted in inconclusive determination of the equilibrium phase. For example, in Figure 2.2c, we show evolution of S_2 for the as-fit NP force field systems at 330 K with nematic and isotropic initial configurations. Even after 500 ns of simulations both systems remained in the original phases, although both of them visited states with S_2~0.4. Additionally, in Figure 2.3, we present the instantaneous order parameter evolutions for all the simulated systems at different temperatures using both POL and NP version of the as-fit force field. Compare to POL (Figure 2.3a), the system using NP force field at 340 K became completely isotropic after about 60 ns (Figure 2.3b). And the NP system at 335 K showed a faster rate of decay of ordering, achieved similar S_2 value as the NP 330 K system after about 150 ns, but after that S_2 began to fluctuating between 0.3 and 0.6, which indicates that this system is right near the critical point between nematic and isotropic phase. Overall, we estimate T_{NI} from NP force field to be between 330 K and 335 K, which is still rather unsatisfactory compared to the experimental value.

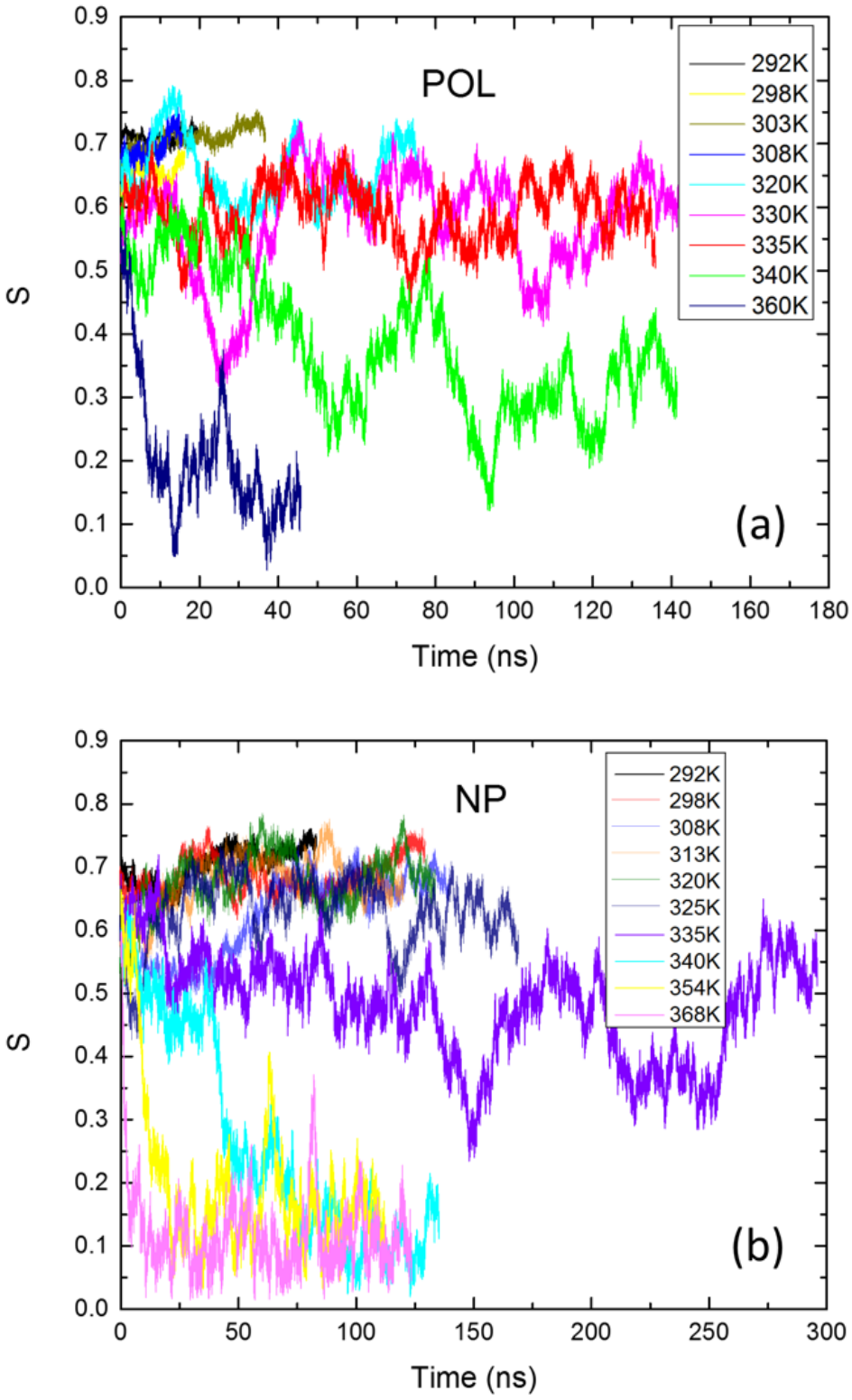

Figure 2.3. Instantaneous order parameter obtained from simulations using (a) POL version of the as-fit force field and (b) using the NP force field at all temperatures investigated.

2.3.1.2 Average Density and Order Parameters

The evolutions of the order parameter clearly indicate that identification of T_{NI} in 5CB bulk system is a challenging task. However, some observations and conclusions can be made regarding the predicted phase behavior by different force field models. To do that we calculated the average density and the order parameter at each temperature as well as the corresponding phase. To identify a phase we used the following criteria: $S_2 > 0.4$ is nematic, $S_2 < 0.4$ is isotropic which is similar to the phase assignments used in the literature.[55,57,58] Furthermore, considering the fluctuations displayed by the systems at temperatures close to T_{NI}, we only use portions of trajectories where S_2 have shown stable fluctuations in one of the phases, e.g., for the POL force field 340 K system shown in Figure 2.2a, we used the data after 90 ns where the system has shown stable fluctuations in the isotropic phase. Figure 2.4b shows the average order parameter $\langle S_2 \rangle$ obtained at each temperature using the POL and NP force fields, while Figure 2.4a reports average densities obtained from simulations and available experiments.[59] From the temperature dependence of $\langle S_2 \rangle$ in Figure 2.4b we can identify the NI phase transition temperature range of 330-340 K for both force fields. For both models, the predicted densities are in excellent agreement with experiment, where at all temperatures the deviation is less than 2%. However, the additional attraction forces from induced dipoles in POL force field model resulted in a systematic overestimation of density by ~2% compared to experimental data. For the NP force field, the predicted densities are within less than 1% from experimental values, with the nematic phase deviation less than 0.5% and only slight underestimation (still less than 1%) at higher temperatures. This agreement for the density is very encouraging, taking into account that many previous simulation works struggled to

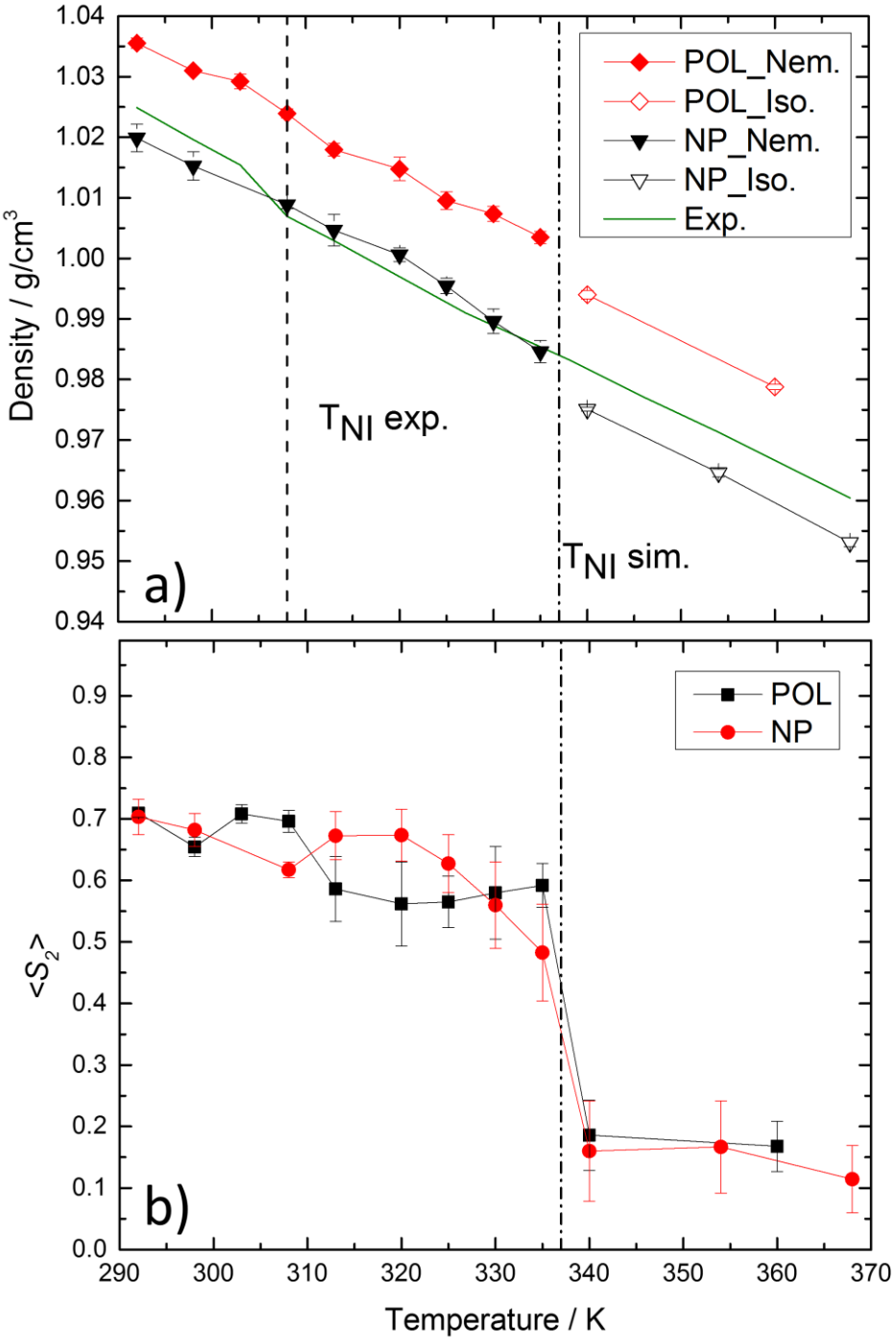

Figure 2.4. Average densities (a) and average order parameter (b) of 5CB liquid as a function of temperature as obtained from simulations using POL, NP force fields and experiments. The dotted vertical lines indicate estimated T_{NI}.

capture the density of 5CB bulk systems.[21,31,60,61]

The comparison of POL and NP force fields indicates that while the predicted densities differ by about 2% (with the POL model being more dense) there is almost no difference in predicted T_{NI} (at least within the accuracy of determining T_{NI} in our simulations). Note that for a given force field (model) the influence of density on the T_{NI} is usually quite noticeable. If for example, we would modify the NP force field to yield the same density as the POL force field (e.g., by rescaling slightly the parameters of dispersion interactions) the T_{NI} in such system would shift to noticeably higher temperatures. Therefore, while the magnitude of the induced dipole is relatively small compare to the magnitude of the permanent dipole of the 5CB molecule (0.83 D for the average induced dipole vs 6.0 D average total dipole of 5CB molecule in the bulk) the presence of the induced polarization interactions in the POL force field is significant enough to offset the increased density (compared to NP force field model) such that both models predict the same transition temperature. Nevertheless, both force fields predict T_{NI} near 340 K which is a significant overestimation compared to experimental values of 306-308 K.[9,10]

2.3.2 Force Field Refinement

Based on the results presented above it was clear that the original version of the force field needed a refinement to better reproduce T_{NI} regardless of whether POL or NP model is used. Here we briefly explain the philosophy for two force field modification strategies: a) adjustment of a torsional potential for biphenyl unit which we refer to as *modT* force field, and b) rescaling of the permanent dipole moment which is referred as *modD* force field.

2.3.2.1 *ModT* Force Field

It is known that due to the interplay of competing energetic and entropic interactions in LC systems, a subtle change in the internal molecular geometry can generate strong impact on the phase behavior of these materials, and often can control the formation and stability of their mesophases. One way to study this effect is to perturb a particular molecular interaction parameter and study the outcomes.[8] In particular for 5CB and its homologues, the molecule conformation can be changed rather easily due to the relatively low inter-ring torsional energy barrier, and as a consequence, have a larger influence on the behavior of its mesophase.[62] Therefore, one can naturally expect that thermodynamic properties of bulk 5CB can be affected through modification of torsional energy parameters. As mentioned earlier, one of force field parameters specifically fit for the 5CB was the dihedral angle φ_1 between the two rings in the biphenyl group. In the *modT* force field we slightly perturbed this dihedral potential and obtained a new torsional potential energy profile as shown in Figure 2.1c. With everything else being the same, the employment of the new force constant caused the aforementioned dihedral angle distribution curve to shifted about 7°, now having a minimum at 45°, instead of 38°. Rather surprisingly, such small change actually brought significant change in the thermodynamic properties of 5CB, which as we discuss below.

Indeed, the changes in biphenyl dihedral potential parameters (*modT* force field) have noticeably decreased the T_{NI}, from 330-340 K, predicted by the original force field, down to 308-320 K range. Specifically, for the *modT*_POL systems shown in Figure 2.5a, we see that the 308 K system displayed very stable nematic phase for over 200 ns and showed no signs of NI phase change. However, the 313 K system from nematic phase started to show

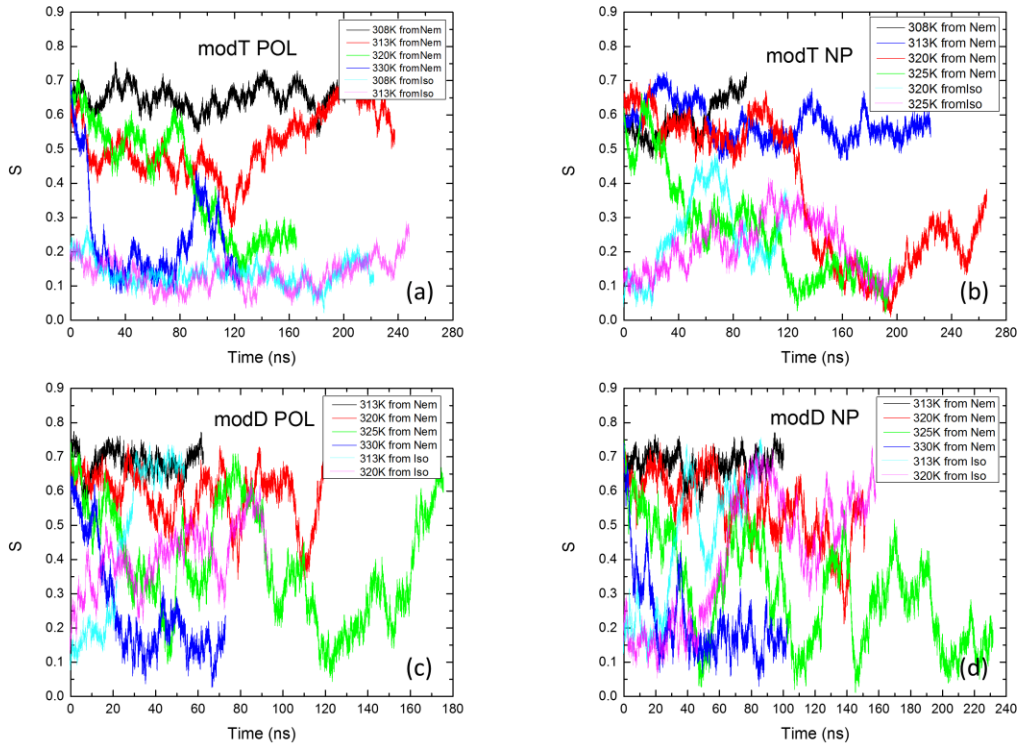

Figure 2.5. Order parameter evolution obtained from simulations using *modT*_POL (a), *modT*_NP (b) and *modD*_POL (c), *modD*_NP (d) force fields.

big fluctuations of orientational orders, indicating that this system is approaching T_{NI}. And in Figure 2.5b we note that unlike the NP version of original force field, the combination of reduced biphenyl torsional energy barrier and the lack of polarization effect in the *modT*_NP force field actually stabilized the nematic phase slightly. Such changes allows a very stable nematic phase to be present in the systems with temperature lower than the presumed T_{NI} of just below 320 K. It took around 125 ns for 320 K to transition to isotropic phase, compare to the 80 ns needed for the same temperature using *modT*_POL force field. Lastly, in order to test whether the equilibrium state has been reached, we have also examined selected systems with isotropic initial condition (mimic cooling). As illustrated in Figure 2.5a, for temperatures of 308 and 313 K, we are within the window of thermal hysteresis, where the coexistence of two different phases for same temperature are possible. And in Figure 2.5b the 320 K system with isotropic initial condition displayed thermal fluctuations mimic its counterpart, and the 325 K system from isotropic showed convergence of P2 with its counterpart. It is worth to point out that running systems with same temperature but from two different initial conditions not only can serves as a way to test for system equilibrium state but also can be considered as a continuation of runs provided that they show convergence of order parameter.

Figure 2.6 shows the averaged S_2 and densities as obtained from simulations using the *modT* force field. The modification of the torsional parameters of the biphenyl group not only significantly lowered the predicted T_{NI} (Figure 2.6b) but also led to lower densities as well. As shown in Figure 2.6a, for both POL and NP versions of the *modT* force field (*modT*_POL and *modT*_NP), the density predictions reduced by about 0.5% compared with the original POL and NP force fields. The density obtained from simulations using

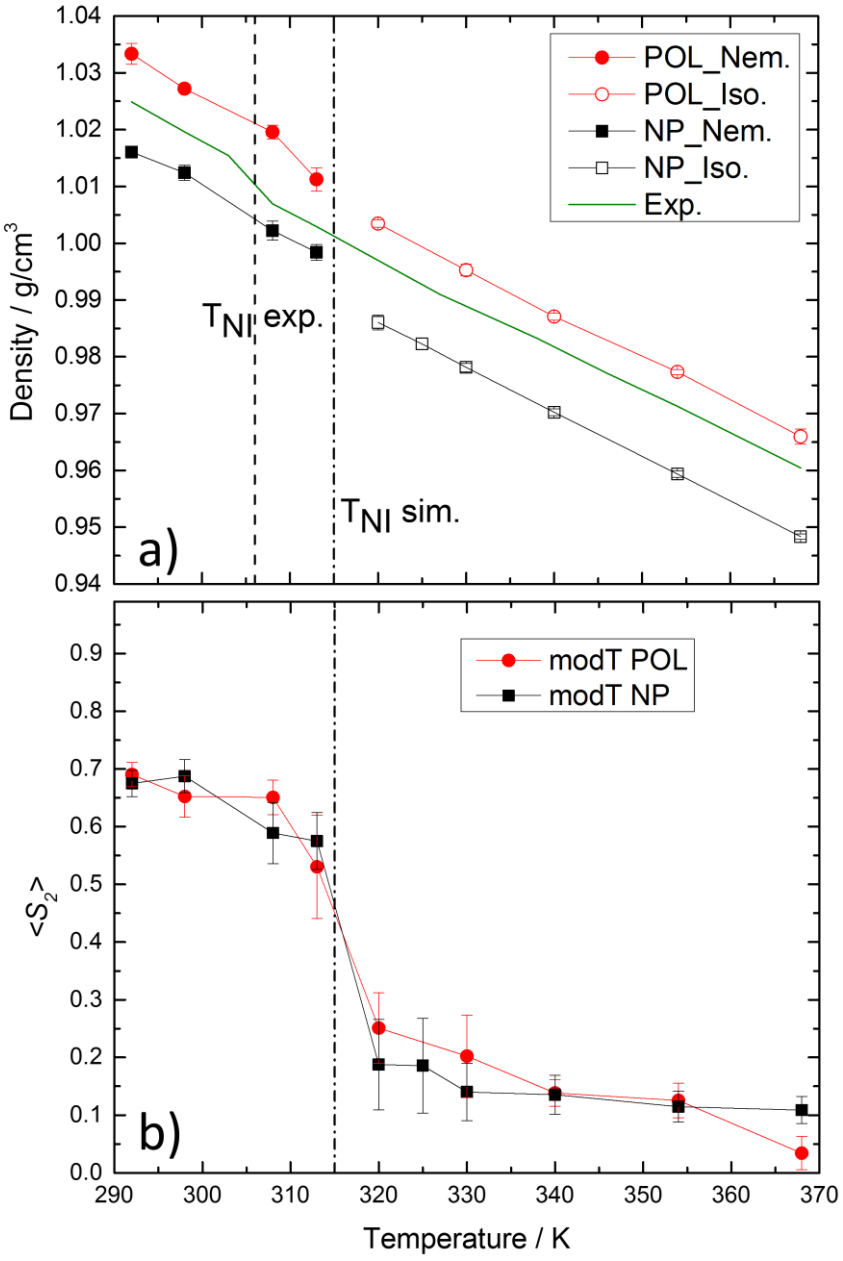

Figure 2.6. Average densities (a) and average order parameter (b) of 5CB liquid as a function of temperature as obtained from simulations using modT force fields and experiments. The dotted vertical lines indicate estimated T_{NI}.

*modT*_POL force field showed small (around 0.5%) overestimation compared to experimental data over the entire temperature range, while those obtained using the *modT*_NP force field showed slight underestimation, ranging from less than 0.5% in the nematic phase to approximately 1% in the isotropic phase. Overall, the reduction in density by the *modT* force fields can be attributed to the subtle increase in the optimal dihedral angle between the two phenyl rings in the 5CB molecule which leads to less planar orientations of CB units. This makes it harder to accommodate the intermolecular attraction from the π-π stacking and hence weakens the attractive interactions between 5CB molecules as well as gives rise to excluded volume interactions[63] between CB units.

2.3.2.2 ModD Force Field

For the second force field modification we focused on the adjustment of partial atomic charges. As previously mentioned in the force field development section, the initially fit partial charges yielded a dipole moment of 6.0 D, which represents almost a 30% overestimation when compared to the experimental estimates of 4.6-4.9 D,[64,65] although one has to keep in mind that the 5CB dipole moments in those experiments were determined based on the measurements of 5CB solutions with various solvents. Therefore, in the second modification we empirically lowered the atomic partial charges to achieve a total dipole moment of 5.0 D which is much closer to the experimental values. Figure 2.1a shows the atom numbering scheme of the 5CB molecule used in the simulation, and in Table 2.1, we report the corresponding partial atomic charges for the original fit (POL, NP, *modT*_POL, and *modT*_NP force fields) and the *modD* force fields. By lowering the molecular dipole moment we expect the system density and T_{NI} to decrease due to reduction

Table 2.1. Partial atomic charges of 5CB in original, *modT* and *modD* force fields. Atom numbering corresponds to Figure 2.1a.

Atom label	Original and *modT*	*modD*
N1	-0.4119	-0.309
C2	0.1604	0.1201
C3	0.1681	0.126
C4,11	-0.2309	-0.1732
H5,12,17,20	0.2057	0.1543
C6,9,14,21	-0.1237	-0.0927
H7,10,15,22	0.1614	0.1211
C8,13	0.0584	0.0437
C16,19	-0.5541	-0.4156
C18	0.5932	0.445
C23	-0.09	-0.0765
H24,25,27,28,30,31,33,34	0	0
C26	0.0598	0.0538
C29,32	0	0
C35	-0.15	-0.15
H36,37,38	0.05	0.05

of electrostatic interactions between molecules. Note that due to reduction of magnitude of the permanent dipole moment, the induced dipole moment per molecule in bulk 5CB also reduced to a value of ~0.64 D (compared to 0.83 D in the original POL force field).

Figure 2.5c and d provides plots of the order parameter evolutions for simulations using modD force fields. An interesting behavior for the 325 K system with *modD*_POL force field can be observed. In this system, the nematic order parameter shows fluctuations/transitions between highly ordered nematic phase and almost disordered isotropic phase. The observed multiple switches between two phases over a relatively short time scale of 230 ns indicates that this behavior is likely caused by close proximity of this temperature to the innate T_{NI}. And with respect to the *modD*_NP force field, once again the absence of induced dipole interactions made some interesting impact on the phase behavior

of 5CB. As can be seen in Figure 2.5d, the absence of polarization effect resulted a less violent phase behavior, and after 200 ns the system is able to stay in isotropic phase. Figure 2.5c also shows selected systems starting in isotropic phase using *modD*_POL force field, for 313 K system displayed a very fast and clean NI transition, and is able to maintain same level of P2 value compare with the 313 K system from nematic phase. However, for 320 K systems the same conclusion cannot be drawn as easily, as both systems are showing big fluctuations, with P2 overlapping serval times, a signage of system approaching T_{NI}. The validation of equilibrium state for systems with *modD*_NP are shown in Figure 2.5d, for T=313 K with isotropic initial condition, the system transitioned to nematic phase quickly, and the fluctuations between 40 and 70 ns can be ascribed to the lack of polarization effect as a stabilizing element. Regardless, this system did eventually reach similar P2 value as its counterpart, indicating that nematic phase is preferred for this temperature. Like many previous systems that are close to T_{NI}, both phases are actually thermodynamically stable, thus allowing the fluctuations between different phases without changing the free energy.

Figure 2.7 shows the average order parameter and densities obtained from simulations using *modD*_POL and *modD*_NP force fields. The T_{NI} has moved down to ~325 K which is about 15 K reduction compared to the original force fields. As expected, the lowered partial charges led to overall lower densities (Figure 2.7a) due to weaker columbic interactions between 5CB mesogens. The comparison of the *modD*_POL and *modD*_NP force fields indicates that induced polarization effects are responsible for increasing density by approximately 1%. Compared to experimental data, the *modD*_POL force field now slightly underestimates density (by approximately 1%), while the *modD*_NP force field model results in about 2% underestimation, indicating that further reduction of the

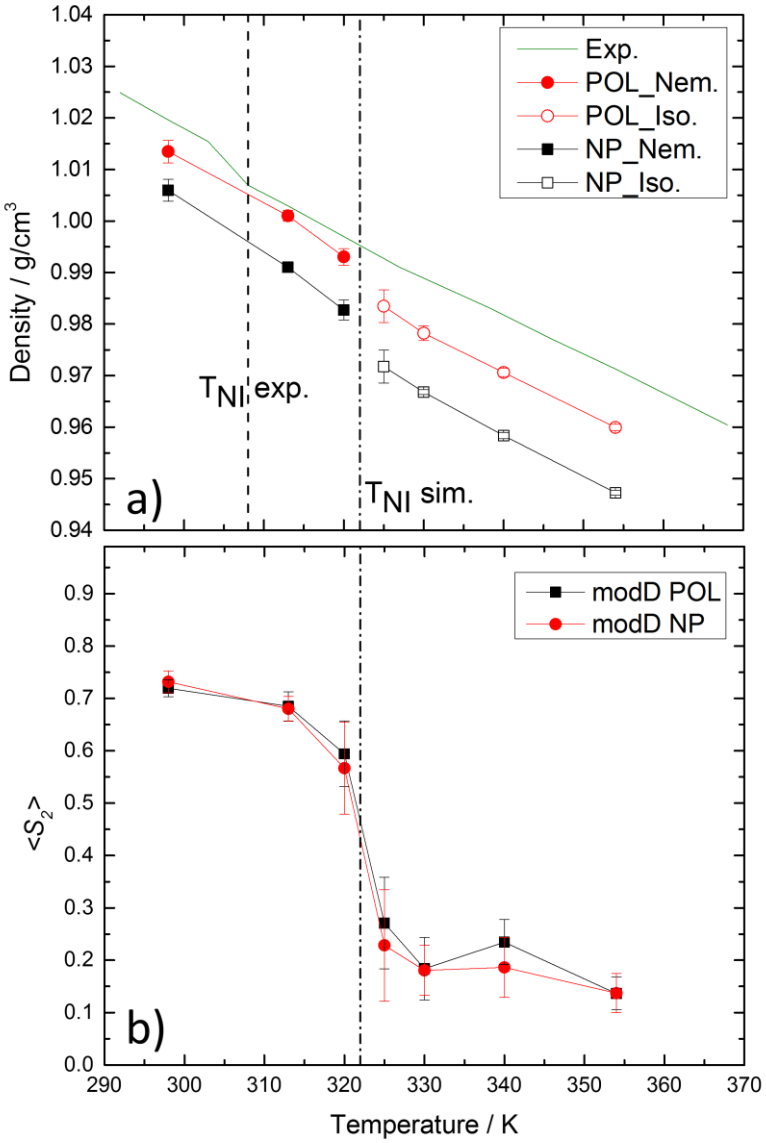

Figure 2.7. Average densities (a) and average order parameter (b) of 5CB liquid as a function of temperature as obtained from simulations using *modD* force fields and experiments. The dotted vertical lines indicate estimated T_{NI}.

permanent dipole moment (without changing other force field parameters) will likely lead to unsatisfactory description of densities, even if such reduction might simultaneously lower TNI towards experimental values.

2.3.3 Dynamic Properties

Lastly, we examined the influence of force fields on the prediction of dynamic properties of bulk 5CB, specifically the self-diffusion coefficient of 5CB molecules. It is well established that upon transition to nematic phase the self-diffusion coefficient becomes highly anisotropic.[66–68] The experimental study of Dvinskikh and Romanova showed that in the nematic phase the diffusion parallel ($D_{\parallel}$) to the nematic order director is about factor of two higher than the diffusion coefficient in the perpendicular ($D_{\perp}$) direction. To assess the accuracy of prediction of dynamical properties from simulations using the force fields discussed above we have calculated the values of $D_{\parallel}$ and $D_{\perp}$. In these calculations we first identified the nematic director vector and then decomposed each molecule displacement between two consecutive snapshots in the simulation trajectory into components parallel and perpendicular to the instantaneous director. Averaging those displacements over multiple time origins and all molecules allowed us to obtain $D_{\parallel}$ and $D_{\perp}$ that are reported in Figure 2.8 for all force field variations discussed above.

For the POL force field at 308 K, the calculated $D_{\parallel}$ and $D_{\perp}$ values are 2.93×10^{-11} and 1.05×10^{-11} m^{-2}/s, respectively, while the NP force field predicts somewhat smaller diffusion. Compared to the experimental values of 7.1×10^{-11} and 3.6×10^{-11} m^{-2}/s for $D_{\parallel}$ and $D_{\perp}$, respectively, the diffusion from simulations using original force fields is almost three times lower. Similar trend is observed at other temperatures as shown in Figure 2.8a

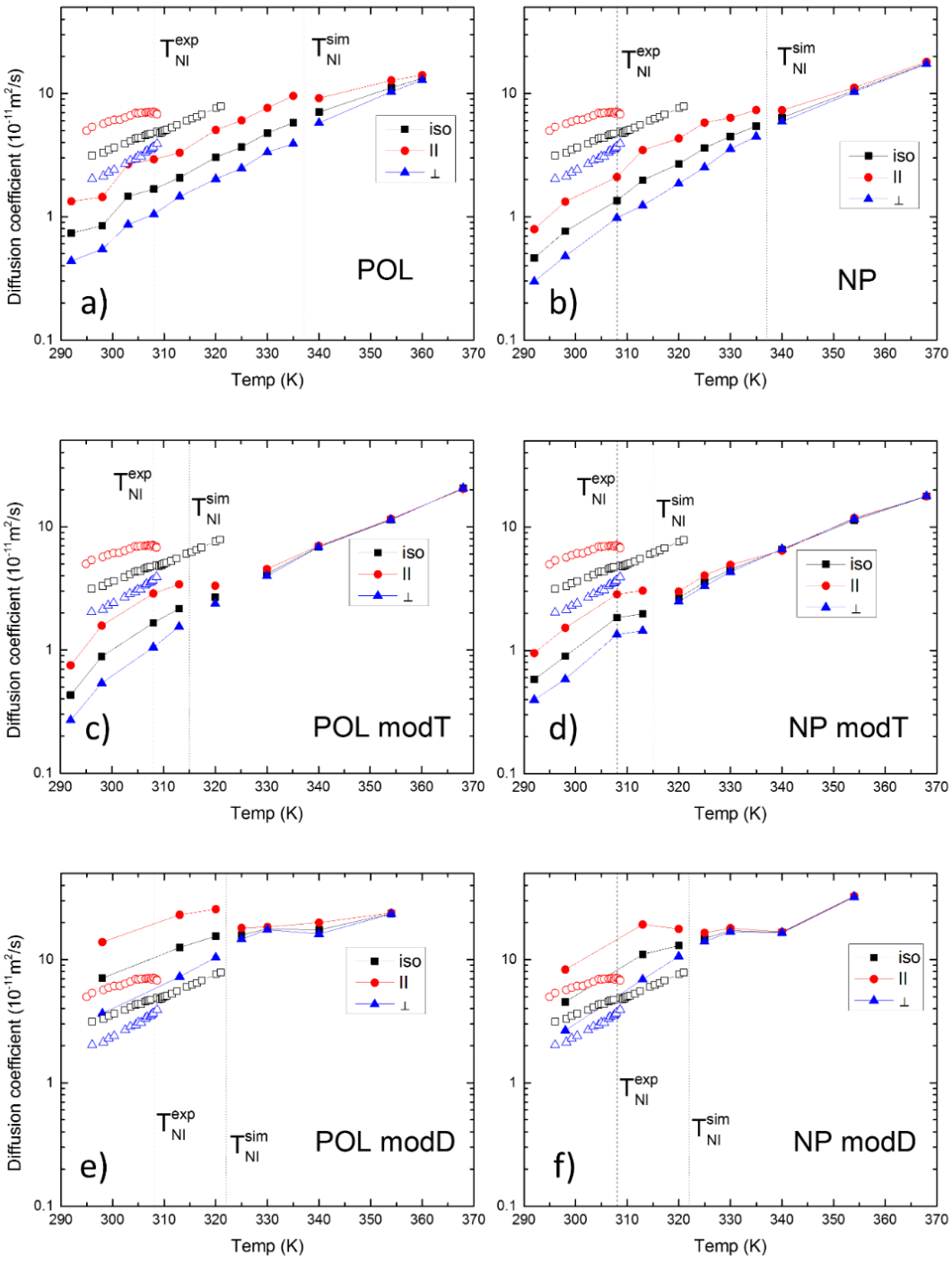

Figure 2.8. 5CB self-diffusion coefficients at different temperatures obtained from simulations using (a) POL, (b) NP, (c) *modT*_POL, (d) *modT*_NP, (e) *modD*_POL, and (f) *modD*_NP force fields, the open symbols correspond to experimental values. The estimated error bars are less than 0.05×10^{-11} m^{-2}/s for all systems investigated.

and b, and the general trend indicates that in the nematic phase both $D_{\parallel}$ and $D_{\perp}$ values are 3-5 times lower than experiments. Nevertheless, in the nematic phase the predicted diffusion anisotropy ratio $D_{\parallel}/D_{\perp}$ was about 2.5 for both POL and NP force fields, which is in a good agreement with 1.9-2.6 values obtained in experiments,[67] and therefore suggesting that the simulation using these force field capture very well the diffusion anisotropic arising from the anisotropy of 5CB molecules and their interactions.[69] It is also worth pointing out that at the NI phase transition point all components of the self-diffusion coefficient converge to similar values further confirming the T_{NI} identified based on the order parameter and density temperature dependencies.

As discussed above, the *modT* force field has resulted in significantly reduced T_{NI}, however, as can be seen in Figure 2.8c and d, the change in torsional energy barrier has an inconsequential effect on the self-diffusion coefficient. At 308 K the *modT*_POL force field gives almost the same $D_{\parallel}$ and $D_{\perp}$ as those predicted by the original force field, both $D_{\parallel}$ and $D_{\perp}$ are still 3-5 times smaller than experimental values. This finding suggests that the small changes in the geometry of the biphenyl group does not affect the self-diffusion coefficient. The diffusion anisotropy ratio $D_{\parallel}/D_{\perp}$ is also similar to that of the original force field. In addition, just like the original force field, the induced polarizability has little impact on the self-diffusion coefficient. On the other hand, as illustrated in Figure 2.8e and f, lowering the molecular dipole moment in the *modD* force fields resulted in significant increase of self-diffusion coefficients. At 298 K the *modD*_POL force field predicts 13.8×10^{-11} and 3.65×10^{-11} m^{-2}/s values for the $D_{\parallel}$ and $D_{\perp}$, respectively, which is in excellent agreement for $D_{\perp}$ and less than a factor of two overestimation for $D_{\parallel}$. The self-diffusion coefficients

predicted by the *modD*_NP force field (8.29×10^{-11} and 2.65×10^{-11} m^{-2}/s) are in excellent agreement with experiment. The observed larger jump in self-diffusion coefficients between the original as-fit and *modD* force fields is due to the reduction of intermolecular electrostatic (attractive) forces at close separations, which leads to the reduction of density and overall viscosity. Interestingly, the presence of induced polarization interactions has a significantly larger effect on the diffusion in the direction parallel to the director of the nematic phase, similar effect has also been reported in our previous simulation in ionic liquids.[39]

2.4 Conclusions

In this work, we have investigated the influence of the details of electrostatic interactions and conformational flexibility of 5CB molecules on the thermodynamic, structural, and dynamic properties of liquid phases of this material as obtained from MD simulations using an all-atom model. We found that induced polarization interactions have limited influence on the thermodynamic properties, with the polarizable force fields predicting densities ~2% higher than their nonpolarizable counterparts while showing little impact on the nematic-isotropic transition temperature. We demonstrate that utilization of partial atomic charge distributions fit directly to the high-level quantum chemistry calculations results in overestimation of the 5CB dipole moment, therefore leading to overestimation of the nematic-isotropic transition temperature (T_{NI}) by about 30 K degrees. Rescaling partial atomic charges (*modD* force field) to allow the molecular dipole to be closer to experimentally reported values of 5CB dipole in condensed phases (i.e., about 5.0 D) significantly improves the prediction of T_{NI} as well as other thermodynamic and

dynamic properties of isotropic and nematic phases. We also demonstrate how structural, thermodynamic and dynamic properties of bulk 5CB are affected by variations of some key force field parameters, e.g., the flexibility of the central biphenyl dihedral (*modT* force field). While the modification of parameters of biphenyl dihedral can significantly influence the T_{NI} it has very little influence on molecules self-diffusion coefficient and structural correlations. Having compared the simulation predictions using six different force fields we conclude that the nonpolarizable version of the force field with reduced dipole moment (*modD*_NP) provides the most consistent set thermophysical and dynamical properties for 5CB liquids in the wide temperature range.

2.5 References

[1] G.W. Gray, K.J. Harrison, and J.A. Nash, Electron. Lett. **9**, 130 (1973).

[2] S. Tanaka, C. Kato, and K. Horie, J. Mol. Struct. **735-736**, 27 (2005).

[3] D. Demus and T. Inukai, Liq. Cryst. **26**, 1257 (1999).

[4] I. Zgura, R. Moldovan, T. Beica, and S. Frunza, Cryst. Res. Technol. **44**, 883 (2009).

[5] I. Musevic, M. Skarabot, U. Tkalec, M. Ravnik, and S. Zumer, Science (80-.). **313**, 954 (2006).

[6] Y. Xia, R. Verduzco, R.H. Grubbs, and J.A. Kornfield, Abstr. Pap. 234th ACS Natl. Meet. Boston, MA, United States, August 19-23, 2007 **91125**, POLY (2007).

[7] M.D. Kempe, N.R. Scruggs, R. Verduzco, J. Lal, and J.A. Kornfield, Nat. Mater. **3**, 177 (2004).

[8] M. Glaser, in *Adv. Comput. Simulatons Liq. Cryst.*, edited by P. Pasini and C. Zannoni (Springer Netherlands, 2000), pp. 263–331.

[9] G.A. Oweimreen and M.A. Morsy, Thermochim. Acta **346**, 37 (2000).

[10] T. Mansaré, R. Decressain, C. Gors, and V.K. Dolganov, Mol. Cryst. Liq. Cryst. **382**,

97 (2002).

[11] S.J. Picken, W.H. de Jeu, S.J. Picken, W.F. van Gunsteren, P.T. van Duijnen, and W.H. de Jeu, Liq. Cryst. **33**, 1359 (2006).

[12] J.G. Gay and B.J. Berne, J. Chem. Phys. **74**, 3316 (1981).

[13] J. Brown, M. Allen, E. Martín del Río, and E. Miguel, Phys. Rev. E **57**, 6685 (1998).

[14] M.A. Bates and C. Zannoni, Chem. Phys. Lett. **280**, 40 (1997).

[15] A. Cuetos, J.M. Ilnytskyi, and M.R. Wilson, Mol. Phys. **100**, 3839 (2002).

[16] S. Izvekov, A. Violi, and G.A. Voth, J. Phys. Chem. B **109**, 17019 (2005).

[17] S.J. Marrink, H.J. Risselada, S. Yefimov, D.P. Tieleman, and A.H. de Vries, J. Phys. Chem. B **111**, 7812 (2007).

[18] J. Zhang, J. Su, Y. Ma, and H. Guo, J. Phys. Chem. B **116**, 2075 (2012).

[19] G. Megariotis, A. Vyrkou, A. Leygue, and D.N. Theodorou, Ind. Eng. Chem. Res. **50**, 546 (2011).

[20] J. Zhang and H. Guo, J. Phys. Chem. B **118**, 4647 (2014).

[21] J. Zhang, J. Su, and H. Guo, J. Phys. Chem. B **115**, 2214 (2011).

[22] B. Stevensson, A. V. Komolkin, D. Sandström, and A. Maliniak, J. Chem. Phys. **114**, 2332 (2001).

[23] C.W. Cross and B.M. Fung, J. Chem. Phys. **101**, 6839 (1994).

[24] A. V. Komolkin, A. Laaksonen, and A. Maliniak, J. Chem. Phys. **101**, 4103 (1994).

[25] Z. Wang, J.A. Lupo, S. Patnaik, and R. Pachter, Comput. Theor. Polym. Sci. **11**, 375 (2001).

[26] F. Chami, M.R. Wilson, and V.S. Oganesyan, Soft Matter **8**, 6823 (2012).

[27] Y. Lansac, M. Glaser, and N. Clark, Phys. Rev. E **64**, 1 (2001).

[28] C. McBride and M.R. Wilson, Mol. Phys. **97**, 511 (1999).

[29] I. Cacelli, S. Campanile, G. Prampolini, and A. Tani, J. Chem. Phys. **117**, 448 (2002).

[30] C. Amovilli, I. Cacelli, S. Campanile, and G. Prampolini, J. Chem. Phys. **117**, 3003 (2002).

[31] I. Cacelli, G. Prampolini, and A. Tani, J. Phys. Chem. B **109**, 3531 (2005).

[32] I. Cacelli, L. De Gaetani, G. Prampolini, and A. Tani, J. Phys. Chem. B **111**, 2130 (2007).

[33] M. Cifelli, L. De Gaetani, G. Prampolini, and A. Tani, J Phys Chem B **112**, 9777 (2007).

[34] A. V. Komolkin, A. Laaksonen, and A. Maliniak, J. Chem. Phys. **101**, 4103 (1994).

[35] S. Sinton and A. Pines, Chem. Phys. Lett. **76**, 263 (1980).

[36] G. Tiberio, L. Muccioli, R. Berardi, and C. Zannoni, ChemPhysChem **10**, 125 (2009).

[37] S.J. Weiner, P.A. Kollman, D.A. Case, U.C. Singh, C. Ghio, G. Alagona, S. Profeta, and P. Weiner, J. Am. Chem. Soc. **106**, 765 (1984).

[38] M.G. Martin and J.I. Siepmann, J. Phys. Chem. B **102**, 2569 (1998).

[39] O. Borodin, J. Phys. Chem. B **113**, 11463 (2009).

[40] D. Bedrov, O. Borodin, Z. Li, and G.D. Smith, J. Phys. Chem. B **114**, 4984 (2010).

[41] Y. Wang, L. Xing, W. Li, and D. Bedrov, J. Phys. Chem. Lett. **4**, 3992 (2013).

[42] D. Bedrov, G.D. Smith, and A.C.T. Van Duin, J. Phys. Chem. A **116**, 2978 (2012).

[43] L. Xing, J. Vatamanu, O. Borodin, G.D. Smith, and D. Bedrov, J. Phys. Chem. C **116**, 23871 (2012).

[44] O.N. Starovoytov, O. Borodin, D. Bedrov, and G.D. Smith, J. Chem. Theory Comput. **7**, 1902 (2011).

[45] J.B. Hooper, O.N. Starovoytov, O. Borodin, D. Bedrov, and G.D. Smith, J. Chem. Phys. **136**, 194506 (2012).

[46] D. Bedrov and O. Borodin, J. Phys. Chem. B **114**, 12802 (2010).

[47] O. Borodin and D. Bedrov, J. Phys. Chem. C **118**, 18362 (2014).

[48] D. Bedrov, O. Borodin, G.D. Smith, T.D. Sewell, D.M. Dattelbaum, and L.L. Stevens, J. Chem. Phys. **131**, 224703 (2009).

[49] J.B. Hooper, G.D. Smith, and D. Bedrov, J. Chem. Phys. **139**, 104503 (2013).

[50] M.J. Frisch and G.W. Trucks, Gaussian, Inc. (2009).

[51] O. Borodin and G.D. Smith, J. Phys. Chem. B **110**, 6279 (2006).

[52] U. Essmann, L. Perera, M.L. Berkowitz, T. Darden, H. Lee, and L.G. Pedersen, J Chem Phys **103**, 8577 (1995).

[53] B.J. Palmer, J. Comput. Phys. **104**, 470 (1993).

[54] G.J. Martyna, M.E. Tuckerman, D.J. Tobias, and M.L. Klein, Mol. Phys. **87**, 1117 (1996).

[55] P.J. Collings and M. Hird, *Introduction to Liquid Crystals: Chemistry and Physics* (1997).

[56] A. Sanchez-Castillo, M.A. Osipov, and F. Giesselmann, Phys. Rev. E - Stat. Nonlinear, Soft Matter Phys. **81**, 1 (2010).

[57] P.G. de Gennes and J. Prost, *The Physics of Liquid Crystals*, 2nd ed. (Clarendon Press, 1995).

[58] S. Chandrasekhar, *Liquid Crystals* (Cambridge University Press, Cambridge, 1992).

[59] J. Deschamps, J.P.M. Trusler, and G. Jackson, J. Phys. Chem. B **112**, 3918 (2008).

[60] S.J. Picken, W.F. Van Gunsteren, P.T. Van Duijnen, and W.H. De Jeu, Liq. Cryst. **6**, 357 (1989).

[61] L. De Gaetani, G. Prampolini, and A. Tani, J. Phys. Chem. B **110**, 2847 (2006).

[62] C. J. Adam S. J. Clark M. R. Wilson, Mol. Phys. **93**, 947 (1998).

[63] L. Onsager, Ann. N. Y. Acad. Sci. **51**, 627 (1949).

[64] K.P. Gueu, E. Megnassan, and A. Proutiere, Mol. Cryst. Liq. Cryst. **132**, 303 (1986).

[65] E.P. Raynes, Mol. Cryst. Liq. Cryst. Lett. **1**, 69 (1985).

[66] S. V. Dvinskikh, I. Furó, H. Zimmermann, and A. Maliniak, Phys. Rev. E - Stat. Nonlinear, Soft Matter Phys. **65**, 1 (2002).

[67] S. V. Dvinskikh and I. Furó, J. Chem. Phys. **115**, 1946 (2001).

[68] E.E. Romanova, F. Grinberg, A. Pampel, J. Kärger, and D. Freude, J. Magn. Reson. **196**, 110 (2009).

[69] P. Ilg, Phys. Rev. E - Stat. Nonlinear, Soft Matter Phys. **71**, 1 (2005).

CHAPTER 3

INFLUENCE OF FORCE FIELD DETAILS ON STRUCTURAL BULK PROPERTIES OF CYANOBIPHENYL LIQUID CRYSTALS

3.1 Introduction

Over the years, atomistic MD simulations have been extensively used for probing the molecular scale structure of soft mater materials including LC materials. Particularly for LC materials, the understanding of bulk properties (e.g., transition between mesophases, anchoring behavior, etc.) are directly linked to the specific inter and intramolecular correlations. While it is well established that formation of long-range ordering and mesophases in LC materials are dictated by the shape and conformations of LC molecules[1], it is extremely difficult to sample these microscopic level structural details experimentally. On the contrast, atomistic MD simulations can easily access those highly detailed structural correlations and therefore became a great tool for the investigation of LC materials in different mesophases. In this chapter, we analyze the influence of variation in the force field parameters (discussed in Chapter 1) on several key orientation and structural correlations predicted by MD simulations for bulk 5CB phases. Using the NP and POL versions of original, *modD* and *modT* force fields we focus on the comparison of conformational properties, structural, and orientational correlations, and distributions of dipole moments in nematic and isotropic phases of 5CB.

3.2 Intramolecular Conformations

It is known that the inter-ring and ring-tail dihedral angle φ1 and φ2 play an important role on the stability of nematic phase of 4-n-pentyl-4'-cyanobiphenyl (5CB).[2] Experimentally, Sinton et al.[3] measured φ1 to be 32±1° using the multiple quantum proton NMR technique, they used the minimum energy configuration of the dihedral potential when fitting the dipolar couplings. Celebre et al.[4] refitted Sinton's data taking into account the entire rotational potential distribution and estimated a φ1 value of 38.4 ± 0.1°. Catalano et al.[5] measured 32° via maximum-entropy analysis of their NMR data. Using Double-Quantum ^{13}C NMR method, Sandstrom et al.[6] measured φ1 to be 36° after fitting the dipolar couplings with both rotational isomeric state and continuous mean-field approximation methods. Emsley et al.[7,8] measured φ1 and φ2 to be 37° and 90°, respectively, from their NMR study.

On the simulation side, Zhang et al.[9] in their united atom (UA) simulation using reoptimized TraPPE-UA force field accurately reproduced the experimental values of φ1 and φ2 at 35° and 90°, respectively. While Komolkin et al.[10] predicted φ1 to be 0° using UA model and ±25° in their all-atom model at 300 K. They attribute the absence of the repulsion force between the adjacent inter-ring ortho-protons in the UA model for the failure in reproducing value of φ1. Simulations of Pizzirusso[11] correctly reproduced φ1 compared to experiment, their results also agreed with the *ab initio* calculation done by Cacelli et al.[12] However, it has been shown[13,14] that due to the relative flat potential energy barriers all confirmations can be sampled even at low temperatures, a small perturbation in the environment can often lead to different conformations. Previous studies[13] have also exposed the poor transferability of the torsional potentials from CB to 5CB, therefore, it is

necessary to have an accurate *ab initio* fit of the torsional energy curves describing those dihedral angles.

3.2.1 Effect of Polarizability and Temperature

Dihedral energy profiles in 5CB and its homologues are known to have strong influences on the molecule conformations, which, in turn, have a strong influence on the stability of its mesophases.[15] Therefore, it is important to investigate these angles as predicted by our force fields. Figure 3.1 identifies the two key dihedral angles of 5CB, where 0° marks the cis configuration, which is the same definition used by other groups.[9,16] One cannot discuss the inter-ring dihedral angle without mentioning biphenyl (2P), which is an important moiety for the nCB liquid crystals family. 2P itself is a nonrigid molecule with strong coupling between molecular conformation and the structure of local environment, its dihedral angle is determined by the repulsion between the adjacent ortho-protons on the two phenyl rings.[17] Like many other oligoaromatic molecules, the inter-ring dihedral angle of 2P is around 44° in the gas phase[18] while almost 0° in the crystal phase.[19] However, NMR experiments have shown that in nematic LC solvents, the 2P has a preferred inter-ring angle of around 35°.[20–22] In 5CB, the additional linkage to cyano and alkyl function groups causes small deviation of the inter-ring dihedral angle. In comparison, Figure 3.2 shows the angle distribution of φ1 and φ2 obtained from our simulations using the POL version of the original force field. In the first quadrant the φ1 has a peak at 38° whereas φ2 at 90°, both predictions agree well with aforementioned experimental values. In Figure 3.2 we also compared the dihedral angle distribution between POL and NP force field. The additional induced dipole interaction has little effect

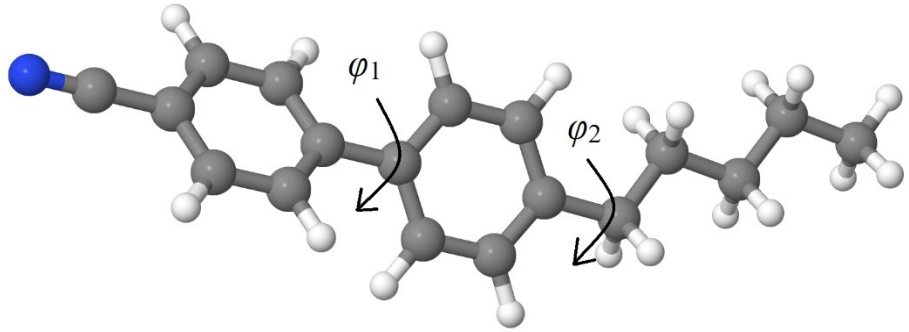

Figure 3.1. All-atom model of 5CB molecule. Dihedral angles φ1 and φ2 are designated to depict the inter-ring and ring tail conformations.

on the conformation of 5CB molecule, which is expected considering the energy of induced dipole is orders of magnitude less than the intramolecular forces.

In order to understand the conformational behavior of 5CB at different temperatures, a comparison was made for φ1 and φ2 distributions both in the nematic and isotropic phases. As shown in Figure 3.3, while the difference is quite small for φ1, we notice a change in distribution for φ2. While typically at higher temperatures distribution of dihedral angles become broader (due to large thermal fluctuations allowing more frequent access of higher energy conformations) we can see that with increasing temperature (and the corresponding switching from nematic to isotropic phase) the peak at 90° for φ2 become sharper. This trend indicates that at lower temperature, the nematic phases imposes additional constrains on the φ2 angle distribution, and in this phase, precludes full expression of the desired angle. In the isotropic phase those local molecular orientational effects are eliminated, therefore allowing the φ2 to reorient to the preferred 90° angle.

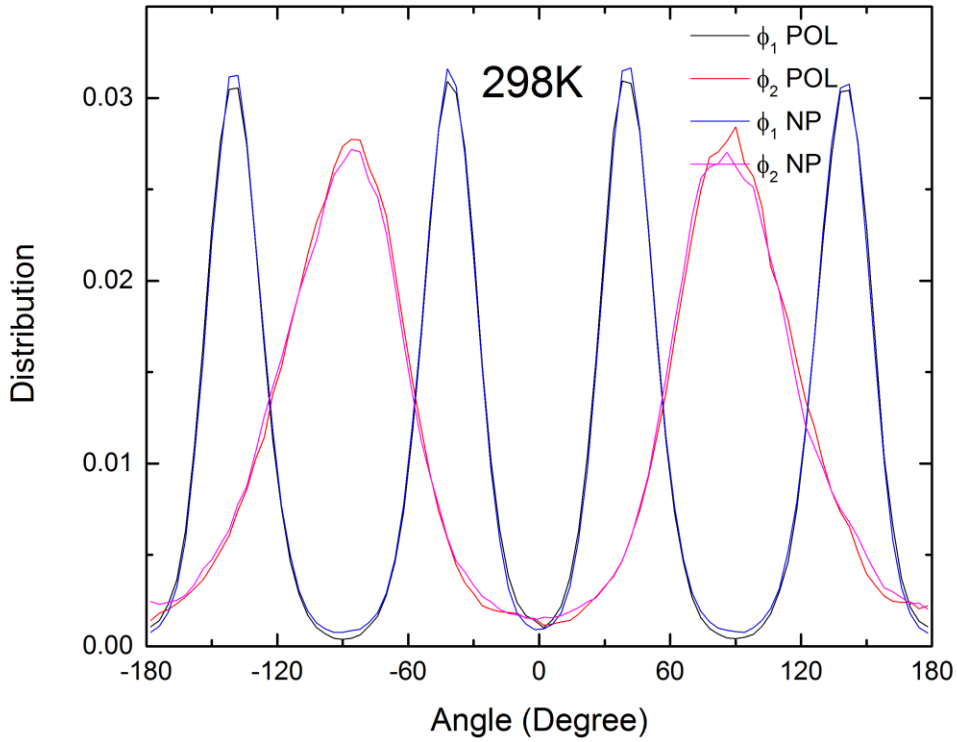

Figure 3.2. Distribution of inter-ring dihedral angle φ1 and ring-tail dihedral angle φ2 using POL and NP version of original force field in the nematic phase

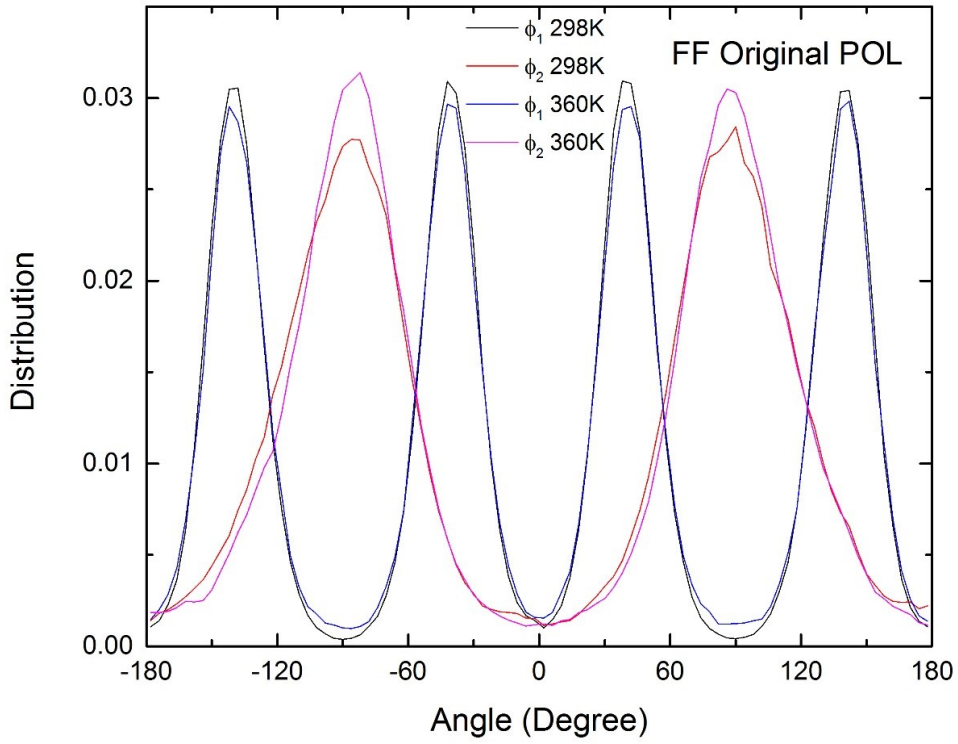

Figure 3.3. Comparison of φ1 and φ2 angle distribution in the nematic (298 K) and isotropic (360 K) phases.

3.2.2 Force Field Refinement and 5CB Conformations

Figure 3.4 shows the comparison of φ1 distributions as obtained from simulations using the original, *modT* and *modD* versions of the force field that has been discussed in Chapter 2. As mentioned previously, the polarizability has minimal influence over the shape of 5CB, therefore, we only show distributions for POL force fields. The modification of the inter-ring dihedral parameters in the *modT* force field has changed the distribution of φ1 in two ways. First, a noticeable shift of the peak location from 38° to 45°, which would to some extent affect the molecular shape and particularly the planarity of the CB unit. This

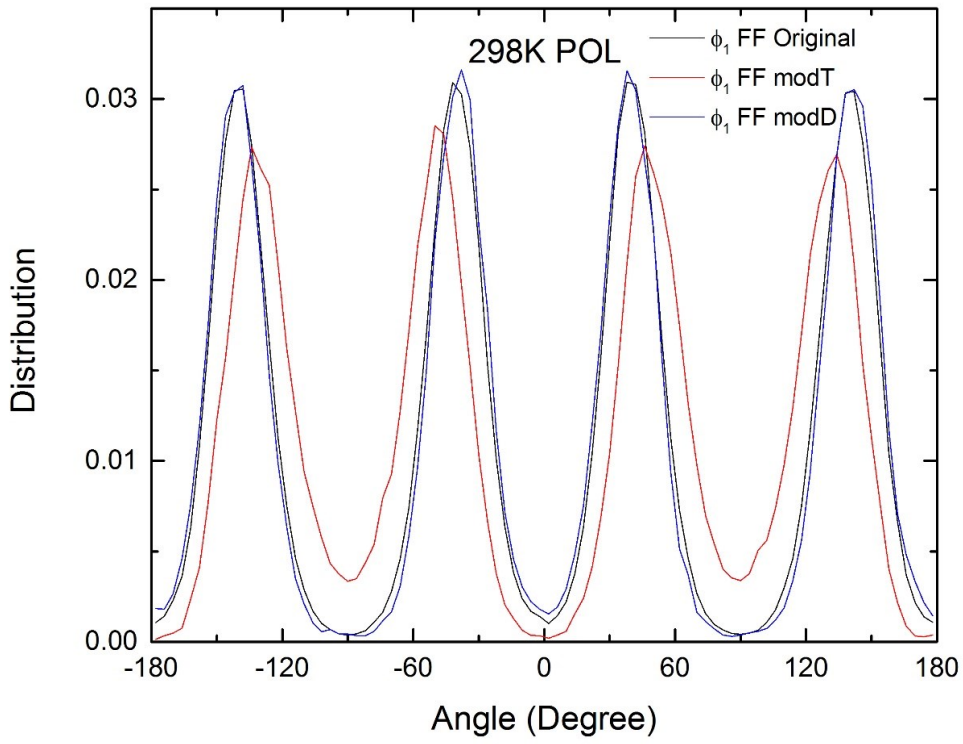

Figure 3.4. Inter-ring dihedral angle φ1 comparison for the original, *modD*, and *modT* versions of the POL force field.

shift would influence the packing of 5CB mesogens, and is likely the primary reason for the decrease of T_{NI} observed for this force field (see Chapter 2). Second, the lowering of rotational barrier increases the rotation rate the biphenyl rings relative to each other, and in turn, can be coupled with molecule mobility. On the other hand, compare to *modT*, the distribution curves between the original and *modD* force fields appeared to be virtually identical, indicating the scaling of atomic partial charges has no impact on the confirmation of 5CB molecule. For φ2, all three force fields predicted the same dihedral angle distribution (same as shown in Figure 3.2).

3.3 Intermolecular Structural Correlations

3.3.1 Structural Correlations in the Nematic Phase

Next we analyze several positional and orientational distribution functions as shown in Figure 3.5. First, we examine the radial distribution function *g(r)* for the center-of-mass of 5CB molecules in the nematic phase (298 K). *g(r)* is defined as,

$$g(r) = \frac{1}{4\pi r^2 \rho_N} \left\langle \delta \left| r_i^k - r_j^m \right| - r \right\rangle \tag{3.3}$$

where *r* is the distance between the specified sites (e.g., the center-of-mass) k and m on molecules *i* and *j*, respectively, ρN is the number density, and the <…> denotes the ensemble average. We also define orientational radial distribution function *g1(r)* as,

$$g_1(r) = \left\langle cos\, \theta_{ij}(r) \right\rangle \tag{3.4}$$

where θij is the angle between two end-to-end vectors of molecules *i* and *j*, *r* is the distance between the center-of-mass of those two vectors. The values of *g1(r)* range from -1 to 1, representing perfect antiparallel and parallel arrangements, respectively.

Figure 3.5a indicates that there is very little difference between *g(r)* obtained from simulations using POL and NP force fields. Both of them show a well-defined first peak within 7.5 Å separations that can be associated with molecules in the first coordination shell. Integration of the *g(r)* allows us to obtain the apparent coordination number as a function of *r* which is also shown in the figure. Figure 3.5a clearly shows that each 5CB molecule on average has about four 5CB molecules within its first coordination shell. Similar result is obtained if one examines the *g(r)* for the phenyl rings connected to the cyano groups as illustrated in Figure 3.5b. Here, the first peak is split into two parts, with the first one having a maximum at about 5.0 Å. This separation corresponds to configuration-1 shown in Figure 3.5e where two phenyl rings are almost parallel and on

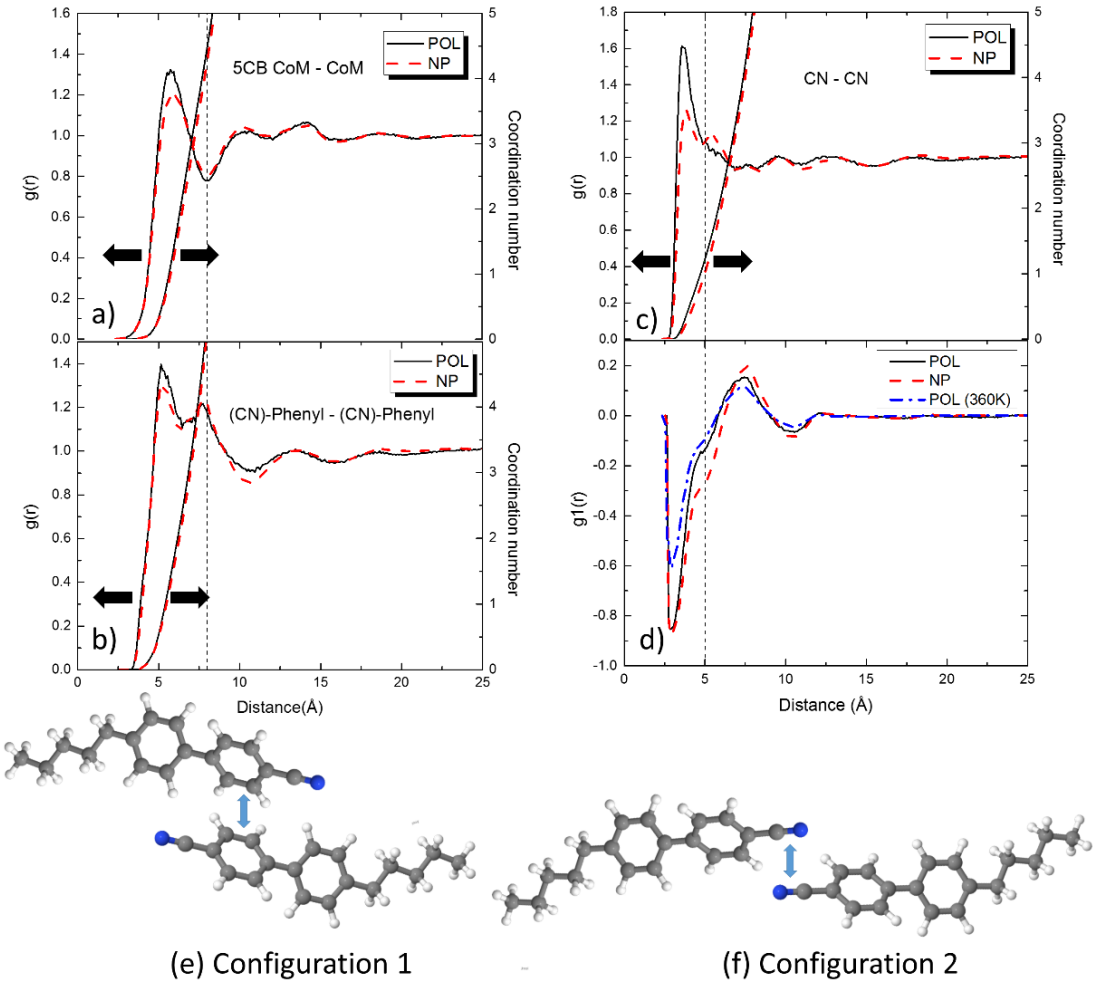

Figure 3.5. The radial distribution function *g(r)* and coordination number calculated for (a) the center of mass of 5CB molecules, (b) the center of mass of the cyano group and (c) center of mass of the phenyl ring connected to the cyano group as obtained from simulations using POL and NP force fields at 298 K (nematic phase). (d) Orientational correlation function *g1(r)* of the cyano group for POL and NP models at 298 K. Also shown is the *g1(r)* at 360 K (isotropic phase) for the POL force field. (e and f) Two preferred configurations of neighboring 5CB molecules are illustrated schematically.

top of each other. The examination of the coordination number for this correlation indicates that within distance of 6.5 Å (the location of a shoulder between the first and the second parts of the phenyl-phenyl peak) we can see that about 2.5 molecules have such a close approach and a dimer geometry similar to configuration-1.

Examination of *g(r)* for the center-of-mass of cyano groups (Figure 3.5c) indicates that there is a strong peak within 5.0 Å separation that corresponds to a very close approach of cyano groups. Figure 3.5d, which shows the orientational correlation function *g1(r)* for the CN vectors, also indicates that if two cyano groups approach each other within 5.0 Å their orientation is antiparallel (negative values of *g1(r)*) as illustrated by configuration-2 in Figure 3.5f. However, the examination of coordination numbers indicates that on average each 5CB molecule has such close approach (within 5.0 Å) only with one other 5CB molecule. In fact, even in isotropic phase, if two cyano groups approach each other within 5.0 Å, their relative orientation will likely be antiparallel as can be seen in Figure 3.5c where *g1(r)* obtained from simulations at 360 K is shown for comparison. This phenomenon of local parallel orientation is consistent with the prediction of Landau-de Gennes theory for temperatures above T_{NI}[2].

Summarizing the analysis of Figure 3.5 we can conclude that out of four nearest neighbors of 5CB molecule in the nematic phase only one of them has orientation similar to configuration-2 (Figure 3.5f) while position and orientation of other neighbors is more similar to configuration-1 (Figure 3.5e).

3.3.2 Force Field Refinement and Structural Correlations

Here, we would like to examine the effect of force field modification on the structure properties of our 5CB systems in the nematic phase. Compare to original POL original, the *g1(r)* obtained from simulations using *modD*_POL force field exhibited a slight shift to the left, as shown in Figure 3.6. The negative peak is now at 2.75Å vs. 2.9Å in the POL original force field. The difference is more noticeable in the first positive peak, where the curve from the system using *modD*_POL has shifted to 6.58Å from 7.45Å. Such changes are expected from lowering the partial atomic charges on cyano group. Now for *modD*_NP force field, lowering the permanent dipole moment exhibited little effect on the first negative peak at 2.95Å, as the two peaks are virtually identical, however, both the first positive peak at 7.55Å and second negative peak at 10.4 Å became less pronounced, indicating a weaker antiparallel parallel arrangement pattern between two 5CB molecules at close approach. This is consistent with weaker Columbic interactions due to smaller dipole moment on the cyano group. Figure 3.7 shows only negligible difference between cyano group center of mass *g(r)* for original and *modD* versions of POL and NP force fields mostly within the first peak, indicating that influence of force field parameters on both structural and orientational properties is very local, i.e., within first coordination shell. It is clear that switching POL to NP form of the force field has a noticeably larger effect on the local structure that reduction of the dipole moment (i.e., original vs. *modD*).

Figure 3.8 compares the changes in spatial correlation of 5CB in the nematic phase after the modification of the torsional energy parameter for φ1. For both *modT*_POL and *modT*_NP force fields the modification of torsional potential resulted in a broader first positive peak at 7.5Å, suggesting a slower decay of antiparallel arrangement at distances

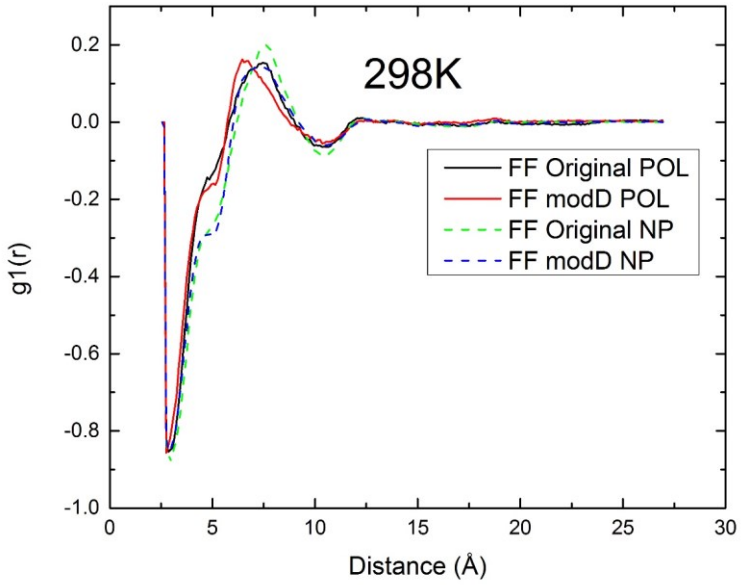

Figure 3.6. The orientational correlation function *g1(r)* of the cyano group in 5CB in nematic phase obtained from simulations using both POL (original and *modD*) and NP (original and *modD*) versions of force field.

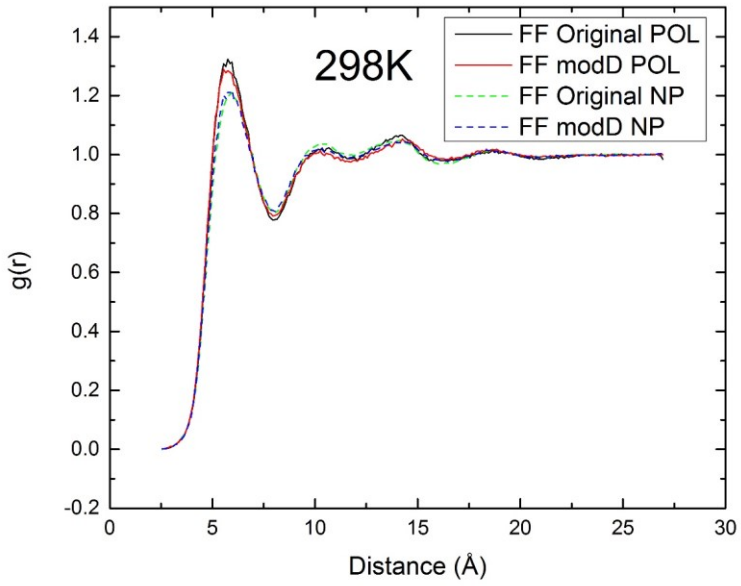

Figure 3.7. The radial distribution function *g(r)* calculated using the center of mass of the cyano group of 5CB in the nematic phase obtained from simulations using both POL (original and *modD*) and NP (original and *modD*) versions of force field.

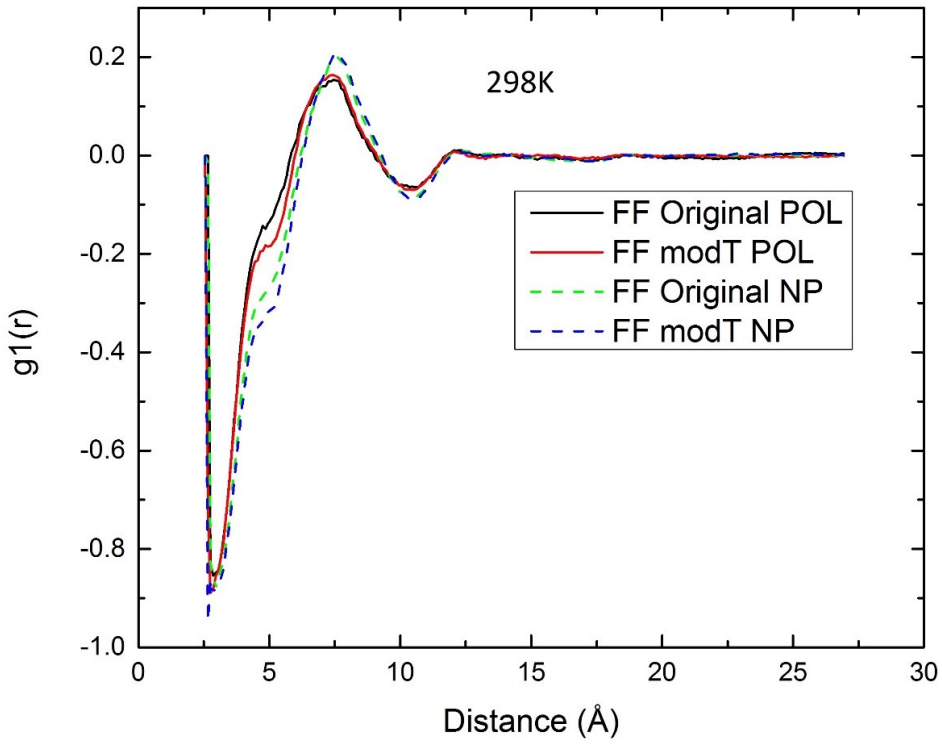

Figure 3.8. The orientational correlation function *g1(r)* of the cyano group in 5CB in nematic phase obtained from simulations using both POL (original and *modT*) and NP (original and *modT*) versions of force field.

between 4.63Å and 5.23Å, which means the average angle between molecules in those coordination shells are slightly more obtuse. This feature is caused by the stronger volume exclusion effect of the rounder biphenyl group in 5CB with *modT* version of the force field, which, in turn, affects the dipole-dipole antiparallel alignment tendency in the neighboring 5CB molecules. Similar to the discussion on the influence of dipole moment adjustment comparison in Figure 3.7, the center of mass *g(r)* shown in Figure 3.9 shows a minimal influence on the number of surrounding molecules. Overall, unlike the impressive changes in thermodynamic properties, the modification of dihedral potential for φ1 did not lead to any significant change in structural and orientational correlations between 5CB molecules.

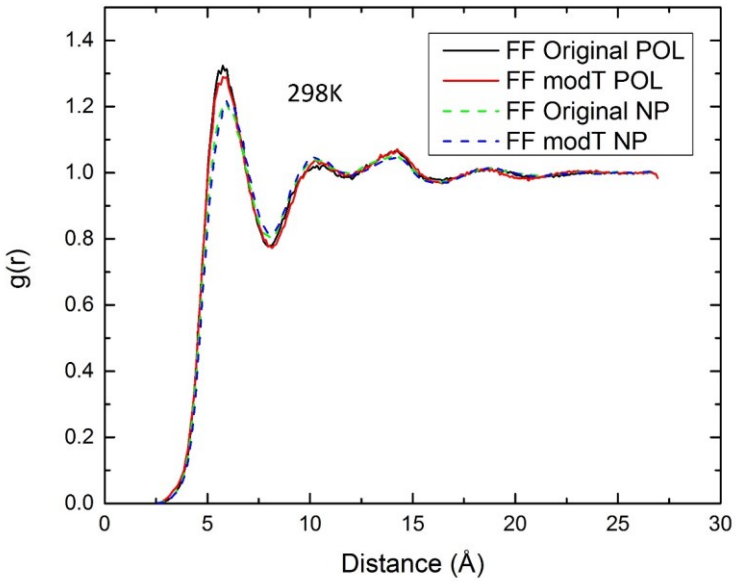

Figure 3.9. The radial distribution function *g(r)* calculated using the center-of-mass of the cyano group of 5CB in nematic phase obtained from simulations using both POL (original and *modT*) and NP (original and *modT*) versions of force field.

3.4 Permanent and Induced Dipole Correlations

To obtain a better understanding on the effect of induced dipole moment on 5CB phase behavior, we have calculated the probability distribution of angles between the permanent dipole and induced dipole moment based for investigated force fields as shown in Figure 3.10. In addition, in Table 3.1 we compared the absolute magnitudes for both types of dipoles. As we can see from Figure 3.10, the angle between induced and permanent dipole is about 80° for all three versions of the force field. Considering that the direction of the permanent dipole is primarily determined by the cyano group, this means that the molecular induced dipole moment is likely to be oriented perpendicular to the long axis of the 5CB molecule. Such distribution explains why the total dipole moment of 5CB is less than the combined value of permanent and induced dipole moments, as shown in Table 3.1.

Table 3.1. Average molecular dipole moment of 5CB in nematic phase at 298 K.

298 K	Permanent (Debye)	Induced (Debye)	Total (Debye)
FF Original	6.41	0.83	6.59
FF *modT*	6.42	0.83	6.61
FF *modD*	4.98	0.64	4.98

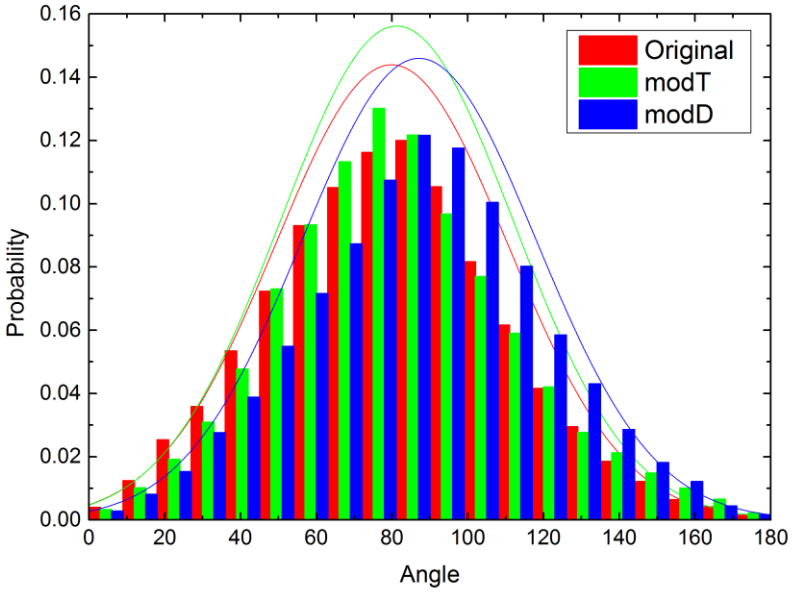

Figure 3.10. Distribution of angles between permanent and induced dipole moment in 298 K nematic phase using original, *modT* and *modD* force field.

Explanation for this Gaussian-like distribution is provided based on the direction of the local electric field generated by the charge separation of the permanent dipole moments, which is determined by the antiparallel arrangement of 5CB molecules. Under such structural/orientational arrangement of 5CB molecules, the local electric field will be perpendicular to the permanent dipole, and since polarizability is a scalar tensor to the electric field, the induced dipole moment must be aligning parallel to the local electric field (i.e., perpendicular to the permanent dipole moment). As a result, the attraction force due

to these polarization interactions is responsible for the closer intermolecular distances seen in Figure 3.5, Figure 3.7, and Figure 3.9 for all POL force fields. The angle distribution obtained from the *modD* force field shows a slight shift of the distribution towards 90°, which is probably related to slight differences in local orientation observed in Figure 3.6 between original and *modD* force field for POL model.

3.5 Conclusions

In this chapter, we investigated the influence of induced dipole moment on the molecular conformations and structural correlation properties of 5CB bulk system as obtained from MD simulations and force fields discussed in Chapter 2. For conformational properties of 5CB, both the original and *modD* force fields accurately predicted the inter-ring and ring-tail average dihedral angles φ1 and φ2 when compared to available experimental data, while the *modT* force field overestimated φ1 by about 7°. The influence of polarization interactions has shown to be inconsequential for the dihedral angle distributions owing to the weak nature of the induced dipole attraction force. The analysis of intermolecular structural correlations indicated two preferred spatial/orientational arrangements for neighboring 5CB in nematic phase, both are antiparallel and interdigitated. Overall, the modifications of force field had limited effect on the structural correlations of bulk 5CB. This indicates that while thermodynamic properties and the phase equilibrium of 5CB liquid phases are strongly sensitive to the force field details, the underlying structure of the nematic and isotropic phases are primarily determined by the anisotropy of 5CB chemical structure and geometry.

3.6 References

[1] M.R. Wilson, Chem. Soc. Rev. **36**, 1881 (2007).

[2] P.G. de Gennes and J. Prost, *The Physics of Liquid Crystals*, 2nd ed. (Clarendon Press, 1995).

[3] S. Sinton and A. Pines, Chem. Phys. Lett. **76**, 263 (1980).

[4] G. Celebre, M. Longeri, E. Sicilia, and J.W. Emsley, Liq. Cryst. **7**, 731 (1990).

[5] D. Catalano, L. Di Bari, C.A. Veracini, G.N. Shilstone, and C. Zannoni, J. Chem. Phys. **94**, 3928 (1991).

[6] D. Sandström and M.H. Levitt, J. Am. Chem. Soc. **118**, 6966 (1996).

[7] J.W. Emsley, T.J. Horne, G. Celebre, G. De Luca, and M. Longeri, J. Chem. Soc. Faraday Trans. **88**, 1679 (1992).

[8] B. Aldridge, G. De Luca, M. Edgar, S.J. Edgar, J.W. Emsley, M.I.C. Furby, and M. Webster, Liq. Cryst. **24**, 569 (2010).

[9] J. Zhang, J. Su, and H. Guo, J. Phys. Chem. B **115**, 2214 (2011).

[10] A. V. Komolkin, A. Laaksonen, and A. Maliniak, J. Chem. Phys. **101**, 4103 (1994).

[11] A. Pizzirusso, M.E. Di Pietro, G. De Luca, G. Celebre, M. Longeri, L. Muccioli, and C. Zannoni, ChemPhysChem **15**, 1356 (2014).

[12] I. Cacelli, G. Prampolini, and A. Tani, J. Phys. Chem. B **109**, 3531 (2005).

[13] C. J. Adam S. J. Clark M. R. Wilson, Mol. Phys. **93**, 947 (1998).

[14] J. Crain and A. V. Komolkin, AdV. Chem. Phys. **109**, (1999).

[15] C.D. Wick, J.M. Stubbs, N. Rai, and J.I. Siepmann, J. Phys. Chem. B **109**, 18974 (2005).

[16] J. Peláez and M. Wilson, Phys. Chem. Chem. Phys. **9**, 2968 (2007).

[17] A. V. Komolkin, A. Laaksonen, and A. Maliniak, J. Chem. Phys. **101**, 4103 (1994).

[18] J. Zhang and H. Guo, J. Phys. Chem. B **118**, 4647 (2014).

[19] G. Charbonneau and Y. Delugeard, Acta Crystallogr. **32**, 1420 (1976).

[20] G. Celebre, G. De Luca, M. Longeri, and J.W. Emsley, J. Chem. Soc. Faraday Trans. **87**, 2623 (1991).

[21] R. Berardi, F. Spinozzi, and C. Zannoni, Mol. Cryst. Liq. Cryst. Sci. Technol. Sect. A. Mol. Cryst. Liq. Cryst. **290**, 245 (1996).

[22] G. Celebre, G. De Luca, and M. Longeri, Liq. Cryst. **37**, 923 (2010).

CHAPTER 4

A MOLECULAR SIMULATION STUDY ON THE INTERFACIAL ANCHORING EFFECT OF CYANOBIPHENYL LIQUID CRYSTALS

4.1 Introduction

In recent years, anchoring behavior of thermotropic liquid crystal (LC) at aqueous interfaces have attracted a considerable amount of attention due to the exciting prospects of various practical applications (e.g., bio-sensors) as well as the desire to understand the fundamental microscopic origin of the observed macroscopic anchoring behaviors. The presence of a surface (air, liquid, or solid) provides a symmetry breaking to the nematic phase of bulk LC, providing the potential for many interesting surface phenomena. The depth of this perturbation, ξ, is on the order of 20-100Å, the LC molecules within this range of the surface are aligning to a particular direction **a**, which is defined as the anchoring direction. The breaking of translational symmetry can create a positional order to the LC at the interface as well. Both the orientational and positional alignment may then be imposed on the bulk LC via realignment of the bulk phase in order to minimize the elastic contribution to the free energy from induced, long-range correlations in dense, potentially ordered phase.[1] Among LC mesogens, 4-cyano-4′-pentylbiphenyl (5CB) has been a popular choice to study the anchoring effect due to its rather simple chemical structure, the stability of its nematic phase at room temperature, and the remarkable sensitivity of its

orientational ordering at the interfaces.

In particular, for 5CB in the nematic phase, it has been shown[2, 3] that the molecules near a free surface will assume a homeotropic (i.e., perpendicular to the interface) orientation, with the alkyl tails in direct contact with air.[4] However, as demonstrated by Magda et al.,[5] the presence of a water surface will alter the interfacial director of 5CB away from the easy axis (i.e., the director orientation with the lowest free energy) in the bulk and lead to a degenerate planar anchoring, where all directions of anchoring tangent to the interface are equivalent in terms of surface interaction energy. On the solid substrate of pyrolytic graphite[6] or MoS_2[7], 5CB will form a 2D crystalline order due to adsorption of its alkyl tail. Recently, a tremendous amount of research has been conducted by Abbott's group on the interfacial ordering of 5CB in contact with immiscible aqueous phases.[8–10] These studies have shown that a wide variety of adsorbates can induce drastic changes on the ordering of 5CB near the surface. For example, they have demonstrated that self-assembled aggregates formed by surfactants or lipids can change the alignment of 5CB at the interface from planar to homeotropic,[8–10] and further investigations[11–13] have found that the tail conformation of surfactant plays an important role in dictating the reorientation of 5CB molecules. Furthermore, the comparable mobility between the lipid monolayer at the LC-aqueous interface and lipid bilayer membranes has enabled two distinct classes of interactions: First, between the biomolecule of interest and lipids and then the reorganized lipids will trigger to the ordering change of 5CB. Some recent examples include the specific binding between enzyme phospholipase A_2 and lipid D-R-dipalmitoylphosphatidylcholine in the presence of Ca^{2+} and the subsequent homeotropic to tilted 5CB ordering transition.[14] Studies[15,16] have shown that the bulk phase transition of 5CB has a strong influence on the

lipid monolayer, which can be expected as the isotropic phase can cause disruption of tail interactions between 5CB and the lipid, leading to a change in the interfacial elastic energy of 5CB. Overall, these research studies showed a great potential for the use of 5CB as sensors for reporting biological events.

One approach to explain the anchoring effect of the nematic 5CB involves the surface excess free energy. This energy arises from balancing electric dipole (and quadrupole) moments of the 5CB mesogen under the electric field generated at the interface due to local charge density mismatch with the short range van der Waals and steric interactions of the mesogens with the interface. The presence of the interface dictates a short-range interaction due to volume exclusion and van der Waals attractions, which causes the 5CB mesogens to align to minimize these short-range but strong interactions. In response, longer-range interactions are generated by the polarization of the strongly polar 5CB molecules when the local directors are distorted at the interface.[17] Thus, the presence of an interface breaks the translational symmetry of the nematic phase 5CB, which creates a gradient in the electric quadrupolar density, leading to an effective dipolar density.[18] Other theories[19–21] have also been proposed to explain the 5CB anchoring effect and have had varying degree of success, but due to the complex nature of the interactions occurring at the interface, better understanding at the molecular level is still desperately needed.

There are multiple advantages of using MD simulations to study the LC interface systems, such as the direct sampling of interfacial interactions at the molecular level, as well as providing the microscopic origin of the macroscopic anchoring effect, and the results can often guide the design of better performing materials/systems. As has been demonstrated in previous chapters our MD simulations of bulk 5CB phases have shown

that we are able to accurately capture the thermodynamic, dynamic, and structural properties,[22] while previous works[23–29] involving aqueous and surfactant systems have provided the validated force field components necessary for simulation of those portions of a 5CB/water interface. Therefore, here we investigate several 5CB interface systems as a natural extension of modeling of this LC material. In this work, we have extensively investigated the interfacial anchoring behavior of 5CB in contact with three different surface environments: the free surface in vacuum, water, and water with cationic surfactant. Simulations have been performed in both the nematic and isotropic phases, using the all-atom MD simulations, with sufficient simulation time scale to capture the anchoring transitions of 5CB mesogens at all three surfaces.

4.2. Methodology

4.2.1 Force Field Development

In this work, the parameterization of the 5CB force field was carried over from our previous study on the properties of bulk 5CB as discussed in Chapter 2. For simulations of interfaces we selected the *modT*_NP and *modD*_NP force field in this work to study the anchoring effect of 5CB. The water model used was the standard TIP4P 2005 model[30] while the surfactant models were taken from the APPLE&P force field, with BF_4^- being explicitly present and the parameters for the decyltrimethylammonium (C_{10}TAB) cationic species being derived from transferrable potentials originally developed for pyrrolidinium based ionic liquids.[31] In order to allow for interactions between water and other species, an effective exp-6 water potential which may be employed with our APPLE&P potentials via mixing rules was fit against *ab initio* approach paths for 1 or 2 water molecules to BF_4^- and

imidazolium cation. Further empirical adjustments of water-ionic interactions were made until thermodynamics of bulk aqueous BF_4^-/imidazolium solutions was achieved.

4.2.2 Simulation Protocol

To study the interfacial anchoring behaviors of 5CB, three different surface systems comprised of free surface in vacuum, pure water and surfactants in aqueous solution were created (see Figure 4.1 for molecule models). For the free surface system, the simulations were carried out in an NVT ensemble with a rectangular box with fixed X, Y, and Z of dimensions of 35Å, 35Å, and 180Å, respectively. The water interface systems were run in the NPT ensemble with the same X and Y dimensions, and fluctuations of cell dimension only allowed in Z direction. The Z dimension of the box was between 183Å and 200Å depending on the temperature. The size of the water layer was sufficiently large to achieve bulk water density in the middle of water layer, indicating that the interfaces are completely independent of each other. Periodic boundary conditions were employed for all systems. The 5CB phase in each system was comprised of 384 molecules (14592 atoms), while the water and surfactant phases are comprised of 2048 and 64 molecules, respectively. The surfactant used in this study was C_{10}TAB. All simulations were conducted using our in-house molecular simulation software.[32] The Ewald summation method[33] was used for electrostatic interactions between partial atomic charges, while the velocity-Verlet form of the SHAKE algorithm[34] was employed to constrain bond lengths. All van der Waals interactions and the real part of the electrostatic interactions in the Ewald summation were cut off at 10 Å. A multiple timestep integration method[35] was employed with three different time scales: a short timestep of 0.5 fs for intramolecular interactions (bonding, bending,

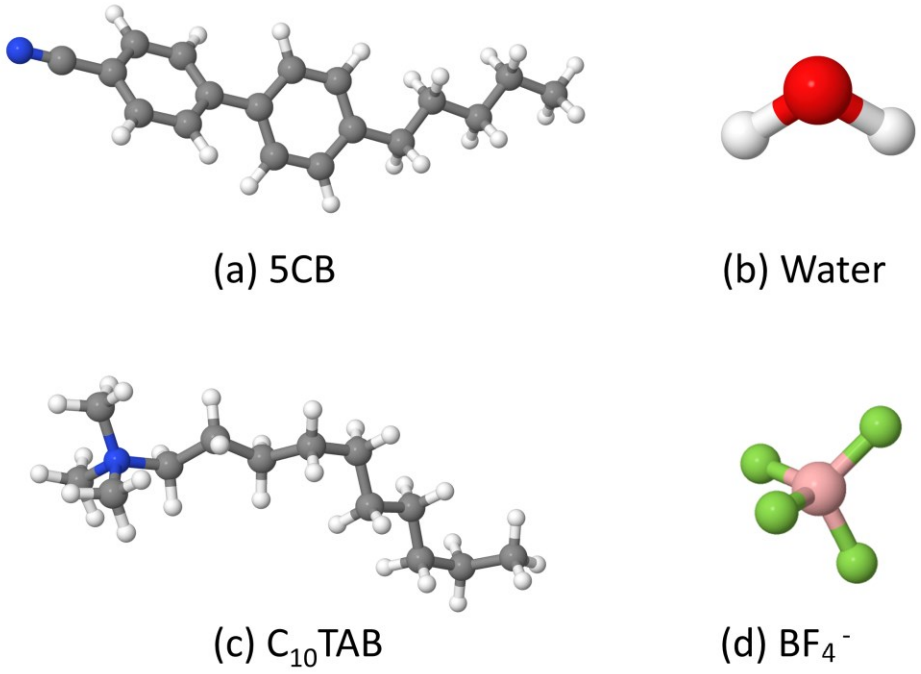

Figure 4.1. Chemical structure and notation of molecules used in MD simulations of interfaces.

dihedral, and out-of plane deformation motions), a medium timestep of 1.5 fs for dihedral and short-range (7.0 Å) nonbonded interactions, and a large timestep of 3 fs for full-range nonbonded interactions and the reciprocal part of electrostatic interactions. A thermostat and barostat[35] were used for temperature and pressure control in the NPT ensemble with frequencies of 0.01/fs and 0.005/fs, respectively.

All three interface systems were initially prepared at 308 K with the bulk 5CB in a stable nematic phase with order parameter around 0.7. We then duplicated each system and increased the temperature to 340 K to create conditions that favored the isotropic phase in the 5CB bulk. The production run times for each system were more than 200 ns. Such

trajectory length was long enough for 5CB molecules to reach the diffusive regime. With respect to the water/surfactant systems, the C_{10}TAB were initially placed at the surface in a roughly expected configuration, with the hydrophilic end in the water phase and hydrophobic tail in the 5CB phase in order to circumvent potential difficulties with surfactant self-assembly (micellization) in the aqueous phase as well as potential kinetic effects of surfactant penetration into the LC phase. The anionic BF_4^- counterions were initially placed in the water.

4.3 Results and Discussion

In order to investigate the LC anchoring effect at the interface and in the bulk, the simulation box has been partitioned into 50 thin slabs along the Z direction and the origin positioned at the center of mass of the bulk 5CB phase to ensure symmetry in the analysis of density and order parameter profiles. Such division results in an average slab thickness of 3.6-3.8 Å depending on the system. Considering that the length of 5CB and C_{10}TAB is about 15 Å, this slab resolution is high enough to distinguish different moieties in the molecules of interest while still have enough statistics to keep the noise low.

4.3.1 5CB/Vacuum Interface

4.3.1.1 Local Number Density

We begin our study by examining a snapshot of equilibrated 5CB/vacuum system at 308 K (Figure 4.2a). Here, the nematic ordering can be clearly seen across the simulation box, while a pair of 5CB highlighted in red indicates one of the preferred interdigitating structural arrangements in the nematic phase. To gain a more quantitative insight into the

interfacial structure and anchoring, we calculated the local number density profile in Z direction for both the cyano and alkyl moieties in 5CB. Such calculations help to elucidate the positional ordering of 5CB both at the interface and in the bulk. To monitor the anchoring transition of 5CB at different phases, we analyzed the local number density profile at the beginning and the end of the simulation for both nematic and isotropic system. For 5CB in the nematic phase, comparing between Figure 4.2b and 4.2c, the free surface imposed symmetry breaking led to the formation of an interfacial layer with strong positional ordering (smectic-like) on both interfaces at the end of simulation, while elsewhere in the bulk the nematic ordering has been greatly enhanced, indicating that the whole bulk is now coupled to the homeotropic anchoring at the 5CB free surface. Such organized monolayers at the free surface have been predicted by both theory[36] and experiment.[37] For the 5CB system in isotropic phase, shown in Figure 4.2d, only slight layering can be identified by the end of the simulation run.

We also investigated the correlation between the conformation of 5CB and its anchoring behavior at the free surface, by using a modified biphenyl torsional parameter force field (*modT*). As indicated by Figure 4.3b, at the end of the anchoring transition, the "softer" torsional parameters in the *modT* force field allowed more pronounced positional ordering to be induced by the homeotropic anchoring near the interface, registering a number density magnitude of more than 4 atoms/nm^3 for the cyano group, whereas in simulations using the *modD* force field it was around 3.5 atoms/nm^3. Similar effect can also be seen in the isotropic systems in Figure 4.3c, while the homeotropic anchoring effect disappears after 30Å from the interface for both force fields, the positional order of *modT* force filed is still stronger than in the *modD* force field. To explain this phenomenon, we

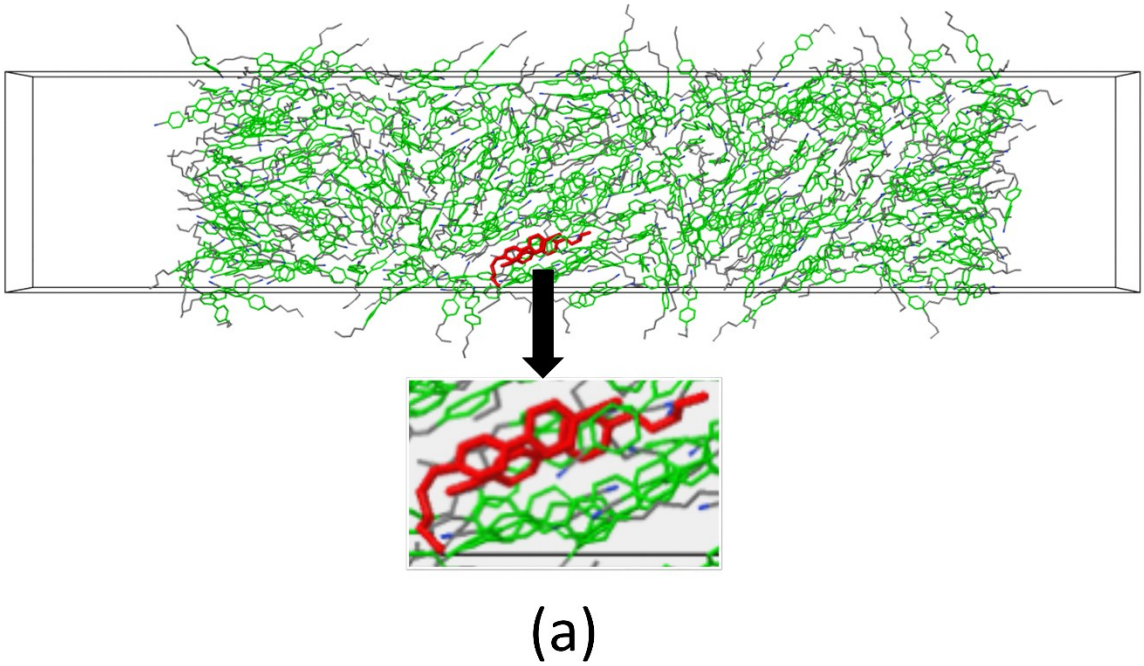

Figure 4.2. Panel (a): Snapshot of equilibrated 5CB/vacuum system at 308 K temperature, the pair of 5CB molecules highlighted in red (insert shown the zoom in picture) was chosen to show the interdigitating configuration typical for the nematic bulk phase. Panels (b – d): Local number density of cyano (black solid line) and alkyl groups (red dash line) of 5CB, (b) and (c) shows the number density profiles before and after the anchoring transition in the nematic. Panel (d) shows density profiles analyzed at the end of the simulation run. Results are obtained from simulations using *modD*_NP force field.

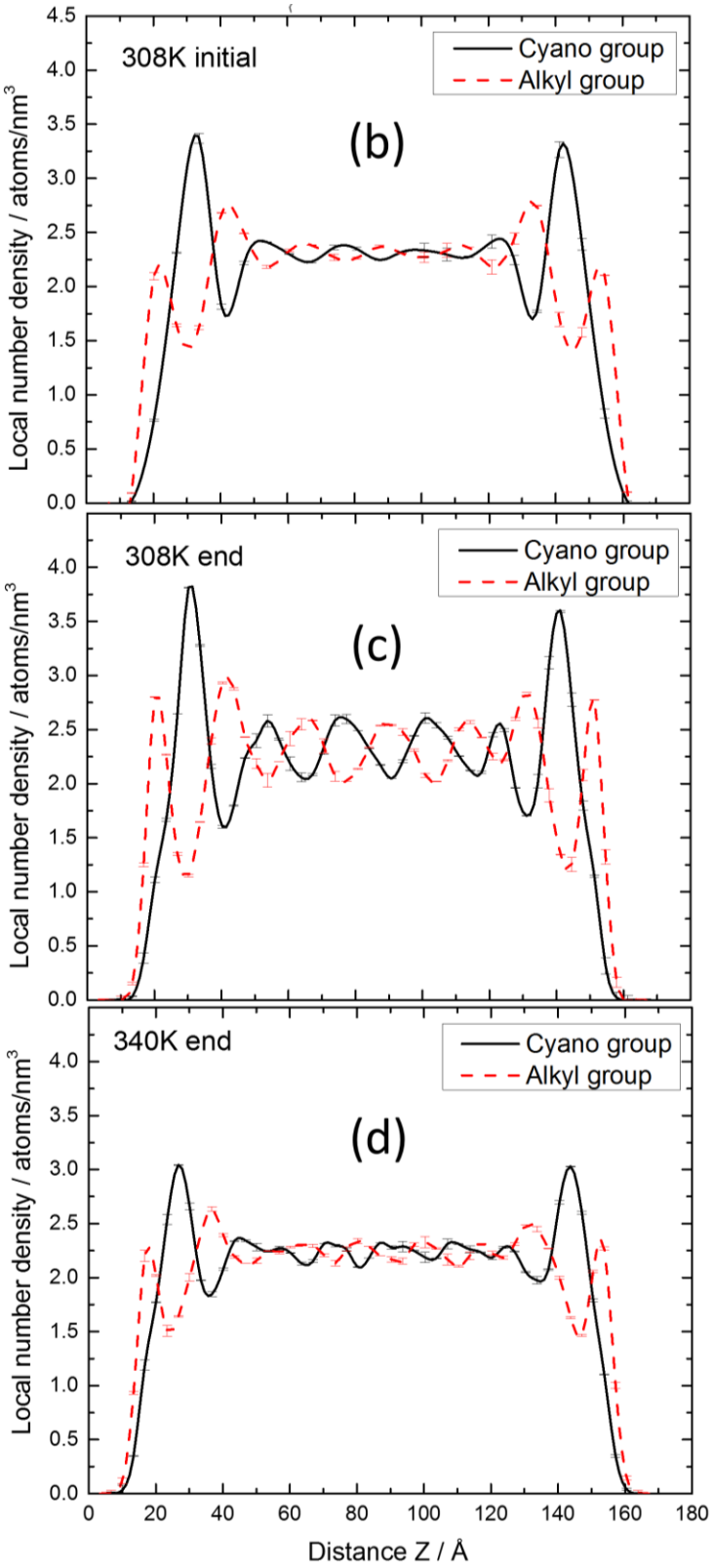

Figure 4.2 Continued.

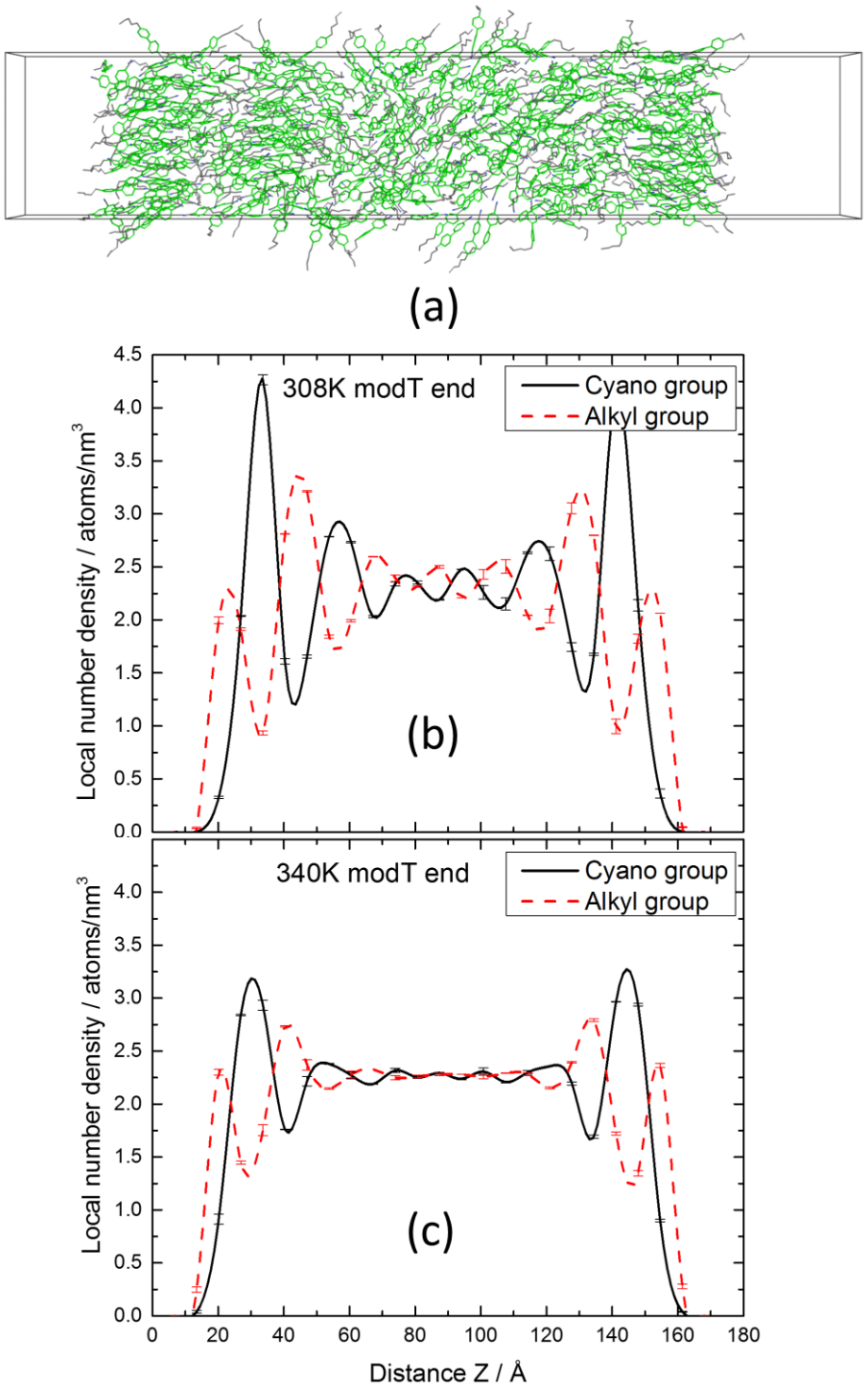

Figure 4.3. Panel (a): Snapshot of equilibrated 5CB/vacuum system at 308 K using *modT* force field. Panel (b – c): Local number density of cyano (black solid line) and alkyl groups (red dash line) of 5CB, (b) and (c) shows the influence of *modT* force field on the local number density of 5CB in nematic and isotropic phases.

postulate that the steric effect is enhanced by the "rounder" biphenyl group in the *modT* force field which is more energetically prohibitive for interdigitation to occur among 5CB molecules, and as a result, the head to tail configurations become more favorable, which leads to the formation of a bilayer structure close to the interface (Figure 4.3a).

Lastly, from the system snapshots in Figure 4.2a and local number density profile in Figure 4.2c and 4.2d, we can see that for both phases (isotropic and nematic) the alkyl tail of 5CB are exposed to vacuum, which is in good agreement with experimental observations.[2] Here we should add that the smectic-like layers were never formed in our previous study[22] of bulk 5CB using either of the force fields. This observation shows once again the sensitivity of 5CB liquid structure to outside perturbations such as the anchoring effect in this case.

4.3.1.2 Local Order Parameter

To further understand the local structure, we have calculated the order parameter in each slab. The nematic order parameter S_2 is defined as the maximum eigenvalue corresponding to the average ordering tensor

$$S_{\alpha\beta} = \frac{1}{N}\sum_{i=1}^{N}\left(\frac{3}{2}\mu_{\alpha}^{i}\mu_{\beta}^{i} - \frac{1}{2}\delta_{\alpha\beta}\right), \quad (4.1)$$

where μ_{α}^{i} $(\alpha, \beta = x, y, z)$ are the Cartesian components of the molecular axis unit vector of molecule *i*. For LC molecules like 5CB we took the long axis of the biphenyl core as the axis of the molecule. The value of S_2 equal to 1 in a perfectly aligned system where all molecules are aligned along the director **n** and 0 in the isotropic system, and the corresponding maximum eigenvector represents the director **n** in the particular layer. However, due to the finite system size in typical MD simulations, the value of S_2 cannot

reach zero exactly, instead it approaches a small value around 0.1-0.2. To obtain better sampling statistics, we do not calculate the order parameter for the outmost slab at the interface when there are less than ten 5CB molecules. The calculation of local order parameter profiles as a function of distance along Z direction allows to directly monitor the transition of the orientational ordering. Together with the positional ordering information obtained from the local number density, this provides a better picture of the structure of the interface systems.

The local order parameter of the free surface system is shown in Figure 4.4a, where, after the completion of the anchoring transition, the homeotropic anchoring-induced layer at the interface led to an apparent increase of order parameter for both nematic and isotropic system. Compare to the bulk, the values of S_2 at the interface are about 50% and 30% higher in the nematic and isotropic system, respectively, and the thickness of the homeotropic interface is around 30Å for the both systems, which suggests the formation of a homeotropic bilayer structure of 5CB. Interestingly, the free surface induced homeotropic alignment helped the isotropic system to sustain a higher order parameter of about 0.3 in the bulk, compare to our previous study on the bulk 5CB systems using the same *modD* force field which yield S_2 value of ~0.1. Such results are in good agreement with experimental measurements,[37,38] where excess orientational order is observed at the interface near T_{NI}. We also compared the anchoring behavior of 5CB of different shapes using the *modT* force field, however, the results suggest that the orientation ordering is insensitive to the details of dihedral potential of 5CB molecule.

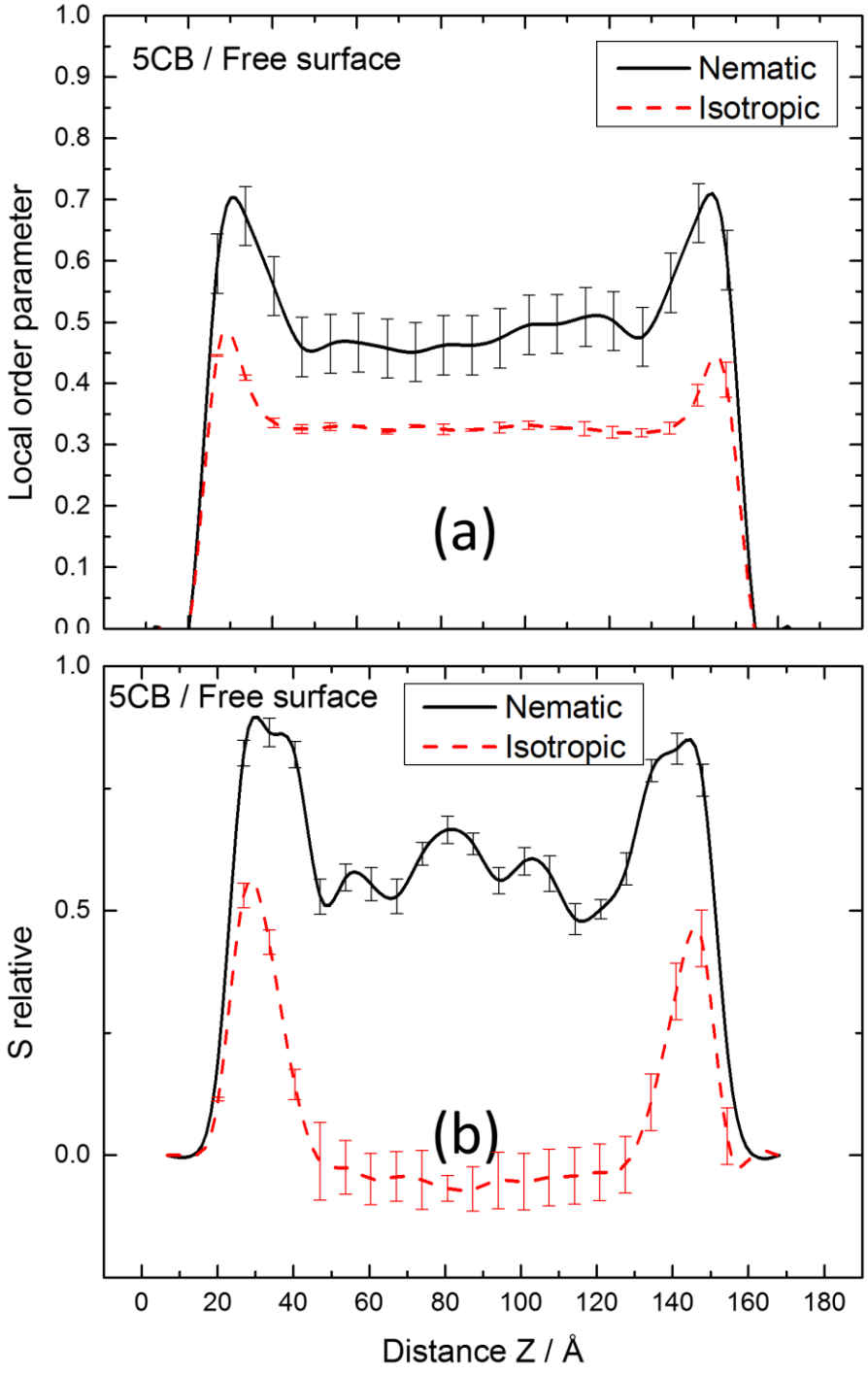

Figure 4.4. Order parameter profile (a) and relative order parameter (b) of 5CB vacuum interface system calculated in each slot for both nematic and isotropic phase systems.

4.3.1.3 Relative Polar Order Parameter

To study the 5CB anchoring effect more closely, in addition to the positional and orientational ordering information obtained by the local number density and local order parameter calculation, we also need to know the state of alignment of 5CB molecules. Due to the rotational symmetry of the nematic phase, this angular information need to be obtained from the calculation of relative order parameter between the 5CB molecules and the interface normal, the alignment is defined as

$$S_{relative} = \frac{1}{2}\langle 3cos^2\psi - 1\rangle \quad (4.2)$$

where ψ is the zenithal angle between the long axis of 5CB and the interface normal (coincide with Z axis), $S_{relative}$ = 1 if the alignment is parallel, -0.5 if they are perpendicular and $S_{relative}$ = 0 for degenerate state where the orientations of 5CB molecules are entirely random. The $S_{relative}$ gives unambiguous information on the alignment compared to direct angle calculation.

As shown in Figure 4.4b, for the nematic system, after the homeotropic anchoring transition has reached equilibrium state, the value of $S_{relative}$ close to the free surface is about 0.9, indicating the local director there align almost perfectly parallel to the Z axis, and the average alignment of the director is about 30° in the bulk. Compare to the initial configuration, the easy axis of 5CB at the interface became more parallel to the interface normal while the angle of between Z and the bulk easy axis has shifted from about 50° to 30° due to the anchoring effect. And for the system in isotropic phase, $S_{relative}$ is lower at the interface compare to the nematic system, and the value of $S_{relative}$ suggests a tilted alignment, while in the bulk $S_{relative}$ is about to 0, which correspond to a random distribution of local director. These observations of 5CB anchoring alignments at the free surface in the

isotropic phase are in good agreement with experimental observations[38,39], where the presence of a nematic layer was found between the isotropic 5CB and vapor interface.

4.3.2 5CB/Water Interface

4.3.2.1 Local Number Density

After initial 3 ns run, where water was brought in contact with 5CB previously equilibrated at vacuum interface, we visually examined the water system to obtain a qualitative picture of the effect of water molecules on the anchoring of 5CB in nematic phase. As can be seen from Figure 4.5a, the 5CB molecules at the interface reoriented to form a flat layer parallel to the interface. To have a quantitative understanding of this phenomenon we again resorted to the local number density calculation. Figure 4.5b and 4.5d shows the local number density of 5CB/water interface systems in nematic and isotropic temperatures after anchoring transition (i.e., at the end of a 200 ns simulation run). Compare to the vacuum interface system, several differences immediately became evident. First, at the water interface the number densities of cyano and alkyl groups are very close to each other, both in terms of absolute values and distribution. This anchoring behavior of 5CB is significantly different than at the free surface, where the alkyl group were exposed into the vacuum phase even at high temperatures. Taking into account the rod-like molecular structure of 5CB, these density profiles suggest the formation of planar layer at the interface, Figure 4.5a can also help to visually confirm the planar layer. Second, from Figure 4.5b, one can see that the nematic ordering is well preserved in the bulk phase at low temperature, whereas the homeotropic anchoring in the 5CB/vacuum interface led to enhanced nematic ordering in the bulk. Thirdly, we note that planar anchoring alignment

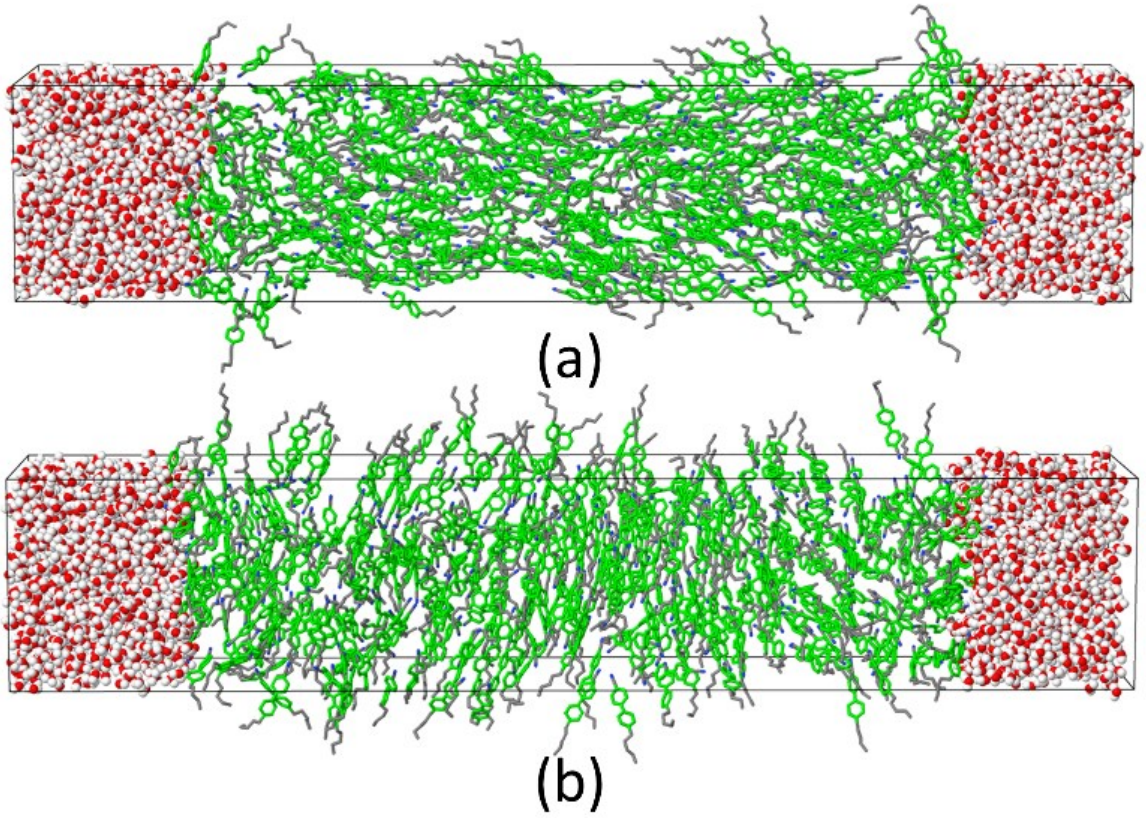

Figure 4.5. Panels (a - b): Snapshots of 5CB/water interface systems at 308 K, initial system configuration (a) and after 200 ns of simulations (b). Panels (c - d): Local number density of cyano (black solid line), alkyl groups (red dash line), and water (blue dots) for the 5CB/water interface system in the nematic (c) and isotropic (d) phases after anchoring transition.

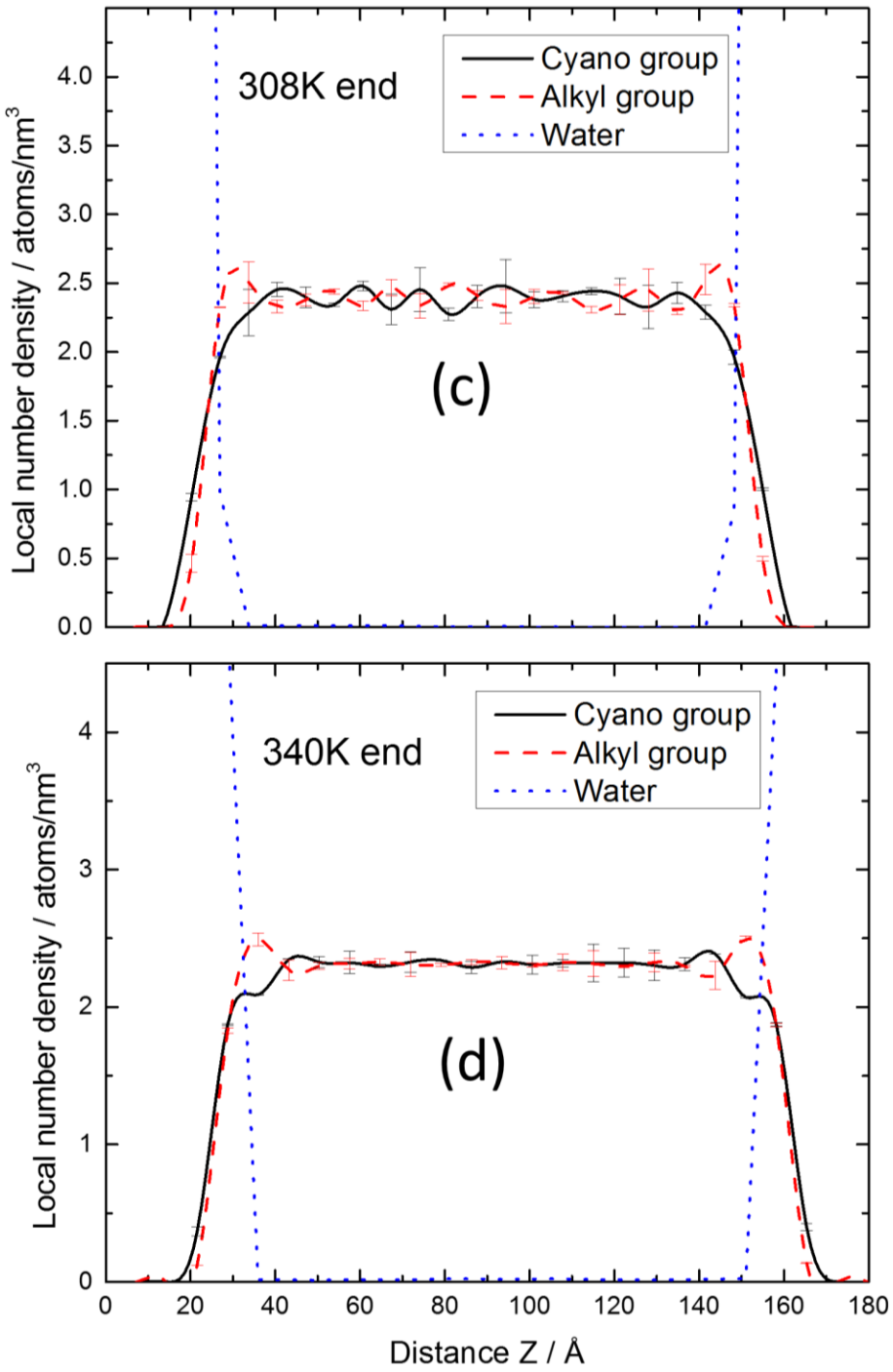

Figure 4.5 Continued.

persists even in the high temperature 340 K isotropic phase system, shown in Figure 4.5d by the lack of separation in Z between the cyano and alkyl groups, such result is in qualitative agreement with experimental observation.[11]

4.3.2.2 Local Order Parameter

Figure 4.6a shows the orientational ordering of 5CB in contact with water after equilibration. At the water interface, the 5CB molecules in both nematic and isotropic states exhibit spontaneous formation of isotropic layers, the value of S_2 is about 0.35 for both cases, indicating that the planar anchoring of 5CB at the interface is in homogeneous degenerate state where all possible tangent alignments to the interface are energetically equivalent. Such phenomenon is also supported by previous experimental studies.[1,40,41] The thickness of the planar interface is about 30Å and after that the orientational ordering of the nematic phase is quickly regained showing an order parameter of 0.75. Both effects can be visually confirmed in Figure 4.6a. For the high temperature system, we see a consistent isotropic behavior in all layers. Similar orientational behavior was found in the *modT* force field, which suggests that the conformational distribution of 5CB is less important for the anchoring effect. Here we notice an interesting phenomenon from the positional and orientational ordering information obtained from local number density and local order parameter calculation for the nematic phase system. The mesogens in the highly ordered nematic bulk and at the isotropic interface all have the planar alignment (consistent with the local number density profiles), yet the difference in order parameter values at the interface and in the bulk suggests that some preferred directions for 5CB mesogens exist in the bulk. To illustrate this we turn to the analysis of relative order parameter.

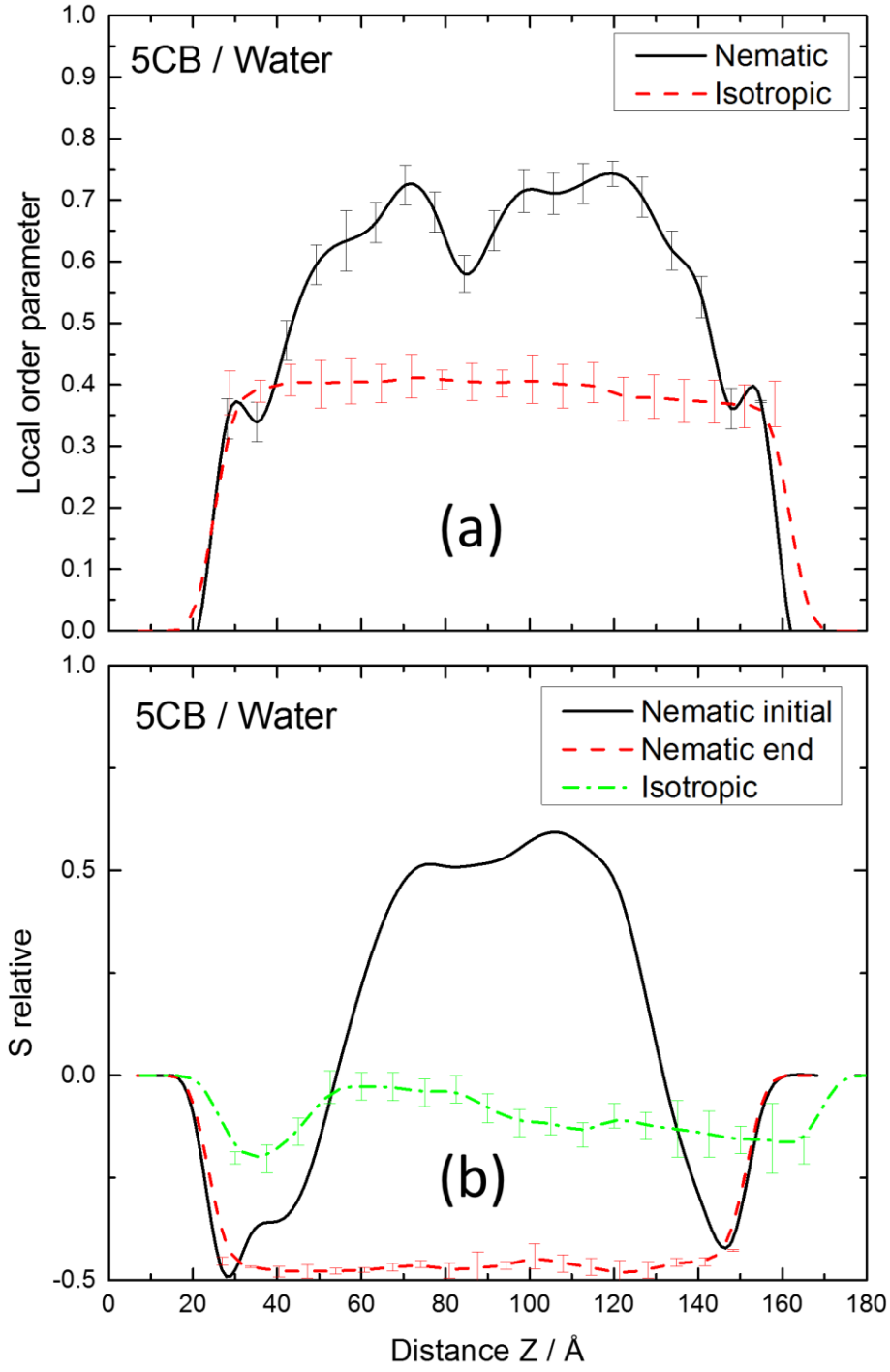

Figure 4.6. Order parameter profile (a), and relative order parameter (b) of 5CB/water interface system calculated in each slot, respectively, for both nematic and isotropic phase systems. In panel (b) we also show the different director field alignments before and after the anchoring transition.

4.3.2.3 Relative Polar Order Parameter

The presence of water molecules at the surface has led to drastic changes of the molecular organization of 5CB, both at the interface and in the bulk, as shown in Figure 4.5a. To study this planar anchoring transition more closely, we have compared the initial and post transition relative ordering of 5CB in nematic phase, as shown in Figure 4.6b. Before the anchoring equilibrium was reached, only mesogens in the interfacial region of ~30Å had a preferred perpendicular alignment with respect to the interface normal, i.e. the value of $S_{relative}$ close to -0.5, while outside of the interface region, the planar anchoring was lost as the average director of 5CBs showed a tilted easy axis of around 50° relative to the Z axis, which is the same as the initial condition of 5CBs in the bulk of the free surface system. In order to accommodate such distortions of director field, the mesogens must sustain both splay and bend strains, therefore making this arrangement as energetically unfavorable, and therefore, a reorientation of the director field in the bulk is expected. Indeed, as shown in Figure 4.5b, after the system equilibrated for more than 200 ns, we observed that the director field across the entirety of the box rearranged to display planar alignment, with $S_{relative}$ of -0.5 throughout the box.

Combining the information from the analysis of density and order parameters profiles together, we can summarize a complete picture of the effect of planar anchoring of 5CB at the water surface: After the transition all molecules adapt a planar configuration that is parallel to the interface, but as the local order parameter profile indicates, rather than adapting to the degenerate planar anchoring as at the interface, the mesogens in the bulk have a preferred orientational ordering. This tilted to planar anchoring transition of the easy axis in the bulk can be explained by the Frank-Oseen elasticity model,[42] where the

discontinuous transition of director field between these two alignments requires both splay and bend deformations. Compare to the twist deformation, the splay and bend deformations are 2-10 times more energetically prohibitive,[43] therefore from the free energy point of view, the 5CB molecules in the bulk must adopt the planar anchoring of the interface. After the tilted to planar transition, the nematic alignment tendency have led to the re-establishment of a preferred orientational ordering, and transition region deformation (degenerate to nematic) is absorbed by the much weaker twist strain. It is also worth to point out that the recovery of nematic ordering while maintaining the overall director parallel to the surface implies that the bulk 5CBs are not bound to the surface layer by finite size effects, but instead, due to the translational restriction of the LC being pinned at the surface a true-2D "nematic" system is formed in the bulk, which also includes the destruction of the long-range ordering. For the isotropic phase system, due to high temperature, we notice significant fluctuations of relative order parameter profile throughout the production run, so we averaged the $S_{relative}$ using the entire trajectory. Shown in Figure 4.6b as green dash dot line, the values of $S_{relative}$ are close to 0 in the bulk, while showing limited planar anchoring behavior near the water surface, indicating the random distortions of the director field throughout the system.

4.3.3 5CB/Water/Surfactant Interface

4.3.3.1 Local Number Density

Encouraged by the success of our simulations in reproducing both the homeotropic and planar anchoring effect at the vacuum and pure water interface systems, we continued with investigation of the influence of amphiphilic surfactants on the anchoring behavior of 5CB

at aqueous solution interface. Experimentally, the classical surfactant family, alkyltrimethylammonium halides (C_nTABs, n > 8) is known to cause homeotropic anchoring for 5CB at the aqueous-liquid crystal interface, while the C_nTABs with shorter alkyl tails (n < 8) do not induce the orientation change for 5CB at the interface.[12] The tail length dependence of the anchoring behavior indicates that the interactions between the surfactant's alkyl tail and the 5CB play an important role in the anchoring reorientation at the interface.[11]

Starting from the 5CB/water system, we placed the C_{10}TAB surfactants at the interface at 308 K, which as discussed previously has a planar anchoring alignment. After more than 300 ns production run to allow reorientation to occur, we observed that, according to the system snapshot in Figure 4.7a as well as the positional ordering information provided by the local number density calculation shown in Figure 4.7b, the 5CB molecules at the aqueous-LC interface with C_{10}TAB had reoriented to a nematic structure, which means that the mesogens experienced planar to either homeotropic or tilted anchoring transition. For the isotropic system at 340 K Figure 4.7c suggests that the addition of surfactant also caused the anchoring transition to occur. Compare between the homeotropic anchoring behavior of 5CB at the vacuum free surface (Figure 4.2a) and in the aqueous solution (Figure 4.7a), one significant difference can be directly observed from the relative positions of 5CB moieties in terms of anchoring effect: instead of exposed alkyl group to the surface in the vacuum, the cyano group of 5CB is now exposed to the aqueous phase. Also indicated by Figure 4.7b and 4.7c is that both the positively charged hydrophilic C_{10}TAB head groups and the cyano group of 5CB are in direct contact with the water molecules, an effect due to the favorable direct electrostatic interactions (both water and the cyano moiety

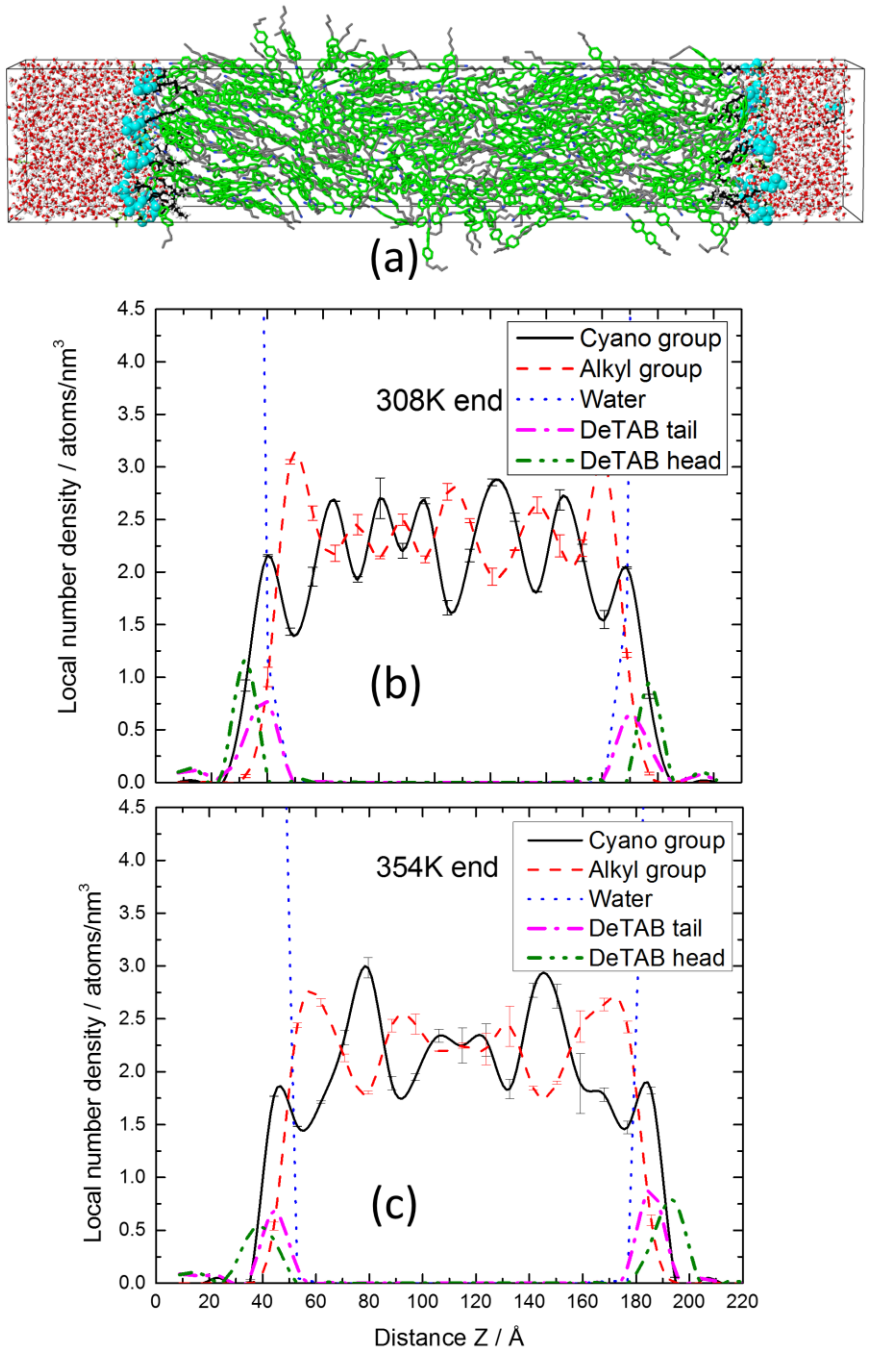

Figure 4.7. Snapshots of 5CB interface system with 5CB/aqueous solutions of C_{10}TAB at 308 K (a), showing surfactant C_{10}TAB induced homeotropic anchoring of 5CB at the aqueous interface. The cyan and black colors mark the head and tail group of C_{10}TAB, it can be seen that the hydrophobic tail of C_{10}TAB is inside the 5CB – aqueous interface while its hydrophilic head is inside water phase. Panels (b - c): Local number density of cyano (black solid line), alkyl groups (red dash line), water (blue dots), C_{10}TAB head (pink dash dot) and tail (green dash dot dot) of the 5CB/Water/Surfactant Interface systems in the nematic (b) and isotropic (c) phases.

are polar and the anion $BF4^-$ of the cationic $C_{10}TAB$ are well shielded by the surrounding water, therefore leaving the cationic surfactant to interact directly with the cyano groups of 5CB). As a consequence of such structural correlation, the strong interdigitation effect between the alkyl tail groups of 5CB and $C_{10}TAB$ is observed which is consistent with experiments.[10,12] Inside the LC bulk, both nematic (Figure 4.7b) and isotropic (Figure 4.7c) systems exhibit enhanced positional order. We postulate that such effect is due to the stronger anchoring effect induced by the presence of surfactant molecules.

4.3.3.2 Local Order Parameter

To further elucidate the homeotropic anchoring we again calculated the order parameter profile as a function of Z direction. As shown in Figure 4.8a, for the nematic phase, compare to the vacuum interface system, the aqueous-LC interface system exhibits a much higher order parameter of 0.7 - 0.8 throughout the simulation box, suggesting a highly aligned director field in every statistic slot. Based on the slight decrease of S_2 in the bulk, we estimate the homeotropic anchoring coherence length in 5CB/water/surfactant system to be about 50Å, which is much longer than both vacuum and water interface system. The enhanced anchoring effect can be attributed to the tail interactions where the homeotropically aligned neutral tail of $C_{10}TAB$ impose its orientational order to the alkyl tails of 5CB at the interface through van der Waals and steric interactions. For the isotropic system also shown in Figure 4.8a, the director field in every slab is still slightly ordered (in our bulk 5CB study the typical value of S_2 at such high temperature is about 0.1), suggesting that the strong homeotropic anchoring effect helps to stabilize the nematic ordering of 5CB at the interface and in the bulk.

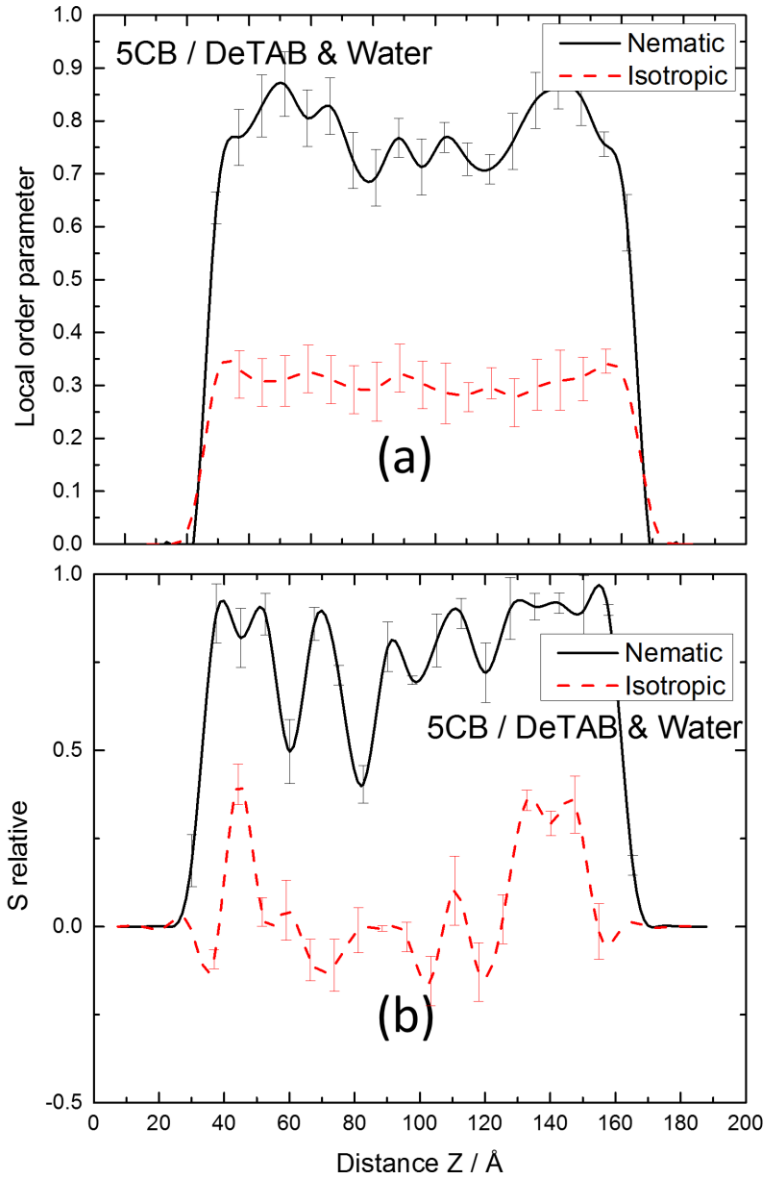

Figure 4.8. Order parameter profile (a) and relative order parameter (b) of the aqueous solution system calculated in each slot for both nematic and isotropic phase systems.

4.3.3.3 Relative Polar Order Parameter

To have a better picture of the planar to homeotropic anchoring transition at the LC-aqueous interface after the addition of C_{10}TAB, we now turn to the relative order parameter profile. The comparison between Figure 4.8b and Figure 4.6b shows that after 300 ns the surfactant molecules have fully reoriented the director field of 5CB in the nematic temperature, with the preferred anchoring direction again almost perfectly parallel to the surface normal near the interface (Figure 4.7a). The slight decrease of $S_{relative}$ further implies that the LC molecules in the transition region of the bulk are under elastic strains due to the competing forces exerted by both the interface homeotropic anchoring and the bulk nematic director field, which has the same easy axis of about 30° as the free surface system. For the isotropic temperature system, the value of $S_{relative}$ is close to 0 in the bulk, suggesting that there is no preferred alignment relative to the Z direction. However, at the interface we can still see a slight increase of $S_{relative}$ due to the homeotropic anchoring induced by the surfactant.

4.4 Conclusion

In this chapter, we discussed results of all-atom MD simulation utilizing non-polarizable force field to study the anchoring effect of 5CB, both in nematic and isotropic phases, at three different interfaces. The results show that overall our force field correctly predicts the qualitative anchoring effects observed in 5CB in contact with vacuum, pure water, and aqueous solutions of C_{10}TAB. For the free surface system, a small change of the biphenyl torsional parameter of 5CB are shown to lead to stronger positional ordering both at the interface and in the bulk, which again show the extreme sensitivity of 5CB to

small perturbations. Both for the nematic and isotropic temperatures, the homeotropic anchoring created an interfacial layer with strong positional ordering, with alkyl tail of 5CB being exposed in the vacuum phase, and in the bulk, the elastic force of homeotropic anchoring created a distortion of director field for nematic system whereas the isotropic system exhibits a random distribution of the director field. For the pure water interface with nematic 5CB, a complete homeotropic to planar anchoring transition occurred, as the preferred axis of 5CB gradually shifted from parallel to perpendicular alignment with respect to the interface across the box. At higher temperature, the bulk remains isotropic, consistent with the Frank-Oseen theory. Lastly, the investigation of 5CB-C_{10}TAB in aqueous solution interfacial ordering shows that our simulations are fully capable of capturing the crucial planar to homeotropic anchoring reorientation of 5CB in a very complex four component environment. Molecular scale analysis have demonstrated that the alkyl tail interactions between 5CB and C_{10} TAB are responsible for the homeotropic anchoring effect, which is consistent with experimental observtions[10,11]. Ultimately, the successful reproduction of the anchoring behavior of 5CB at different interfaces has paved a way for future studies on the LC interface anchoring mechanisms with variety of other components (other surfactants, different solutes, biomolecules, etc.) and can become as an invaluable tool for developing better LC-based sensors.

4.5 References

[1] B. Jerome, Reports Prog. Phys. **54**, 391 (1991).

[2] V. Nazarenko and A. Nych, Phys. Rev. E. **60**, R3495 (1999).

[3] H. Kasten and G. Strobl, J. Chem. Phys. **103**, 6768 (1995).

[4] H. Hsiung and Y.R. Shen, Phys. Rev. A **34**, 4303 (1986).

[5] J.W. Kim, H. Kim, Lee Myoungbae, and J.J. Magda, Langmuir **20**, 8110 (2004).

[6] D.P.E. Smith, J.K.H. Hörber, G. Binnig, and H. Nejoh, Nature **344**, 641 (1990).

[7] D.P.E. Smith and W.H. Heckl, Nature **346**, 616 (1990).

[8] J.M. Brake, M.K. Daschner, Y-Y. Luk, and N.L. Abbott, Science **302**, 2094 (2003).

[9] A.D. Price and D.K. Schwartz, J. Am. Chem. Soc. **130**, 8188 (2008).

[10] J.M. Brake and N.L. Abbott, Langmuir **18**, 6101 (2002).

[11] N.A. Lockwood, J.J. De Pablo, and N.L. Abbott, Langmuir **21**, 6805 (2005).

[12] J.M. Brake, A.D. Mezera, and N.L. Abbott, Langmuir **19**, 6436 (2003).

[13] P.D.I. Fletcher, N.-G. Kang, and V.N. Paunov, Chemphyschem **10**, 3046 (2009).

[14] J.M. Brake and N.L. Abbott, Langmuir **23**, 8497 (2007).

[15] J.K. Gupta, M.-V. Meli, S. Teren, and N.L. Abbott, Phys Rev Lett **100**, 48301 (2008).

[16] D. Hartono, X. Bi, K.-L. Yang, and L.-Y.L. Yung, Adv. Funct. Mater. **18**, 2938 (2008).

[17] R.B. Meyer, Phys. Rev. Lett. **22**, 918 (1969).

[18] J. Prost and J.P. Marcerou, J. Phys. **38**, 315 (1977).

[19] A.D. Rey, Langmuir **20**, 11473 (2004).

[20] M.J. Uline, S. Meng, and I. Szleifer, Soft Matter **6**, 5482 (2010).

[21] C. Bahr, Phys. Rev. E **73**, 030702 (2006).

[22] X. Wei, J.B. Hooper, and D. Bedrov, Liq. Cryst. **ASAP**, (2016).

[23] D. Bedrov, O. Borodin, Z. Li, and G.D. Smith, J. Phys. Chem. B **114**, 4984 (2010).

[24] J.B. Hooper, G.D. Smith, and D. Bedrov, J. Chem. Phys. **139**, 104503 (2013).

[25] J.B. Hooper, O.N. Starovoytov, O. Borodin, D. Bedrov, and G.D. Smith, J. Chem. Phys. **136**, 194506 (2012).

[26] D. Bedrov and O. Borodin, J. Phys. Chem. B **114**, 12802 (2010).

[27] D. Bedrov, M. Pekny, and G.D. Smith, J. Phys. Chem. B **102**, 996 (1998).

[28] D. Bedrov, G.D. Smith, K.F. Freed, and J. Dudowicz, J. Chem. Phys. **116**, 4765 (2002).

[29] G.D. Smith and D. Bedrov, J. Phys. Chem. B **107**, 3095 (2003).

[30] J.L. Abascal and C. Vega, J. Chem. Phys. **123**, 234505 (2005).

[31] O. Borodin, J. Phys. Chem. B **113**, 11463 (2009).

[32] The WMI molecular dynamics simulation package is available free of charge. For more information, please contact info@wasatchmolecular.com.

[33] U. Essmann, L. Perera, M.L. Berkowitz, T. Darden, H. Lee, and L.G. Pedersen, J Chem Phys **103**, 8577 (1995).

[34] B.J. Palmer, J. Comput. Phys. **104**, 470 (1993).

[35] G.J. Martyna, M.E. Tuckerman, D.J. Tobias, and M.L. Klein, Mol. Phys. **87**, 1117 (1996).

[36] C.A. Croxton and S. Chandrasekhar, Pramana Suppl. **1**, 237 (1975).

[37] M.G.J. Gannon and T.E. Faber, Philos. Mag. A **37**, 117 (1978).

[38] S. Immerschitt, T. Koch, W. Stille, and G. Strobl, J. Chem. Phys. **96**, 6249 (1992).

[39] D. Beaglehole, Mol. Cryst. Liq. Cryst. **89**, 319 (1982).

[40] R. A. Drawhorn, N.L. Abbott, J. Phys. Chem. **99**, 16511 (1995).

[41] D. Demus and L. Richter, Textures of Liquid Crystals, 1st ed. (Wiley-VCH Verlag, 1980).

[42] F.C. Frank, Discuss. Faraday Soc. **25**, 19 (1958).

[43] M. Majumdar, P. Salamon, A. Jákli, J.T. Gleeson, and S. Sprunt, Phys. Rev. E - Stat. Nonlinear, Soft Matter Phys. **83**, 1 (2011).

CHAPTER 5

TEMPERATURE DEPENDENCE OF THE NOVEL TWIST-BEND NEMATIC PHASE OF THE CYANOBIPHENYL DIMER CB7CB – AN ATOMISTIC SIMULATION STUDY

5.1 Introduction

Recently, a collaborative work between experimental efforts at University of Colorado Boulder and our group has directly confirmed the existence of the new type LC phase,[1] the so called twist-bend nematic (N_{TB}) phase which was first conjectured in theory by Meyer,[2] Dozov[3] and Memmer.[4] Such discovery marks the fifth nematic phase being observed in LC materials since the discovery of the uniaxial nematic phase (N) in the 19th century. Several earlier experiments[5–9] have observed that nematogen dimers connected with odd number of carbons flexible chains in typical nematic phase transitioned to a lower temperature new nematic phase with different textures. However it was not until the freeze-fracture transmission electron microscopy (FFTEM) images obtained in Chen's work[1] that we have conclusive structural evidence for the existence of this novel phase for the nematogen dimer cyanobiphenyl-$(CH_2)_7$-cyanobiphenyl (CB7CB). Specifically, the obtained FFTEM images show 2D curved domains with periodically spaced layers that correspond to a 3D focal conics domains structure with pitch of around 8 nm, which is orders of magnitude less than the chiral N* phase. In the images the fracture plane runs

predominately normal to the helix layers (periodic stacking of sheet-like structures in 3D), therefore ruling out the possibility of smectic C* (SmC*) phase, where the fracture plane tends to be parallel to the layers. To further differentiate between the N_{TB} and SmC* phases, X-ray scattering analysis was performed and the result showed no Bragg peak, which is consistent with a nematic phase behavior where the electron density is uniform. Also from the fracture plane images, a complete 360° rotation of CB7CB molecules around the helix is observed, this consequently ruled out the N* phase where molecules are perpendicular to the helix axis. To mathematically describe the helix structure formed in the N_{TB} phase, one can define a conical polar angle θ and azimuthal angle φ for the spontaneously twisted director **n**, and where **Z** is a vector parallel to the helix axis. The helix pitch P_{TB} and the wavevector **q** are inversely related through $q=\pm 2\pi/P_{TB}$ and, the sign of the wave vector q is used to distinguish the chirality of the helix.

In order to better understand the N_{TB} phase, investigations towards different properties of CB7CB were conducted both experimentally and via simulations. Meyer et al.[10] measured the temperature dependence of the heliconical tilt angle of CB7CB in N_{TB} phase using optical birefringence technique. Their results showed that the tilt angle monotonically increases from 9° at the N–N_{TB} transition temperature of 100°C, to about 37° at 50°C. In the N_{TB} phase the obtained birefringence changes smoothly as a function of temperature and the process is fully reversible without any hysteresis. This characteristic proves that CB7CB formed N_{TB} is a true nematic phase, as opposes to "soft crystal" or "glassy-nematic" suggested by others.[11] Cristina et al.[12] demonstrated the formation of helical structure using a rigid crescent-shaped particle model with generalized Onsager theory of repulsive pair interactions. They concluded that the spontaneous chiral symmetry

breaking is entropy driven, specifically when compare to normal nematic ordering, the excluded volume is smaller as the particles rotate and propagate along the helix axis in the helical arrangement of N_{TB}, and the N–N_{TB} phase transition are primarily determined by shape of particles.

Currently there are two theories providing possible explanations for the formation of N_{TB} phase. In Meyer's model[2] he attributed the transformation from uniaxial nematic to N_{TB} heliconical structure to the spontaneous ferroelectric coupling between polarization effect and bend deformation in the nematic phase. Later, Dozov[3] proposed a negative elasticity model where in a bent-shaped LC molecule the bend elastic constant K_3 could became negative (if the imposed elastic bend is stronger than splay and twist force) and twist-bend nematic ordering could form. In this theory, the twist motion of director **n** is imposed by the bend, resulting a "third dimension escape" of **n** from its geometrical constraints. The same theory was independently proposed by Memmer[4] based on results of Monte Carlo simulations.

To find the origin of N_{TB} phase at microscopic level, it is important to first understand that the shape of LC mesogen plays a significant role on the behavior and stability of a mesophase, through both short range steric effect and long range repulsion-dispersion interactions.[13] The chemical details control the average shape of a given mesogen, and therefore influence the aforementioned properties.[7] Typically, a LC molecule is comprised by rigid and a flexible moieties, it is the latter that enables the transformation of the mesogen shape, especially when the flexible part is located between the rigid parts. The flexible chain affects the shape by both length and parity, for a longer chain the so called odd-even effect[13] often arises from the parity difference, which can significantly affect the

phase transition enthalpy and entropy. The simplest examples related to the N_{TB} phase would be LC dimers with flexible chain in the middle, specifically, two cyanobiphenyl moieties linked together by either a hexane (CB6CB) or heptane chain (CB7CB). The energetically favored molecular conformation is different for CB6CB and CB7CB, where only the latter exhibits N_{TB} phase. Deeper insight to this effect is obtained through our atomistic MD simulations of these two dimers. After 15 ns equilibration run at 360 K, the CB7CB dimers exhibit strong preference toward the bend conformation, and the whole system transitioned into the N_{TB} phase. For the CB6CB dimer the lowest energy conformation is almost linear and the system remains in regular nematic phase. In the CB7CB system, as a result of the bend conformation, the combined effective dipole moment of the cyanobiphenyl groups on the opposite side is likely to be perpendicular to the helix axis. The direction of dipole moment promotes the director field to spontaneously tilt and twist around the helix axis at a constant precession. Aside from the direction of the dipole moment, the shape of LC can affect the elasticity as well. Via the continuous torsional potential surface interaction calculation of conformational distribution for the alkyl chain, Cestari et al.[7] showed that a negative bend elastic constant, K_3, exists for certain conformations of the achiral CB7CB. The negative K_3 promotes the spontaneous bending of the director to be energetically favored, thus enables the formation of the new ground state N_{TB}. Another implication of the achirality of CB7CB is the spontaneous chiral symmetry breaking required by N - N_{TB} phase transition, where the transition need to decompose into doubly degenerate helix domains with opposite chirality.

Although the current experimental observations seem to support the negative elasticity model (K_3 decrease to very low value near the N_{TB} transition as temperature drops,[7,9] the

short pitch of 8-9 nm,[1,14] etc.), the microscopic origin for the spontaneous chiral symmetry breaking from the achiral CB7CB and the mechanism for its propagation into the macroscopic level are still poorly understood by the LC and condensed matter community. The complex energetic and entropic interplay between the flexible achiral dimer and the chiral helix organization of molecules has made the investigations even more challenging. In this chapter we discuss preliminary results from our work-in-progress on the thermodynamic, structural and transport properties for CB7CB in N_{TB}, N, and isotropic phases using atomistic MD simulations. Specifically, since the defining characteristic of N_{TB} is the conical helicoid structure of the local director field controlled by the relative position of the two rigid cyanobiphenyl units, it is useful to analyze conformational and orientational properties of CB7CB.

5.2 Methodology

In this all-atom MD simulation work, each system contains 384 CB7CB mesogens (i.e. 24960 atoms) in a 3D periodic orthorhombic simulation cell. All interaction parameters are directly transferred from the *modD*_NP force field developed for in 5CB[15,16] and discussed in previous chapters. A multiple timestep integration method[17] was used for different types of interactions. The thermostat and barostat used for temperature and pressure control in the NPT ensemble had frequencies of 0.01 fs^{-1} and 0.005 fs^{-1}, respectively. Initially, the mesogens were set up on a regular low-density lattice, the system was then shrunk to the desired dimension, i.e., x, y dimensions about 5.6 nm and 8 nm for the z-direction. During this compression and the subsequent equilibration stage, the mesogens in the system were aligned the along the z axis by applying a biasing potential of weak forces to the cyano

groups at each end of the dimer, pulling them in the opposite directions (+z and -z). As a result, the initially equilibrated configurations were in a well-defined nematic phase with the director field aligned along the Z direction. Subsequently, the biasing potential was turned off and each system was simulated in the NPT ensemble with the x and y dimensions allowed to fluctuate to achieve the atmospheric pressure in the system, while z dimension was kept fixed. Simulations were carried out in the 360 - 420 K temperature range. Production runs were over 100 ns during which no drift in the system energy or order parameters were observed indicating stationary behavior of the targeted equilibrium conditions. The velocity-Verlet form of the SHAKE algorithm[18] was employed to constrain bond lengths. All van der Waals interactions and the real part of the electrostatic interactions in the Ewald summation were cutoff at 11Å.

5.3 Results and Discussion

First, we visually examine the snapshots of systems obtained from production simulations at 360, 390, and 420 K to confirm the formation of N_{TB}, N and isotropic phases, respectively, as shown in Figure 5.1. At 360 K the helix structure with right-handiness can be clearly observed in Figure 5.1a, while at 390 K we can see the uniaxial nematic ordering (Figure 5.1b). At 420 K, the snapshot in Figure 5.1c indicates the CB7CB bulk system has completely transitioned to an isotropic phase. While it is not the aim of this study, it is worth to point out that the transferred force field is in good qualitative agreement with observed experimental N_{TB} – N and N – I phase transition temperatures of 373 and 387.15 K, respectively.[10,19]

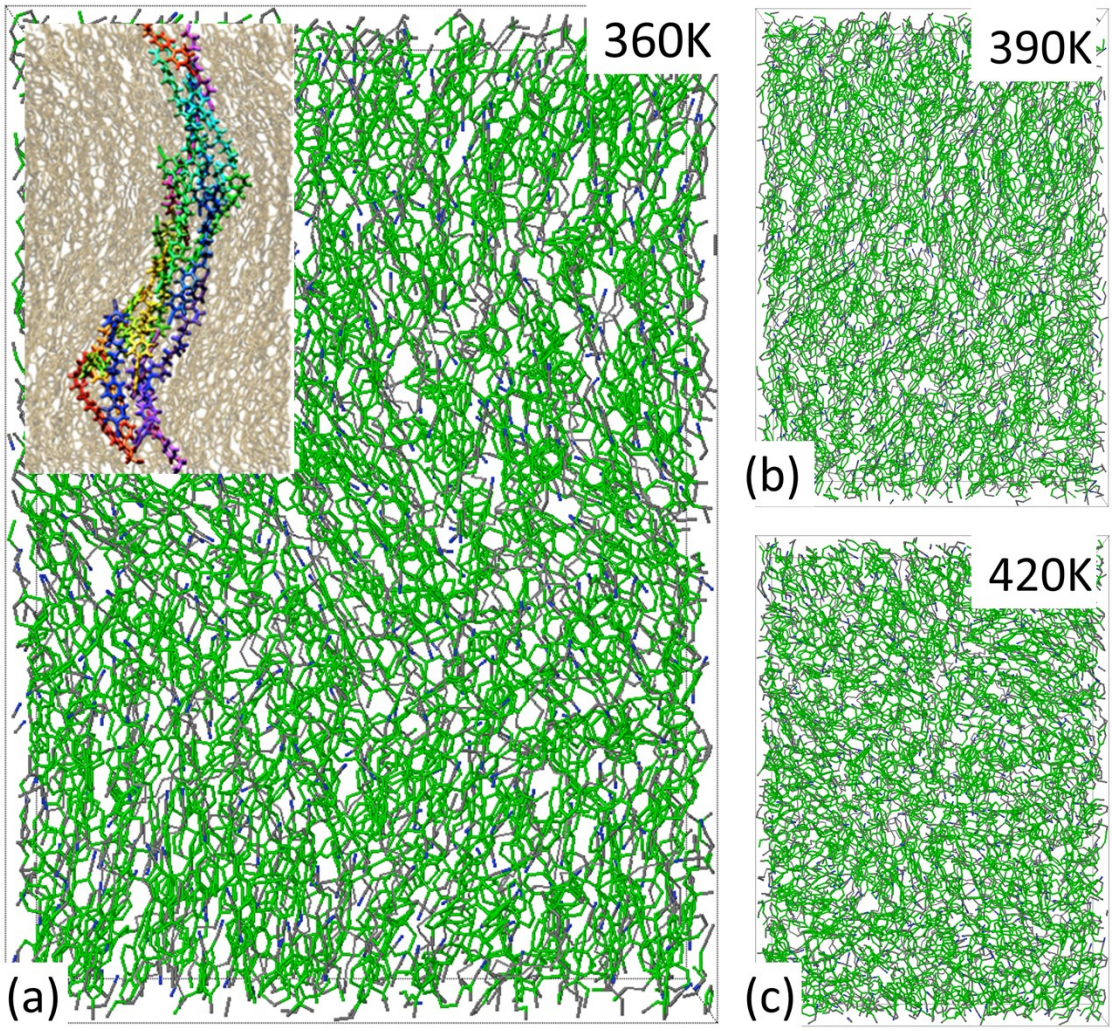

Figure 5.1. Snapshots of CB7CB bulk systems at different temperatures of 360-420 K showing (a) twist-bend nematic (360 K), (b) regular nematic (390 K), and (c) isotropic phase (420 K). The inset in (a) shows twist-bend structure with several molecules highlighting the helical arrangement.

In order to have a preliminary understanding of differences between N_{TB} and N phase, we computed the average bulk orientational order parameter, S_2, as well as the order parameter profile along the Z axis (set parallel to the helix axis) for all three temperatures (Figure 5.2). In order to obtain S_2 we converted both rigid end of the dimer's long axis into two unit vectors and calculated the order parameter separately. The average bulk order parameter for N_{TB}, N, and isotropic phases are 0.48, 0.35, and 0.1, respectively. These results agrees well with the recent X-ray scattering and polarized microscopic studies done by Singh et al.,[20] where the measured S_2 is 0.35 at 360 K N_{TB} phase, and about 0.4 in 390 K nematic phase. From the order parameter profile shown in Figure 5.2 we notice an interesting phenomenon, where the helix structure of N_{TB} phase leads to a much higher order parameter ($\Delta S \sim 0.15$) in each local slab compared to the bulk average S_2. Since slabs are defined perpendicular to the helix axes it is expected that orientational ordering in such subdomains will be higher than the average for the whole system where director from different domains will be averaged out. On the contrary, in the ordinary nematic phase both values are very similar, with local S_2 slightly higher than the bulk average S_2, we attribute this difference to the normalization factor.

To better understand the structural properties of the N_{TB} phase, we calculated the relative bend angle β between two cyanobiphenyl groups on CB7CB as a function of distance, shown in Figure 5.3. This analysis provides submolecular level insight on the conformational transformations of CB7CB mesogens when they spiral along the helix axis, and also can be used to as a way to distinguish the twist-bend phase from typical nematic ordering. As can be seen from Figure 5.3, the average bend angle $< \beta >$ for CB7CB in N_{TB} phase at 360 K is about 125° (previously, we measured it to be about 133° at 370 K using

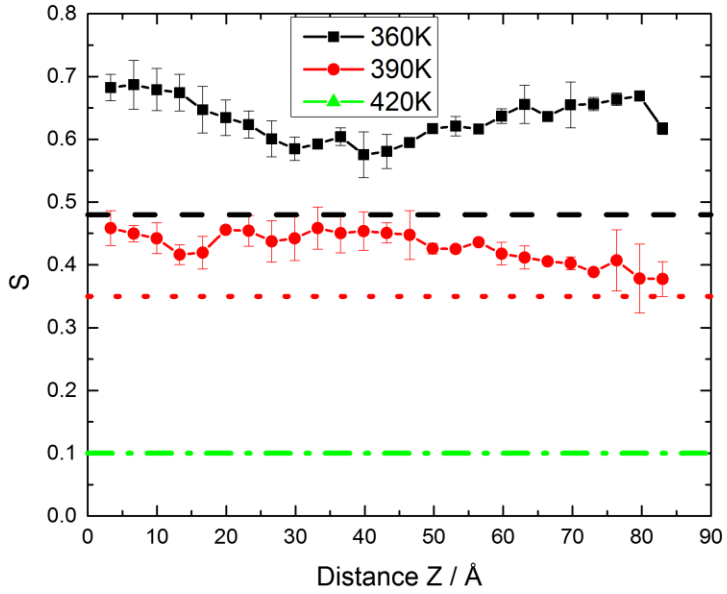

Figure 5.2. Order parameter profile as a function of distance along the Z direction for 360 (black square) and 390 K (red circle) CB7CB system, the black dash, red dot, and green dash-dot lines are the average bulk order parameters of the systems.

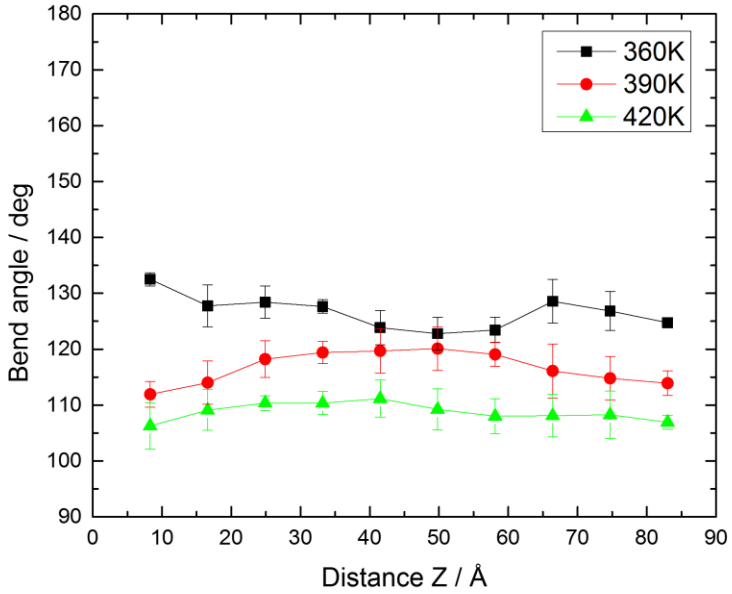

Figure 5.3. Average bend angle between the two cyanobiphenyl groups on the opposite side of CB7CB molecule as a function of Z direction for N_{TB}, N, and isotropic phases.

a slightly different force field[1]). In the nematic and isotropic phases $< \beta >$ is about 115° and 108°, respectively. However, what is more interesting is that, in Figure 5.3 the apparent atomistic scale modulation of bend angle β (black squares) along the helix axis. Such result indicates that the CH_2 units on the flexible alkyl chain in CB7CB undergoes conformational symmetry breaking to accommodate both twist and bend elastic energies as the molecule propagates along the helix. This observation is in accordance with the conformation study of CB7CB by Emsley et al.[21] using residual dipolar couplings technique. For nematic and isotropic phases we observe no apparent variation of $< \beta >$ along the Z direction. We also measured the heliconical precession angle θ in the N_{TB} phase, and the average angle is about 23°, which is well within the experimental measurements[10,14,20] between 17-30°.

So far no experimental data on the dynamic properties of CB7CB in N_{TB} phase have been reported. Here we report the prediction of self-diffusion coefficient for CB7CB in all three different phases using our MD simulations. As shown in Figure 5.4, the self-diffusion coefficient CB7CB in both N_{TB} and N phases is highly anisotropic, where the diffusion parallel ($D_{\parallel}$) to the Z direction (coincide with the helix axis in N_{TB}) is about 2-3 times faster than in the perpendicular ($D_{\perp}$) direction. However, such observation is not unexpected considering that both phases have nematic ordering in the Z direction and such dynamic asymmetry has been well documented in previous experiments[22–24] on 5CB. For CB7CB in N_{TB} phase at 360 K, the values of $D_{\parallel}$ and $D_{\perp}$ are 2.15×10^{-11} and 7.51×10^{-11} m^{-2}/s, respectively, vs. 13.9×10^{-11}, and 5.6×10^{-11} m^{-2}/s in the N phase at 390 K. The diffusion anisotropy ratio $D_{\parallel}/D_{\perp}$ is 3.5 in the N_{TB} phase and drops to 2.46 in the uniaxial N phase. This difference suggest that the spiral motion of the achiral LC molecules along the heliconical structure is encouraged. The contribution of this type of motion is smaller than

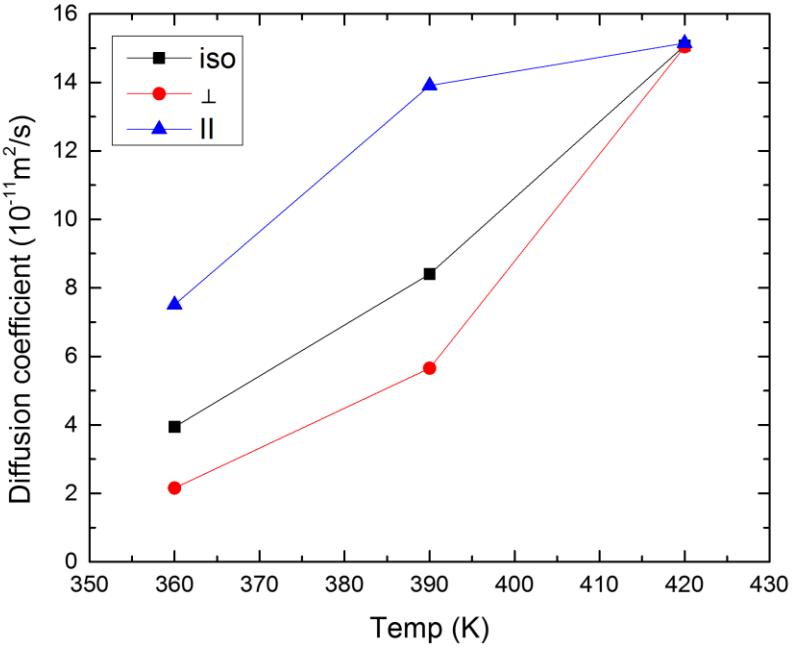

Figure 5.4. Diffusion coefficient of CB7CB in N_{TB}, N, and isotropic phases. The estimated error bars are less than 0.03×10^{-11} m^{-2}/s for all systems investigated.

the regular translational motion in uniaxial N phase. Such postulation is possible considering the experimentally[14] measured extremely low elastic bend modules of CB7CB in N_{TB} phase. Lastly, we note that at 420 K the self-diffusion coefficients become isotropic when all three values merge (15×10^{-11} m^{-2}/s) at 420 K, this unification further confirms that the 420 K system is in true isotropic state.

5.4 Conclusion

In this chapter, we briefly reviewed the exciting initial work that has been done to understand the novel twist-bend nematic phase. Many phenomena observed in the N_{TB} phase are still largely unexplained, such as the spontaneous chiral symmetry breaking from the achiral CB7CB, the microscopic to macroscopic heliconial structure coupling, etc. Although several theories describing this class of materials have been proposed for some time, the complete understanding of what is the true driving force behind the formation of N_{TB} phase is still lacking. Using MD simulations we presented initial data and comparison on structure, conformations, and dynamics of CB7CB in twist-bend nematic, regular nematic, and isotropic phases. The calculated order parameter agrees well with experimental data. In the relative bend angle β profile we noticed nanoscale angular modulation which indicates conformational changes of CB7CB when it twists around the helix. The diffusion anisotropy ratio difference between N_{TB} and N phases suggest that the twist-bend motion encounter less resistance from the bulk than the direct translational motion along the uniaxial director for CB7CB. As far as we know, this is still the only MD simulation work with atomistic level of details available today for this type of materials.

5.5 References

[1] D. Chen, J.H. Porada, J.B. Hooper, A. Klittick, Y. Shen, M.R. Tuchband, E. Korblova, D. Bedrov, D.M. Walba, M.A. Glaser, J.E. Maclennan, and N.A. Clark, Proc. Natl. Acad. Sci. **110**, 15931 (2013).

[2] R.B. Meyer, in *Mol. Fluids*, edited by B. R and W. G (Gordon and Breach, New York, 1976), pp. 271–343.

[3] I. Dozov, Europhys. Lett. **56**, 247 (2001).

[4] R. Memmer, Liq. Cryst. **29**, 483 (2002).

[5] V.P. Panov, M. Nagaraj, J.K. Vij, Y.P. Panarin, A. Kohlmeier, M.G. Tamba, R.A. Lewis, and G.H. Mehl, Phys. Rev. Lett. **105**, 167801 (2010).

[6] V. Görtz, C. Southern, N.W. Roberts, H.F. Gleeson, and J.W. Goodby, Soft Matter **5**, 463 (2009).

[7] M. Cestari, S. Diez-Berart, D.A. Dunmur, A. Ferrarini, M.R. de la Fuente, D.J.B. Jackson, D.O. Lopez, G.R. Luckhurst, M.A. Perez-Jubindo, R.M. Richardson, J. Salud, B.A. Timimi, and H. Zimmermann, Phys. Rev. E **84**, 031704 (2011).

[8] P.A. Henderson and C.T. Imrie, Liq. Cryst. **38**, 1407 (2011).

[9] K. Adlem, M. Čopič, G.R. Luckhurst, a. Mertelj, O. Parri, R.M. Richardson, B.D. Snow, B. a. Timimi, R.P. Tuffin, and D. Wilkes, Phys. Rev. E **88**, 022503 (2013).

[10] C. Meyer, G.R. Luckhurst, and I. Dozov, J. Mater. Chem. C **3**, 318 (2015).

[11] R.J. Mandle, E.J. Davis, C.T. Archbold, S.J. Cowling, and J.W. Goodby, J. Mat. Chem. C. **2**, 556 (2014).

[12] C. Greco and A. Ferrarini, Phys. Rev. Lett. **115**, 147801 (2015).

[13] D. Demus, J. Goodby, G.W. Gray, H.-W. Spiess, and V. Vill, editors , *Handbook of Liquid Crystals Set* (Wiley-VCH Verlag GmbH, Weinheim, Germany, 1998).

[14] V. Borshch, Y.-K. Kim, J. Xiang, M. Gao, A. Jákli, V.P. Panov, J.K. Vij, C.T. Imrie, M.G. Tamba, G.H. Mehl, and O.D. Lavrentovich, Nat. Commun. **4**, 1 (2013).

[15] O.N. Starovoytov, O. Borodin, D. Bedrov, and G.D. Smith, J. Chem. Theory Comput. **7**, 1902 (2011).

[16] X. Wei, J.B. Hooper, and D. Bedrov, Liq. Cryst. **ASAP**, (2016).

[17] G.J. Martyna, M.E. Tuckerman, D.J. Tobias, and M.L. Klein, Mol. Phys. **87**, 1117 (1996).

[18] B.J. Palmer, J. Comput. Phys. **104**, 470 (1993).

[19] D. Chen, M. Nakata, R. Shao, M.R. Tuchband, M. Shuai, U. Baumeister, W. Weissflog, D.M. Walba, M.A. Glaser, J.E. Maclennan, and N.A. Clark, Phys. Rev. E - Stat. Nonlinear, Soft Matter Phys. **89**, 1 (2014).

[20] G. Singh, D.M. Agra-kooijman, M.R. Fisch, and M.R. Vengatesan, 1 (n.d.).

[21] J.W. Emsley, M. Lelli, A. Lesage, and G.R. Luckhurst, J. Phys. Chem. B **117**, 6547 (2013).

[22] S. V. Dvinskikh, I. Furó, H. Zimmermann, and A. Maliniak, Phys. Rev. E - Stat. Nonlinear, Soft Matter Phys. **65**, 1 (2002).

[23] S. V. Dvinskikh and I. Furó, J. Chem. Phys. **115**, 1946 (2001).

[24] E.E. Romanova, F. Grinberg, A. Pampel, J. Kärger, and D. Freude, J. Magn. Reson. **196**, 110 (2009).

CHAPTER 6

CONCLUSION AND FINAL THOUGHTS ON MD SIMULATION STUDIES OF CYANOBIPHENYL-BASED LIQUID CRYSTALS

The research work presented in this thesis contributes to the fundamental understanding of properties of liquid crystal materials. We have made advances in three key areas. We started off by exploring the influence of electrostatic interactions (the value of molecular dipole moment and inclusion of induced polarization effects) on the prediction of thermodynamic and structural properties of bulk liquid crystal systems comprised of 5CB mesogen from atomistic molecular MD simulations. We demonstrated that utilization of partial atomic charge distributions fit directly to the high-level quantum chemistry calculations results in overestimation of the 5CB dipole moment, therefore leading to overestimation of the nematic-isotropic transition temperature by about 30 K degrees. Rescaling the charges to allow the molecular dipole to be closer to experimentally reported values of 5CB dipole in condensed phases significantly improves the prediction of T_{NI} as well as other thermodynamic and dynamic properties of isotropic and nematic phases of 5CB. We observed that the inclusion of induced polarization interaction does not have a significant impact on the structural, thermodynamic and dynamic properties of bulk 5CB. We also showed the rotational flexibility of the biphenyl unit has a strong influence on the stability of nematic phase.

From that work we obtained an optimized force field for 5CB and proceeded to investigation of 5CB anchoring behavior at immiscible aqueous interfaces. The results of the interface study show that we have correctly predicted the anchoring effects observed for 5CB at three different interfaces. For the free surface system, we demonstrated that alkyl tails of homeotropically anchored 5CB are exposed into the vacuum. At the interface with pure water our simulations showed a complete $\pi/2$ rotation of the easy axis across the box due to planar anchoring transition. A planar to homeotropic reorientation of 5CB in a complex four component system demonstrated the capability and the accuracy of our force field and provided the basis for future investigation of other multicomponent interface systems, such as LC based bio-sensors.

Lastly, we provided a brief preview of our current work on the exciting novel twist-bend nematic phase, where the basic understanding for the spontaneous chiral symmetry breaking from achiral LC molecules in nematic phase is still lacking. Nonetheless, after direct adaptation of the 5CB force field to the achiral CB7CB molecule, not only we were able to predict the signature twist-bend heliconical structure in our simulation but also correctly predicted some key structural and thermodynamic properties for the N_{TB} phase.